

EXPERIMENTAL INVESTIGATION OF 3D PRINTED SYNTACTIC FOAM COMPOSITES

Thesis

Submitted in partial fulfillment of the requirements for the degree of

DOCTOR OF PHILOSOPHY

by

BALU PATIL



DEPARTMENT OF MECHANICAL ENGINEERING
NATIONAL INSTITUTE OF TECHNOLOGY KARNATAKA,
SURATHKAL, MANGALORE – 575025

AUGUST, 2019

DECLARATION

I hereby *declare* that the Research Thesis entitled “**EXPERIMENTAL INVESTIGATION OF 3D PRINTED SYNTACTIC FOAM COMPOSITES**” which is being submitted to the **National Institute of Technology Karnataka, Surathkal** in partial fulfillment of the requirements for the award of the Degree of **Doctor of Philosophy** in **Department of Mechanical Engineering** is a *bonafide report of the research work carried out by me*. The material contained in this Research Thesis has not been submitted to any University or Institution for the award of any degree.

Register Number : **165001ME16F01**

Name of the Research Scholar : **BALU PATIL**

Signature of the Research Scholar :

Department of Mechanical Engineering

Place : **NITK, Surathkal**

Date :

C E R T I F I C A T E

This is to *certify* that the Research Thesis entitled “**EXPERIMENTAL INVESTIGATION OF 3D PRINTED SYNTACTIC FOAM COMPOSITES**” submitted by **Mr. BALU PATIL (Register Number: 165001ME16F01)** as the record of the research work carried out by him, is *accepted as the Research Thesis submission* in partial fulfillment of the requirements for the award of degree of **Doctor of Philosophy.**

Research Guide

Dr. Mrityunjay Doddamani

Assistant Professor

Department of Mechanical Engineering

Chairman – DRPC

Date:

ACKNOWLEDGEMENT

I would like to extend my sincere gratitude to Dr. Mrityunjay Doddamani, Assistant Professor, Mechanical Engineering Department for the invaluable constructive guidance and encouragement extended throughout my study. Sincere gratitude is expressed to Prof. Nikhil Gupta, New York University, USA for the encouragement and help provided.

I would like to thank Research Progress Assessment Committee members, Dr. Ramesh M. R. and Dr. Raviraj H. M. for their valuable inputs.

I would like to thank Prof. Shrikantha S Rao, Head of Mechanical Engineering Department and all the faculty members at Mechanical Engineering Department for their support throughout this research work.

Constant encouragement of my family to pursue higher studies has made it possible for me to reach at this stage. I wish to thank all my family members for love, help and encouragement provided. I express my sincere thanks to Dr. Bharath Kumar B. R, Dr. Jaywardhan M. L, Dr. Mahantesh Mathapatti, Dr. Kiran Shahapurkar, Dr. Ashrith H. S, Dr. Sunil Waddar, Mr. Praveen and Advanced Manufacturing Lab research team for their help and kind cooperation extended throughout this research work. Special note of thanks to all my friends and well wishers for their constant help, encouragement and understanding.

ABSTRACT

Polymer matrix composites can reduce the structural weight and result in improved fuel efficiency and performance in transportation applications. Thermoplastic matrix composites have been used for semi-structural and engineering applications. In addition to the ease of fabrication using a wide range of forming processes, thermoplastic polymers are recyclable, which is the strong driving force for their current and future applications.

Rapid production of high quality components is the key to cost reduction in industrial applications. The present work is the first attempt of manufacturing syntactic foams, hollow particle filled lightweight composites using thermoplastic based fused filament fabrication /fused deposition modeling (FFF/FDM) 3D printing process. High Density Polyethylene (HDPE) is used as the matrix material and fly ash cenospheres as the filler. Development of syntactic foams with cenospheres serves dual purpose of beneficial utilization of industrial waste fly ash and reduction in the component cost. Hollow fly ash cenospheres are blended with HDPE to form cenosphere/HDPE blend and is extruded to filament form and finally fed through 3D printer for printing eco-friendly lightweight syntactic foams. Prior to filament development, thermal degradation, melt flow index (MFI) and rheological properties of cenosphere/HDPE blend are studied. MFI decreased by 39.29, 60.54 and 70.51% with increasing cenospheres content of 20, 40 and 60 vol. % respectively. Rheology study of cenosphere/HDPE blend revealed complex viscosities values are maximum at a lower frequency but decreases with an increasing frequency indicating shear thinning behaviour. Both storage and loss modulus showed an increasing trend with filler content and frequency.

Single screw extruder parameters are optimized to develop ecofriendly syntactic foam filament with minimum cenosphere fracture and to obtain homogeneous mixing of constituents. The optimized parameters are used for manufacturing syntactic foams filament with 20, 40 and 60 vol.% cenosphere in HDPE matrix. Further, recycling potential of foam filament is also studied. Density of H40 (HDPE with 40 vol.% of

cenospheres) foams increased in up to two extrusion passes (2X) due to cenosphere breakage and porosity consolidation. Tensile properties of developed filaments are carried out to assess its viability into 3D printer. Tensile modulus and yield strength of neat HDPE filaments increased with each extrusion pass. Specific modulus of 3D printed H40-2X and 3X are 1.6 and 2.6 times higher than the respective filaments, however, fracture strain decreases by up to 40%. For first time extruded (1X) filament with addition of cenosphere density reduces due to intact cenosphere and void formation during extrusion, making it a 3 phase foam material. The void content and weight saving potential increases with increase in filler content and their values are higher for 3D prints than respective filament. Higher filler loading increases filament modulus by 7.72-12.79% as compared to HDPE. Among the foam filaments, H20 composition registered the highest ultimate strength (10.30 MPa) and strain at break (26.20%).

Differential scanning calorimeter and X-ray diffraction analysis of neat HDPE and foam filaments crystallinity is used to assess the parametric optimization of 3D printing process. It is observed that addition of cenosphere reduced crystallinity of HDPE. HDPE and foam filaments exhibit lower crystallinity as compared to respective printed material. Coefficient of thermal expansion (CTE) of 3D printed HDPE and its foam is studied to understand warping and shrinkage phenomenon occurring during printing. It is observed that filler addition in HDPE matrix reduces CTE remarkably. Warpage of the specimen is reduced with filler content and print quality is further improvised by optimizing printer speed, layer thickness, print temperature and cooling conditions.

Tensile tests are carried out on filaments and printed samples. Cenospheres addition resulted in improved tensile modulus and decreased filament strength. Tensile modulus of printed foams increases with filler content. 3D printed HDPE and foams modulus is better than respective feedstock material (filament). Tensile properties of 3D printed HDPE and foams are compared with injection molded samples. 3D printed HDPE registered higher tensile modulus and fracture strength compared to injection molding. Flexural test is conducted on 3D printed sample in two configurations (top

and bottom face of print subjected to the load). Results obtained from both configurations reveals that second configuration has shown better flexural modulus and strength. Neat HDPE print did not show any fracture below 10% strain. Flexural modulus increases with cenosphere content. Highest modulus is exhibited by H60 which is 1.56 times better than neat HDPE print. Raster gaps in 3D prints lowers flexural modulus and strength as compared to fully dense injection molded sample.

Quasi-static and regular strain rate compressive response is investigated on prints. Compressive behaviour of 3D printed foams follow similar trend in quasi-static and regular compressive mode as reported in fully dense injection molded two-phase foams. Modulus of neat HDPE is higher for all strain rates as compared to foams. Yield strength shows an increasing trend with strain rate. Highest specific compressive modulus and yield strength is observed for H60 and H20 respectively at 0.1 s^{-1} among foams. Further, HDPE matrix syntactic foam prints are characterized for their viscoelastic properties by dynamic mechanical analysis. Tests are conducted over 30-125°C temperatures. Storage and loss modulus increase with increasing volume fraction of cenospheres, with a slight difference between HDPE, H20 and H40 vol.%, at all temperatures. Storage modulus decreased with increasing temperature for neat HDPE and foam prints. Storage and loss modulus decrease with increasing temperature in the range of 30-125°C, while $\text{Tan } \delta$ increases. Structure-property correlations of all the investigated properties are presented with the help of exhaustive SEM images to understand underlying mechanisms.

Property maps for selected test conditions are presented for comparative analysis between FFF/FDM based 3D printing of eco-friendly lightweight syntactic foam prints and other processing routes used for thermoplastics. This work is an effort towards making wide material choices availability for FFF based 3D printing industries. Finally, the potential for using the optimized parameters of 3D printing is demonstrated by printing several industrial components as a deliverable of this work.

Keywords: *Syntactic foam filament; 3D printing; FFF; High density polyethylene; Fly ash cenosphere; Crystallinity; CTE; Mechanical properties.*

CONTENTS

| | |
|---|------|
| Declaration | |
| Certificate | |
| Acknowledgement | |
| Abstract | |
| CONTENTS..... | i |
| LIST OF TABLES..... | viii |
| ABBREVIATIONS | ix |
| NOMENCLATURE | x |
| 1 INTRODUCTION | 1 |
| 1.1 Composite Materials | 1 |
| 1.2 Syntactic Foam Composites..... | 4 |
| 1.2.1 Filler/Reinforcement..... | 5 |
| 1.2.2 Matrix..... | 8 |
| 1.3 Processing of Syntactic foams | 10 |
| 1.3.1 Compression Molding..... | 11 |
| 1.3.2 Injection Molding..... | 12 |
| 1.3.3 Additive Manufacturing (AM)..... | 13 |
| 1.4 Literature review | 20 |
| 1.5 Motivation of work | 44 |
| 1.6 Objectives and scope of the work | 45 |
| 1.7 Outline of the thesis | 46 |
| 2 MATERIALS AND METHODS..... | 47 |
| 2.1 Constituents..... | 47 |
| 2.1.1 Fly ash cenospheres | 47 |
| 2.1.2 Matrix..... | 48 |
| 2.2 Blend preparation..... | 48 |
| 2.3 Thermogravimetric analysis (TGA)..... | 50 |
| 2.4 Melt Flow Index (MFI)..... | 51 |
| 2.5 Rheological study of cenosphere/HDPE blend..... | 51 |
| 2.6 Filament development and 3D printing | 52 |

| | | |
|-------|---|----|
| 2.7 | Differential scanning calorimetry (DSC)..... | 55 |
| 2.8 | X-ray diffraction (XRD) | 56 |
| 2.9 | Coefficient of thermal expansion (CTE)..... | 56 |
| 2.10 | Density | 56 |
| 2.11 | Tensile testing | 57 |
| 2.12 | Flexural test..... | 57 |
| 2.13 | Compression test..... | 57 |
| 2.14 | Dynamic Mechanical Analysis | 58 |
| 2.15 | Imaging | 58 |
| 3 | MATERIAL CHARACTERIZATION AND PROCESSING ASPECTS | 59 |
| 3.1 | Blend characterization | 59 |
| 3.1.1 | Thermogravimetric analysis (TGA)..... | 59 |
| 3.1.2 | MFI of HDPE and cenosphere/HDPE blends..... | 60 |
| 3.1.3 | Rheology of HDPE and cenosphere/HDPE blend..... | 61 |
| | <i>Frequency sweep</i> | 61 |
| | <i>Temperature sweep</i> | 62 |
| 3.2 | Filament development..... | 64 |
| 3.3 | 3D printing of HDPE and their foams | 70 |
| 3.4 | DSC of filament and 3D prints | 74 |
| 3.5 | XRD analysis of filament and 3D prints..... | 76 |
| 3.6 | Coefficient of thermal expansion of prints | 77 |
| 4 | TENSILE BEHAVIOR OF FILAMENT and 3D PRINTS..... | 79 |
| 4.1 | Tensile behaviour of HDPE (1X, 2X and 3X) and H40 (2X, 3X) filament | 79 |
| 4.2 | Tensile behaviour of HDPE and H40 (2X, 3X) prints..... | 82 |
| 4.3 | Tensile behaviour of HDPE, H20, H40 and H60 filament | 85 |
| 4.4 | Tensile behaviour of HDPE, H20, H40 and H60 prints | 86 |
| 4.5 | Property map..... | 89 |
| | Conclusions..... | 91 |
| 5 | FLEXURAL RESPONSE..... | 93 |
| 5.1 | Flexural modulus and strength..... | 93 |
| 5.2 | Property map..... | 96 |

| | |
|--|-----|
| Conclusions..... | 98 |
| 6 COMPRESSIVE BEHAVIOR OF 3D PRINTS..... | 99 |
| 6.1 Quasi static compressive behavior of 3D prints | 99 |
| Property map..... | 104 |
| Conclusions..... | 105 |
| 7 DYNAMIC MECHANICAL ANALYSIS..... | 107 |
| 7.1 Temperature sweep | 107 |
| Conclusions..... | 109 |
| 8 3D PRINTED INDUSTRIAL COMPONENTS..... | 110 |
| SUMMARY AND CONCLUSIVE REMARKS | 113 |
| SCOPE OF FUTURE WORK | 117 |
| REFERENCES | 118 |
| RESEARCH OUTCOME IN PRINT MEDIA..... | 133 |
| LIST OF PUBLICATIONS | 134 |
| BIO-DATA | 136 |

LIST OF FIGURES

| | |
|--|----|
| Figure 1.1 Classification of composites based on the nature of reinforcement..... | 2 |
| Figure 1.2 Schematic representation of two, three and multi-phased syntactic foams..... | 5 |
| Figure 1.3 Structure of fly ash particles..... | 7 |
| Figure 1.4 Polymer consumption in India..... | 9 |
| Figure 1.5 Illustration of reinforced syntactic foam fabrication method (Gupta et al. 2013). | 11 |
| Figure 1.6 Constituents of PMCs and manufacturing options..... | 11 |
| Figure 1.7 Work flow of AM/3DP..... | 15 |
| Figure 1.8 Schematic of FFF process. | 17 |
| Figure 2.1 (a) Cenospheres and (b) HDPE matrix used in the present work..... | 48 |
| Figure 2.2 (a) Brabender (b) blending mechanism and (c) cenosphere/HDPE blend from brabender..... | 49 |
| Figure 2.3 Flow chart of the present study. | 50 |
| Figure 2.4 Melt flow indexer (Dynisco LMI5000)..... | 51 |
| Figure 2.5 (a) Schematic representation of the industrial scale single screw extruder and (b) experimental set up. | 53 |
| Figure 2.6 (a) Schematic representation of FFF printer and (b) FFF printer utilized in the present work..... | 54 |
| Figure 3.1 (a) TGA and (b) DTG thermograms of HDPE and cenosphere/HDPE blend..... | 59 |
| Figure 3.2 (a) Complex viscosity (b) storage modulus and (c) loss modulus as a function of frequency for HDPE and their blends..... | 61 |
| Figure 3.3 (a) Storage modulus (b) loss modulus and (c) $\tan \delta$ as a function of temperature for HDPE and their blends..... | 63 |
| Figure 3.4 Micrograph of (a) H40-1X filament at low magnification (b) a higher magnification image (c) H40-2X and (d) H40-3X filaments..... | 65 |
| Figure 3.5 (a) Micro-CT scan image showing reconstructed (i) sagittal ($y-z$) (ii) trans-axial ($x-y$) and (iii) coronal ($z-x$) views of H40-1X specimen (b) & (c) micrographs showing cenosphere walls with porosities and variable thickness and (d) voids present in cenosphere walls can appear to be discontinuities in some slices in the micro-CT scan images of H40.. | 67 |

| | |
|---|----|
| Figure 3.6 Representative H60 filament. | 68 |
| Figure 3.7 Freeze fractured micrographs of (a) filament cross section for H20 at lower magnification (b) H20 (c) H40 and (d) H60 at 250X. | 69 |
| Figure 3.8 Print trials of H40. | 71 |
| Figure 3.9 3D printed (a) HDPE and (b) H40-2X tensile bar. | 71 |
| Figure 3.10 Micrographs showing uniform distribution of cenospheres in 3D printed (a) H40-2X (b) H40-3X (c) high magnification micrograph of H40-2X shows cenospheres that survived the filament manufacturing and 3D printing process and (d) a defect in H40-2X specimen where incomplete filling is observed. | 72 |
| Figure 3.11 3D printed (a) HDPE (b) H20 (c) H40 (d) H60 tensile bar. | 73 |
| Figure 3.12 SEM of representative (a) 3D printed sample in thickness direction (b) freeze fractured HDPE (c) H60 and (d) air gap (marked area) between raster. | 74 |
| Figure 3.13 DSC thermograms for crystallization peak from cooling cycle in (a) filament (c) 3D prints and melting peak from second heating cycle in (b) filament (d) 3D prints. | 75 |
| Figure 3.14 XRD pattern of (a) filament and (b) printed specimen. | 77 |
| Figure 3.15 Representative images of (a) warped neat HDPE print and (b) intact non warped foam print. | 78 |
| Figure 4.1 Representative stress vs. strain curves for tensile behavior of (a) H-1X (b) H-2X (c) H-3X (d) H40-2X (e) H40-3X filaments and (f) The specific modulus versus strain rate plot for H40 filaments versus injection molded H40. | 80 |
| Figure 4.2 Tensile fracture surface of H40-2X filament tested at 10^{-4} s^{-1} at (a) low and (b) higher magnifications. | 82 |
| Figure 4.3 (a) Representative stress-strain curve for HDPE tensile samples at 10^{-3} s^{-1} strain rate, and (b) failure mode for HDPE tensile bar at 50% strain. | 83 |
| Figure 4.4 (a) Representative stress-strain plots for 3D printed H40-2X and H40-3X tensile specimens, (b) intact cenospheres on the fracture surface of a tensile tested H40-3X specimen and (c) failure mode in H40-2X specimen. | 84 |
| Figure 4.5 Representative stress-strain plot of neat HDPE and syntactic foam feedstock filament. | 86 |
| Figure 4.6 Representative stress-strain plot for 3D printed (a) HDPE and (b) their foams. | 87 |

| | |
|---|-----|
| Figure 4.7 Representative failed 3D printed sample of (a) HDPE (b) H60 and (c) SEM of H60 post tensile test..... | 88 |
| Figure 4.8 Tensile modulus and (b) strength of HDPE composites plotted against density (Adhikary et al. 2011, Ayrilmis 2013, Bharath Kumar et al. 2016, Homaeigohar et al. 2006, Khalaf 2015, Liu et al. 2008, Ou et al. 2014, Sim et al. 1997, Yuan et al. 2010)..... | 90 |
| Figure 5.1 Flexural test configuration (a) sample with top face up (b) sample with top face down..... | 93 |
| Figure 5.2 Representative flexural stress strain plot for (a) top face up and (b) top face down configuration..... | 94 |
| Figure 5.3 Flexural tested foam samples (a) H20 (b) H60. | 94 |
| Figure 5.4 Experimentally measured flexural (a) modulus and (b) strength of HDPE and their syntactic foams..... | 95 |
| Figure 5.5 Micrograph of H60 post flexural test. | 96 |
| Figure 5.6 Experimentally measured specific flexural (a) modulus and (b) strength of HDPE and their syntactic foams. | 96 |
| Figure 5.7 Flexural modulus and (b) strength of HDPE composite plotted against density (Adhikary et al. 2011, Ayrilmis 2013, Bharath Kumar et al. 2016, Chen et al. 2006, Gwon et al. 2012, Liu et al. 2008, Liu et al. 2009, Singh et al. 2016, Sood 2014). | 97 |
| Figure 6.1 Micrograph of freeze fractured (a) extruded syntactic foam filament showing circular cross-section of representative H60 filament (b) 3D printed H20 and (c) H60 sample. | 100 |
| Figure 6.2 Representative stress-strain plots for Quasi-static (a) HDPE (b) H20 (c) H40 and (d) H60..... | 101 |
| Figure 6.3 SEM of compression tested samples at 0.1 s^{-1} for H20 (a-b), H40 (c-d) and H60 (e-f) at lower and higher magnifications..... | 103 |
| Figure 6.4 Compressive modulus and strength of thermoplastic composites plotted against density from available studies (Bharath Kumar et al. 2016, Chakravarty et al. 2003, Jayavardhan and Doddamani 2018, Luong et al. 2013, Mahfuz et al. 2006, Saha et al. 2005, Tagarielli et al. 2008)..... | 105 |
| Figure 7.1 (a) Storage modulus (b) loss modulus and (c) $\text{Tan } \delta$ results at 1 Hz..... | 108 |

Figure 8.1 Eco-friendly components printed using 3DP technique 1. Arduino rack 2. Bearing holder 3. Arduino rack upper head 4. Support channel 5. Motor mount with fillet 6. Motor mount 7. Rod end holder 8. Filter ring 9. Motor cover 10. Filter end cap..... 110

Figure 8.2 Prototype components printed in the study: (a) Support channel (b) Motor mount with fillet (c) Motor mount (d) Filter end cap..... 111

LIST OF TABLES

| | |
|---|-----|
| Table 1.1 AM process categories (ASTM F2792-10). | 16 |
| Table 1.2 Literature survey of thermoplastic materials/composites for FFF/FDM process. .. | 21 |
| Table 2.1 Physical, chemical and sieve analysis details of cenospheres*. | 47 |
| Table 2.2 Characteristics of HDPE grade HD50MA180*..... | 48 |
| Table 2.3 Single screw extruder specifications..... | 53 |
| Table 2.4 Specifications of FFF based 3D printer. | 55 |
| Table 3.1 TGA and DTG thermograms of HDPE and their foams. | 60 |
| Table 3.2 Density, void content and weight saving potential of filament and 3D printed samples..... | 69 |
| Table 3.3 Pilot study print settings. | 71 |
| Table 3.4 Optimized printing parameters. | 73 |
| Table 3.5 T_{Cryst} , α_{cryst} and T_{Melt} of samples. | 75 |
| Table 3.6 XRD data of neat HDPE and foam material..... | 77 |
| Table 3.7 CTE values of 3D printed HDPE and their foams..... | 78 |
| Table 4.1 Tensile properties of extruded HDPE and H40 filaments. | 81 |
| Table 4.2 Tensile properties of 3D printed H40-2X and 3X specimens..... | 85 |
| Table 4.3 Tensile properties of filament and 3D printed material..... | 86 |
| Table 4.4 Specific properties of syntactic foams fabricated using a 3D printer. | 89 |
| Table 5.1 Flexural properties of printed HDPE and their syntactic foams. | 94 |
| Table 5.2 Specific flexural modulus and strength for top face down configuration..... | 95 |
| Table 6.1 Quasi-static compression data of 3D printed HDPE and their foams..... | 102 |
| Table 7.1 Comparison of storage modulus at three representative temperatures. | 108 |
| Table 7.2 Comparison of loss modulus at three representative temperatures..... | 108 |
| Table 7.3 Comparison of damping parameter at three representative temperatures..... | 109 |
| Table 8.1 Details of 3DP syntactic foam components..... | 112 |

ABBREVIATIONS

| | |
|------|--|
| ASTM | : American Society for Testing and Materials |
| AM | : Additive Manufacturing |
| CTE | : Coefficient of Thermal Expansion |
| CM | : Compression Molding |
| DSC | : Differential Scanning Calorimetry |
| DTG | : Derivative Thermogravimetry |
| DMA | : Dynamic Mechanical Analysis |
| FFF | : Fused Filament Fabrication |
| FDM | : Fused Deposition Modeling |
| IM | : Injection Molding |
| MFI | : Melt Flow Index |
| PMC | : Polymer Matrix Composite |
| SEM | : Scanning Electron Microscope |
| SF | : Syntactic Foam |
| TGA | : Thermogravimetric Analysis |
| UTS | : Ultimate Tensile Strength |
| XRD | : X-ray Diffraction |
| 3DP | : 3 Dimensional Printing |

NOMENCLATURE

| | | |
|------------------|---|-------------------|
| ρ | Density of the composite | kg/m ³ |
| ρ_f | Density of the filler | kg/m ³ |
| Φ_f | Cenosphere percentage | % |
| ρ_m | Density of the matrix | kg/m ³ |
| V_m | Volume fraction of matrix | % |
| V_f | Volume fraction of filler | % |
| Φ_V | Void content | % |
| ρ^{th} | Theoretical density | kg/m ³ |
| ρ^{exp} | Experimental density | kg/m ³ |
| E_{fM} | Flexural modulus | MPa |
| σ_{fS} | Flexural strength | MPa |
| T_{Cryst} | Melting peak temperature | °C |
| T_{Melt} | Crystallization temperature | °C |
| α_{Cryst} | Degree of crystallinity | % |
| ΔH_m | Heat of fusion | J g ⁻¹ |
| ΔH_m^* | Heat of fusion per gram for 100% crystalline HDPE | J g ⁻¹ |
| A_{cr} | Area of crystalline phase of HDPE | ----- |
| A_{am} | Area of amorphous phase of HDPE | ----- |
| η' | Complex viscosity | Pa.s |
| G' | Storage modulus | Pa |
| G'' | Loss modulus | Pa |
| $Tan \delta$ | Damping factor | ----- |
| E' | Storage modulus | MPa |
| E'' | Loss modulus | MPa |

1 INTRODUCTION

1.1 Composite Materials

The development of mankind is defined in terms of advances in materials: Stone Age, Bronze Age, and the Iron Age. Today the development of any country is decided based on the amount of steel and concrete used. The Industrial revolution largely made possible advances in the use of materials in industrial equipment. In the last half century, the growth of materials technology has been explosive and its impact on our daily lives, pervasive. In last few decades the developments in materials technology is fueled mainly by composite materials. Composite materials are extending horizons of designers in all branches of engineering, and yet the degree to which this is happening can easily pass unperceived. The eye, after all, does not see beyond the glossy exterior or the race performance of a glass fiber reinforced plastics (GRP) yacht, nor does it sense the complexity of the structure of a composite helicopter rotor blade or of a modern carbon fiber reinforced plastics (CFRP) tennis racket. Nevertheless, this family of synthesized materials offers the possibility of exciting new solutions to difficult engineering problems (Harris 1999). In composites, materials are combined in such a way as to enable us make better use of their virtues while minimizing to some extent the effect of their deficiencies. This principle, when extended to physical, chemical and mechanical properties that can accrue, has opened a Pandora's box where the combinations to be thought of and tried for optimizing any of the above properties are only limited by one's imagination. This process of optimization can release a designer from the constraints associated with the selection and manufacture of conventional materials. One can make a use of tougher and lighter materials, with properties that can be tailored to suite particular design requirements.

Composites are classified according to either of the constituents, the matrix or the reinforcement (Chawla 2001). Based on the matrix material, composites are classified as Metal Matrix Composite (MMC), Ceramic Matrix Composite (CMC) and Polymer Matrix Composite (PMC). PMC's are becoming promising materials for variety of structural and automotive applications since these possess favorable combinations of mechanical properties (Benchechou et al. 1998). Metal and ceramic matrix composites find less extensive applications compared to PMC's, because of the involved processing methods and higher cost. The applications of the former two varieties are typically seen in high performance/high

temperature and cost intensive categories. On the other hand, PMC's have particularly attracted a wider usage and lot of interest because of their relative ease of processing, low density, desirable electrical/thermal properties and excellent chemical/corrosion resistance. Hence, they find applications ranging from specialized functions in aerospace and electronics engineering to day-to-day consumer industries construction and transportation. Classification of composites based on the nature of reinforcement is simplified and presented in Figure 1.1 (Agarwal and Broutman 1980).

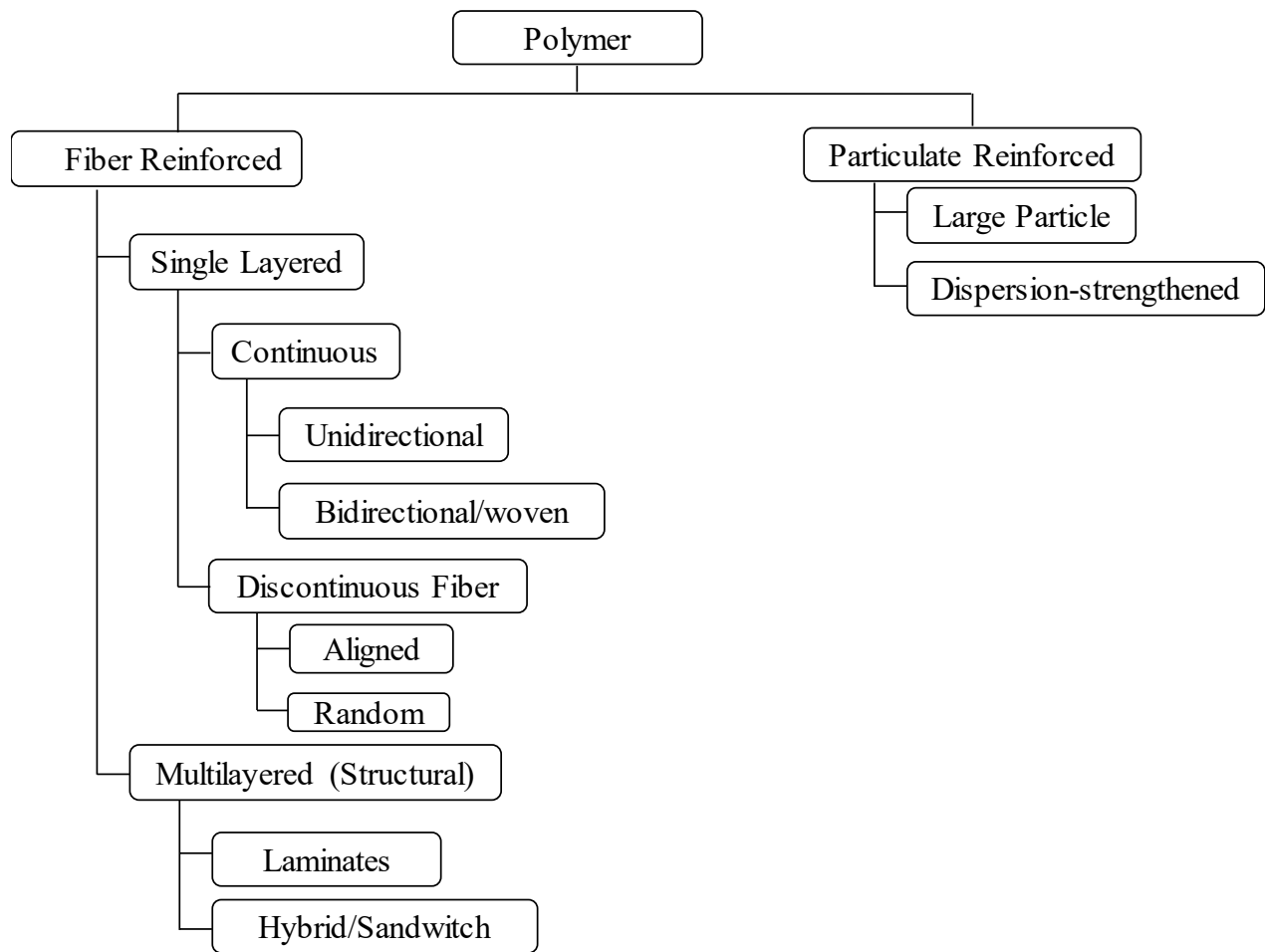


Figure 1.1 Classification of composites based on the nature of reinforcement.

PMCs consists of a polymer (epoxy, polyester, urethane etc.) reinforced by thin diameter fibers (graphite, aramids, boron etc.). The reasons for this are two-fold. Foremost, in general the mechanical properties of polymers are inadequate for many structural designs. In particular, their strength and stiffness is low compared to metals and ceramics. This implies that there is

a considerable benefit to be gained by reinforcing polymers and that the reinforcement, initially at least, did not have to have special properties. Secondly, the processing of PMCs need not involve high pressures and temperatures. It follows that problems associated with the degradation of the reinforcement during manufacture are less significant for PMCs than for composites with other matrices. Further, the equipment required for PMCs are simpler. For these reasons polymer matrix composites developed rapidly and soon became accepted for structural applications. Today glass-reinforced polymers are still by far the most used composite material in terms of volume with the exception of concrete.

To see the advantages in using composite materials, a comparison between their properties and those of newer class of composites should be done in terms of specific values (per unit of weight). When it comes to weight saving without sacrificing structural performance, composites and in particular from the lightweight materials regime, syntactic foam (SF) composites are without doubt far superior to other traditional composites. In the present scenario, SF a special class of structural composite have become very popular due to high specific strength and bending stiffness. Low density of these materials makes them especially suitable for use in aeronautical, space, marine and sports applications (Gupta and Woldesenbet 2004). Syntactic foams are lightweight porous composites that found their early applications in marine structures due to their naturally buoyant behavior and low moisture absorption. This lightweight feature is beneficial in weight sensitive aerospace structures too. Syntactic foams have pushed the performance boundaries for composites and have enabled the development of vehicles for travelling to the deepest parts of the ocean and to other planets. The high volume fraction of porosity in syntactic foams also enabled their applications in thermal insulation of pipelines in oil and gas industry. The possibility of tailoring the mechanical and thermal properties of syntactic foams through a combination of material selection, hollow particle volume fraction, and hollow particle wall thickness has helped in rapidly growing these applications. The low coefficient of thermal expansion and dimensional stability at high temperatures are now leading their use in electronic packaging, composite tooling and thermoforming plug assists. Methods have been developed to tailor the mechanical and thermal properties of syntactic foams independent of each other over a wide range, which is a

significant advantage over other traditional particulate and fibrous composites (Gupta et al. 2005).

1.2 Syntactic Foam Composites

Syntactic foams are examples of particulate composites. These foams are made by mixing hollow particles called cenospheres/microspheres/microballoons in a matrix material. They possess lower density due to the hollow microballoons incorporated in the matrix compared to solid particulate and fiber reinforced composites. These foams are found to possess high specific strength and low thermal conductivity (Gupta et al. 2005). SF's are used in a wide variety of applications. Most of the applications are related to the marine environment, where structural designs depend on the buoyancy obtained from such lightweight materials with high compressive strength and modulus. These materials were developed in the 1960s as buoyancy aid materials, for deep sea applications. Currently they are used in aircraft, spacecraft and ship structures (Gupta and Woldesenbet 2004). One of the major advantages of syntactic foams is their ability to be designed and fabricated according to the physical and mechanical property requirements of the application. Depending upon the service conditions, the matrix resin can be chosen from a wide range of thermosetting and thermoplastic resins. Similarly, microballoons of polymer, ceramic or metal can be chosen based on the availability (Gupta et al. 2013).

A schematic representation of two, three and multi-phase structures of syntactic foams are presented in Figure 1.2. Syntactic foams are usually a two phase structures, namely matrix and microballoons. These foams are classified as closed pore/cell foams, due to the existence of enclosed porosity within the microballoons (Gupta 2007). However, during fabrication of syntactic foams, air or voids might get entrapped in the matrix. The presence of air or voids within the matrix is termed as open cell porosity and thus making syntactic foams a three phase structure. Syntactic foams when reinforced with fibers results in multi-phase structure.

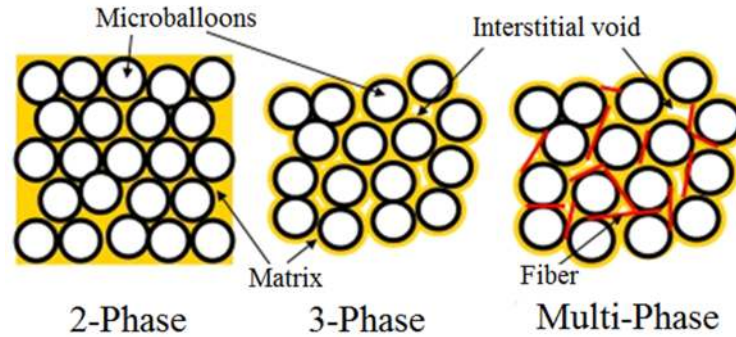


Figure 1.2 Schematic representation of two, three and multi-phased syntactic foams.

Interest in utilizing the advantage of low density of syntactic foams in variety of applications has made it necessary to characterize these materials for mechanical behavior. Though SF's are widely used, thrust on developing these with variety of hollow particulate fillers is overgrowing.

1.2.1 Filler/Reinforcement

Fillers are often incorporated in matrix resin to improve tensile and compressive strengths, tribological characteristics, toughness, dimensional and thermal stability etc. Selection of filler material is primarily dependant on the requirements expected in the end product, the interface compatibility, shape, size and packing factor. Large number of materials can be selected as fillers for the polymers which include particles of minerals, metals, ceramics, polymers and also some industrial wastes (Shaikh and Channiwala 2006). Some common examples of filler materials are particles of alumina, silica, hollow and solid particles of glass, wood chips, fly ash and carbon black. Selection of one of these materials is mainly based on the desired properties of the composite. The shape of the filler particles plays important role in determining the properties of the composite. Spherical particulate fillers are more popular compared to the other types. The principal advantages of spherical fillers are (Ferrigno 1978):

- Low surface area to volume ratio
- Regularity of shape
- Control of surface properties
- High crush strength
- Closely controlled particle size
- Better rheology

One of the materials available in abundance in particulate form as far as fillers are concerned is 'Fly ash'. It has attracted interest lately because of the abundance in terms of material volume generated and the environmental linked problems in the subsequent disposal (Ferrigno 1978). Fly ash is a predominantly inorganic residue obtained from the flue gases of furnaces at pulverized coal power plants. When coal is burnt in pulverized coal boilers, the minerals entrained in the coal are thermally transformed into chemical species that are reactive or could be chemically activated, for example by the addition of calcium hydroxide (Chawla 2001). The finely divided glass phase, the predominant phase in fly ash, reacts as a pozzolan, defined by Manz (Manz 1999) as "...a siliceous and aluminous material that in itself possesses little or no cementitious value but will, in finely divided form and in the presence of moisture, chemically react with calcium hydroxide at ordinary temperatures to form compounds possessing cementitious properties".

Fly ash can be classified as either cementitious or pozzolanic. The cementitious fly ash is labeled as Class C making up at least 50 mass percent. In pozzolanic fly ash, Class F makes up more than 70 mass percent of the total fly ash composition (Kruger 1997, Scheetz and Earle 1998). There are two primary sources of fly ash: fly ash from a pulverised coal power plant and fly ash from a municipal waste incineration plant. The fly ash produced from the burning of pulverized coal in a coal fired boiler is a fine-grained, powdery particulate material that is carried off in the flue gas and usually collected from it by means of electrostatic precipitators, bag houses or mechanical collection devices such as cyclones. It is the finely divided mineral residue resulting from the combustion of ground or powdered coal in electric generating plant (ASTM C618-15). Since the particles solidify while suspended in the exhaust gases, fly ash particles are generally spherical in shape (Kruger 1997) and are usually silt size (0.074 - 0.005 mm). As these have aspect ratios closer to unity, near isotropic characteristics are displayed by them. These are inexpensive and possess good mechanical properties.

Fly ash mainly consists of alumina and silica which are expected to improve the composite properties. It also consists to some extent, hollow spherical particles termed as cenospheres (Mohapatra and Rao 2001, Pedlow 1978) which aid lowering the composite density. A

schematic with SEM image showing the structure of the fly ash particles is presented in Figure 1.3.

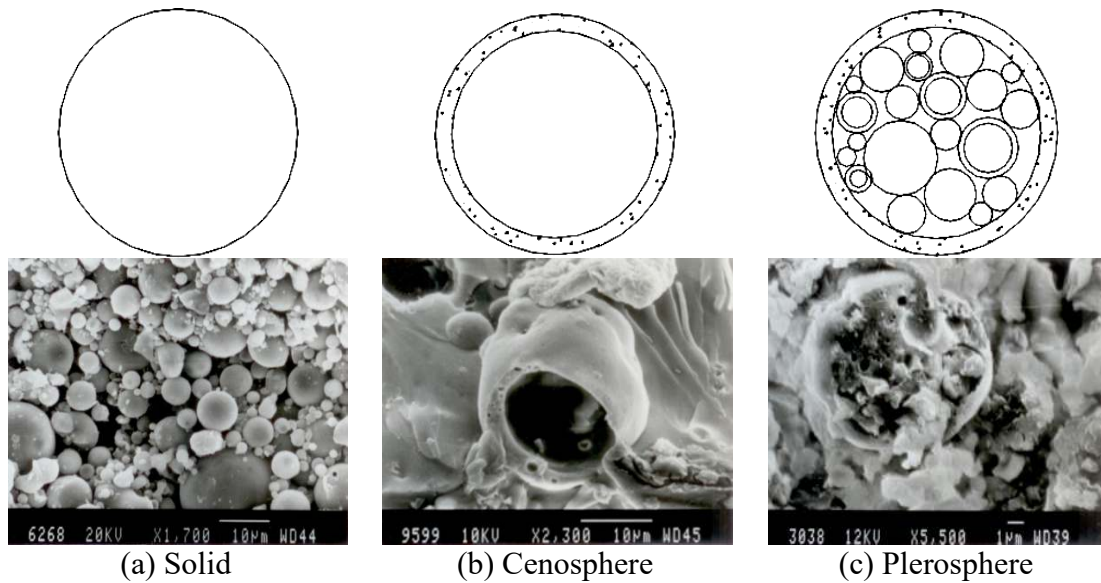


Figure 1.3 Structure of fly ash particles.

Hollow fly ash particles are generally termed as Cenospheres. Composite particles, which consist of smaller solid and hollow spherical particles, are referred as Plerospheres and the SEM picture above displays one such Plerosphere. Cenospheres are unique free flowing powders composed of hard shelled, hollow, minute spheres. A small proportion of the pulverized fuel ash produced from the combustion of coal in power stations is formed as Cenospheres. Cenospheres are made up of silica, iron and alumina. They are also referred to as microspheres, hollow spheres, hollow ceramic microspheres or microballoons. These spheres have been used to improve the properties of a variety of finished consumer products. Thermosetting synthetic foams made with cenospheres have demonstrated superior mechanical properties when compared to those manufactured with fabricated microspheres (Gupta et al. 2014).

When used with well-established matrix materials, these help in reducing the cost and either retain or improve desirable and specific mechanical properties (Scheetz and Earle 1998). The feature of inbuilt porosity in cenospheres is of considerable significance in weight specific applications. As the fillers are of near spherical shape, the resin spread is also better.

Developing newer and utilitarian thermoplastic systems using fly ash displaying near isotropic properties should be an interesting and challenging task.

1.2.2 Matrix

Polymers are long chain organic molecules or macromolecules with many desirable properties such as high ductility, ease of forming and non-corrosiveness (Srinivasan and Ramakrishnan 1983). A wide variety of such materials are available to a designer. Two such classes are thermosetting and thermoplastic polymers. Their initial target applications were in aerospace and later became viable alternative material in the sporting, automotive and in construction industries. In thermosetting polymers, there are covalent cross bonds (cross link) between molecules, in addition to Van der Waals forces. Owing to these cross bonds, a thermosetting polymer remains rigid on heating (Arzamasov B 1989). Thermoplastic polymers can be re-shaped by repeated heating and cooling without losing their properties (Arzamasov B 1989). They soften on heating and become rigid on cooling. On the other hand, thermosets remain rigid during reheating till they are converted into char. This difference in behavior on heating is due to the relatively weak Van der Waals forces acting between the molecules of thermoplastic polymers. On heating, the bonds between the molecules weaken substantially and the material becomes soft and yieldable.

Many thermoplastics are now accepted as engineering plastics. The term engineering plastics probably originated as a classification distinguishing those plastics that can satisfactorily substitute the metals such as Aluminum in small devices and structures requiring lower mechanical properties. Engineering plastics are the main source for developing high performance composites which possess advantages like high stiffness, high strength to weight ratio and increased chemical and atmospheric inertness compared to conventional materials.

Though PMCs have higher initial material costs, low cost ones could be developed from reinforcing plastics with low cost environmental pollutants like cenospheres. In the year 1997, the estimated per capita demand of plastics in India was 0.800 Kgs. which was one of the lowest in Asia (Burgiel et al. 1994, Burgueno et al. 2004, Esha and Rajaram 1997, Scott 2000). The projected demand in 2000 A. D. was 2.16 kg/capita (KSSPMA 1992). A boom in the consumption of plastic in India is experienced with the economic liberalization since 1991.

Plastic consumption in India has more than doubled from 0.85 million tons during 1990-91 to 1.79 million tons during 1995-96. Demand for commodity plastics is growing at the rate of 15% per year.

As per a survey conducted by the All India Plastic Manufacturers Association, the total capacity to produce PE, PVC, PP and PS was 1.39 million mega tonne (MMT) against the demand of 1.55 million MT in 1995 which has increased to 1.8-1.9 million MT for 1996-97. This is concentrated in three major sectors according to the Plast India figures: infrastructure (power, roads, bridges, telecommunications and construction) which is 30% of the total, packaging is 25% of the total and 24% for agriculture and water (Nanavaty 1997). The consumption of polymers in the year 2015 in India is 13 MMT which is 15 times higher than that seen in 1990 and is estimated to grow upto 22 MMT by 2020 (Figure 1.4) (Shekhar 2012). Polymers used in packages have about 50% of share in this consumption.

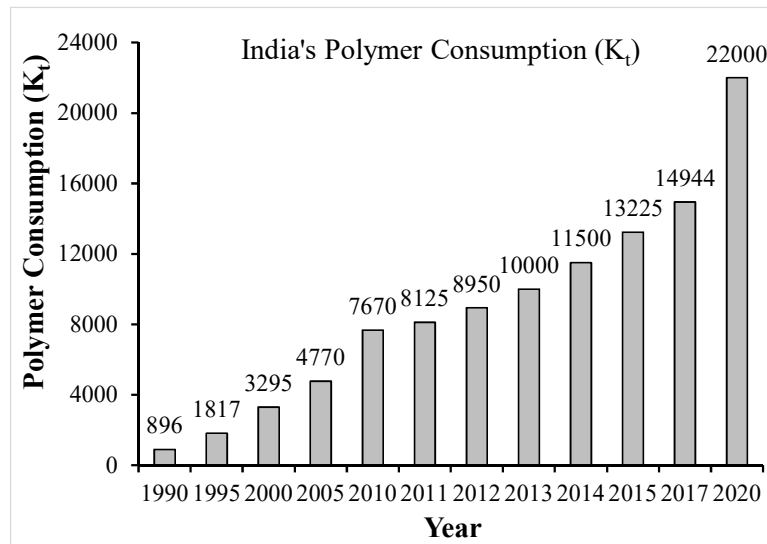


Figure 1.4 Polymer consumption in India.

With such a drastic growth prevailing in the consumption of plastic, thermoplastic syntactic foam composites with filler such as fly ash cenospheres may be an essential requirement to avoid issues regarding plastic management and environmental linked problems. Further, when matrix is reinforced with fillers, role of interface between them and related compatibility issues needs attention.

1.3 Processing of Syntactic foams

Every material possesses unique physical, mechanical and processing characteristics and hence a suitable manufacturing route must be selected to transform the material to its final shape. In the last half of the twentieth century, the processes used for fabrication of parts made from composite materials evolved from operations relying on manual labour to manufacture by automated equipment controlled from sophisticated microprocessor systems. Early pioneers combined raw materials and formed the final structure by hand lay-up or spray-up in open molds. The parts are cured at ambient temperature. As the advantages of PMC's are felt, these synthetic materials began to penetrate virtually every other market worldwide, from consumer products, automotive and marine to primary structural elements of aircraft and bridges. Such widespread growth in product applications mandated corresponding growth in materials technology, design approaches, and fabrication processes (Arza 2012).

In case of syntactic foam composites, if the processing route is not carefully designed, hollow particles reinforcement may provide unintentional effect of increased matrix porosity by stabilizing gas bubbles in polymer matrix. The processing methods are also required to be efficient in promoting wetting of reinforcement by the matrix resin, breaking clusters without fracturing the reinforcement material and obtaining uniform distribution of reinforcement in the matrix resin. In addition, the hollow particles should not be excessively fractured during the manufacturing process. A commonly used fabrication method for reinforced syntactic foams is illustrated in Figure 1.5. In this method, a three-step mixing process is used. In the first step, the reinforcement is added to the neat resin and mixed. After thorough mixing of reinforcement, hollow particles are added and stirred until slurry of consistent viscosity is obtained. In the final step, the hardener or catalyst is added to the resin and stirred slowly. The mixture is cast in molds and cured as per the requirements of the resin. Additional rigorous mixing of reinforcement before incorporation of hollow particles helps in reducing the possibility of hollow particle breakage during processing.

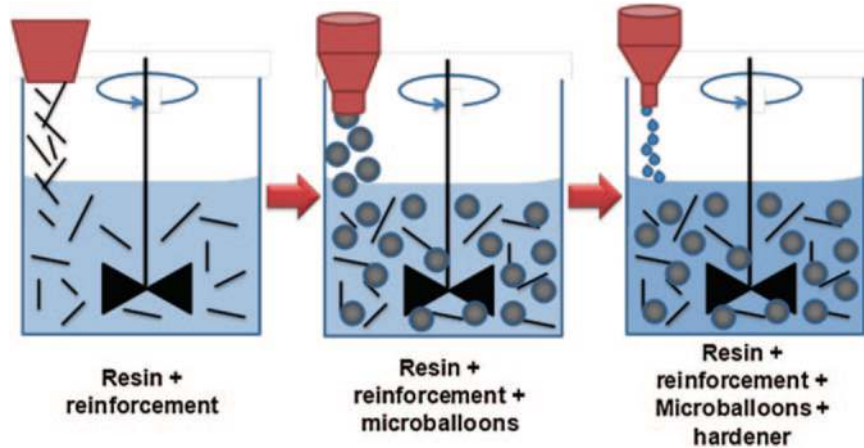


Figure 1.5 Illustration of reinforced syntactic foam fabrication method (Gupta et al. 2013).

Some of the fabrication processes widely practiced on the shop floor include open mold processes like hand layup, autoclave, press cure oven cure process. Closed mold processes include compression molding, injection molding, transfer molding and thermostamping. Some of the processing options for thermoset and thermoplastic materials with variety of reinforcement are presented in Figure 1.6 (Reinhart 1998).

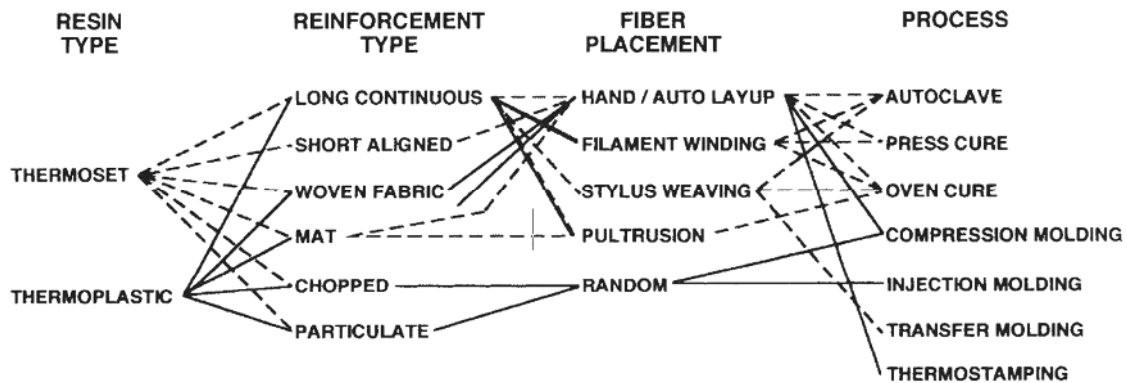


Figure 1.6 Constituents of PMCs and manufacturing options.

Particulate reinforced thermoplastics are processed using Compression and Injection molding routes as seen from Figure 1.6. PMC's can also be processed through FFF/FDM based additive manufacturing.

1.3.1 Compression Molding

Compression molding machine is a kind of press which is oriented vertically with two molding halves (top and bottom). It is high-pressure method suitable for molding complex, high strength

fiberglass reinforcements. Compression mold consists of two components namely male and female plate. Male plate is fixed and the female plate is movable. Thermoplastics blended with filler are placed inside the mold that is been preheated to a set temperature depending on the materials requirement. Pressure is applied through hydraulic means to the preheated mold to form the required shape. Advanced composite thermoplastics can also be compression molded with unidirectional tapes, woven fabrics, randomly oriented fiber mat or chopped strand. Materials such as polystyrene, polypropylene and polythene are used with this method. Compression molding is a cost effective process when compared to the injection molding and stamping. It is the oldest and unique process for molding of plastic components that produce parts of near net shape (Manas and Salil 2006). In compression molding of thermosets, the mold remains hot throughout the cycle. As soon as a molded part is ejected, a new charge of molding powder can be introduced. On the other hand, unlike thermosets, thermoplastics must be cooled to harden. Compression molding of HDPE composites was prepared and characterized for impact and wear performance (Chand et al. 2010). They observed considerable improvement in both the properties. Multi walled carbon nanotubes reinforced cenosphere/HDPE syntactic foam sheets are compression molded at 15 MPa pressure and 160°C temperature and investigated for mechanical properties (Divya et al. 2015). Further, Deepthi and group (Deepthi et al. 2014) developed HDPE reinforced with silicon nitride and nanoclay using compression molding at 15 MPa pressure and 130°C temperature and dealt with mechanical characterization. Compression molding is not as efficient as IM with regard to cycle time, complexity of components and volume of production.

1.3.2 Injection Molding

IM is one of the most widely processes to manufacture thermoplastic products. It is considered as the promising alternative technique for mass-fabrication of the polymer micro/nano engineered surfaces due to rapid cycle time, low material cost and variety of material options. It offers a number of advantages such as low material consumption, improved dimensional stability, shorter cycle time, lower injection pressures and clamp forces. Furthermore, injection molded products show better thermal, acoustic insulation and improved mechanical properties compared to compression molded counterparts. It is a widely used manufacturing method for low and high density polyethylene (LDPE and HDPE), polymethyl methacrylate

and polylactic acid (Alkan et al. 1995, Benchekchou et al. 1998). Injection molding is capable of economically producing precision plastic parts with various shapes and complex geometries at low cost. Use of these resins in fabricating syntactic foams can provide opportunities of saving weight in existing applications and also in developing new material systems (Bunn and Mottram 1993, Gupta et al. 2004). One of the advantages of using thermoplastic resins is the possibility of using rapid manufacturing industrial techniques for making syntactic foam parts. However, the existing studies have not utilized such mainstream industrial production methods for producing syntactic foams. If such rapid manufacturing technique can be developed for syntactic foam parts, the cost of such lightweight eco-friendly components can be lowered (Gupta et al. 2014). The available studies on thermoplastic syntactic foams process materials under controlled conditions at laboratory scale, which usually provides syntactic foams with high quality. However, processing of materials with industrial scale manufacturing equipment may not yield similar quality. Though Injection molding is rapid manufacturing technique, its quite expensive as far as tooling (molds) is concerned. Alternative for this could be a 3D printing having the maximum flexibility of developing any complex shapes. Over the past year there has been an explosion on the consumer market of low cost additive manufacturing machines available for home users. This has brought additive manufacturing machines into focus and interest of the media. Several low cost desktop printers have been developed and the new market segment has influenced a wave of innovation.

1.3.3 Additive Manufacturing (AM)

Rapid growth and advances in manufacturing for global competitiveness drives the promise realization of next generation manufacturing. Innovative materials with manufacturing technologies to make next generation products are a crucial factor for the economic success of any country. AM is a key factor to revolutionize the way products are designed and built. It leads to wealth of opportunities for product customization, improved performance, multifunctionality and lower overall manufacturing costs. Not only does AM remove the traditional limits on part geometry, but highly complex components can also be fabricated faster while consuming less material and using less energy. It eliminates the need for expensive part tooling and detailed drawing packages, lower lead times for concept to commercialization, reduced energy intensity strengthening clean energy economy causing a paradigm shift for the

design-to-manufacture process. AM allows freeform manufacturing without the need for tools or molds. In contrast to traditional reductive methods such as milling or lathing which remove material to create a part, additive manufacturing works by sequentially adding more material to build up a part. AM allows for rapid prototyping and in some cases can be used directly in manufacturing for small-scale production. The method allows manufacturing of complex shapes, otherwise difficult to be made, using conventional methods. It also allows quick and cheap manufacturing of low quantities and also permits iterative changes. For designers this may be invaluable as a tactile sense of a physical object can display characteristics that are hard to interpret from 3D models on a computer screen.

AM is also known by different names coined by 3D printing community from different companies. It is interchangeably used with 3D printing, Layer by layer manufacturing, Rapid prototyping (RP) and Solid freeform fabrication (SFF) etc. According to the ASTM F2792-10, additive manufacturing is the “process of joining materials to make objects from 3D model data, usually layer upon layer, as opposed to subtractive manufacturing methodologies, such as traditional machining”. AM is one of the fastest growing industrial fields in recent years. AM was initially considered useful for prototyping during the component development stage because the time and cost of developing molds, dies and tools associated with methods such as casting and forging are served in this method. This technology accelerated the product development life cycle.

Rapid advancement in AM methods have moved them from prototyping to actual production of components in aerospace, automotive and medical industries are now manufactured using AM methods and deployed in service. A typical AM process chain is illustrated in Figure 1.7 (Chen et al. 2017). The AM process chain starts with the conversion of one’s idea/imagination into a solid CAD model where a definite shape and size is finalized by software through optimization. The model is obtained either from Computer Aided Design (CAD), Computer Topographic (CT) scanning or 3D laser scanning technique and is saved in STL (Stereolithography/Standard Tessellation Language) file format. Further the STL file is opened in slicing software which is the interface platform between 3D printer and computer. Apart from dividing the CAD model into thin layers, it allows to set various process parameters and

support structure geometry generation. The operating console of machine execute software generated G-code which defines printing (tool) path for every single layer. Once the printing starts, the first layer is deposited on the bed/substrate, on the top of first layer next layer is deposited as per model definition and the cycle continues till the entire model prints. Completed part is then removed from bed or substrate and further post processing steps like priming and painting are carried out. Different AM processes have different methods to remove the support structure from the actual part since they vary in method and materials used. The common feature of all the AM processes, even though the details of individual AM processes vary widely, is that fabrication of the part occurs directly from a 3D CAD model of an object by a fast, accurate, highly automated and flexible process.

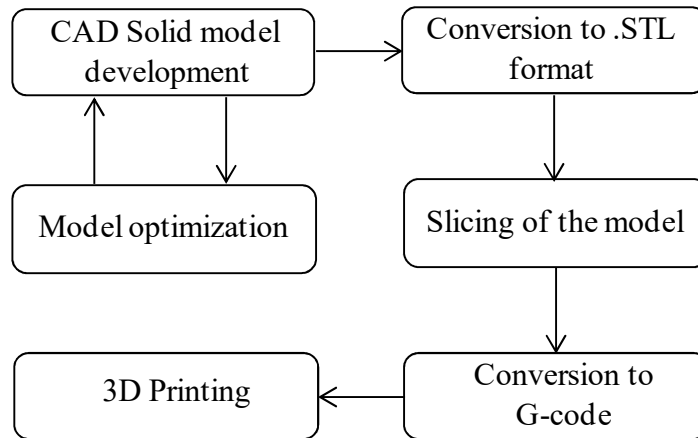


Figure 1.7 Work flow of AM/3DP.

Industrial companies, including the Electro Optical System (EOS) in Germany, Arcam in Sweden, MCP Tooling technologies in the UK and Stratasys, 3D System, Optomec and Z Corporation in the United States, have introduced various AM processes to the commercial market. ASTM F42 committee, classifies the AM processes into seven areas as shown in Table 1.1. Out of the seven AM classes, four types are widely used to process plastics namely Stereolithography (SLA), Selective laser sintering (SLS), Fused filament fabrication (FFF) or Fused deposition modeling (FDM) and Multi-jet/Polyjet modeling (MJM) (Kazmer 2017). In this work, FFF/FDM technology is used to print the thermoplastic based syntactic foam composite. The FFF technology was developed by S. Scott Crump in the late 1980s and later commercialized in 1990 through Stratasys Inc, which he co-founded (Perez 2013). FFF is a

solid-based 3D printing technology, which makes use of thermoplastic filament as feeding material. Heating element and nozzle converts the solid filament into molten plastic, which subsequently gets deposited layer by layer.

Table 1.1 AM process categories (ASTM F2792-10).

| Process Type | Brief Description | Related Technology | Companies | Materials |
|--------------------------|---|---|--|-------------------------------|
| Powder Bed Fusion | Thermal energy selectively fuses regions of powder bed | Electron Beam Melting (EBM), Selective Laser Sintering (SLS), Selective Heat, Sintering (SHS) and Direct Metal Laser Sintering (DMLS) | EOS (Germany), 3Dsystem (US), Arcam (Sweden) | Metals, Polymers |
| Direct Energy Deposition | Focused thermal energy is used to fuse material by melting as the material is being deposited | Laser Metal Deposition (LMD) | Optomec (USA), POM (USA) | Metals |
| Material Extrusion | Material is selectively dispensed through a nozzle or orifice | Fused Filament Fabrication (FFF)/ Fused Deposition Modeling (FDM) | Stratasys (Israel), Bits from bytes | Polymers |
| Vat Photo Polymerization | Liquid photopolymer in a vat is selectively cured by light-activated polymerization | Stereolithography (SLA), Digital Light Processing (DLP) | 3D system (USA), Envisiontec (Germany) | Photopolymers |
| Binder Jetting | A liquid bonding agent is selectively deposited to join powder material | Powder Bed and Inkjet Head (PBIH), Plaster Based 3D Printing (PP) | 3D system (USA), ExOne (USA) | Polymer, foundry sand, metals |
| Material Jetting | Droplets of build material are selectively deposited | Multi-Jet Modeling (MJM) | Objet (Israel), 3D system (USA) | Polymer, waxes |
| Sheet Lamination | Sheets of material are bonded to form an object | Laminated Object Manufacturing (LOM), Ultrasonic Consolidation (UC) | Fabrisonic (USA), Mcor (Ireland) | Paper, metals |

The preliminary step in developing physical part using FFF technique is creating digital model using commonly used CAD packages. Once the CAD model is ready, it can be exported to the slicing software in the stereolithography (STL) file format. There are various slicing software's (Cura, Simplify 3D, Slice3r and Kisslicer).

Software's allows defining various process parameter such as layer height, infill percentage, printing pattern, speed, support structure geometry and part orientation etc. The slicing software uses this information to generate G-code which is followed by the machine. The filament is unwound from a spool and is pulled by electromechanical feeding unit. Sufficient heat to melt the plastic material will be supplied by heated nozzle. Semi-molten material gets deposited on bed in the form of rasters/roads, as time lapse complete part gets printed layer by layer (Dakshinamurthy and Gupta 2018). The schematic representation of FFF process is presented in Figure 1.8.

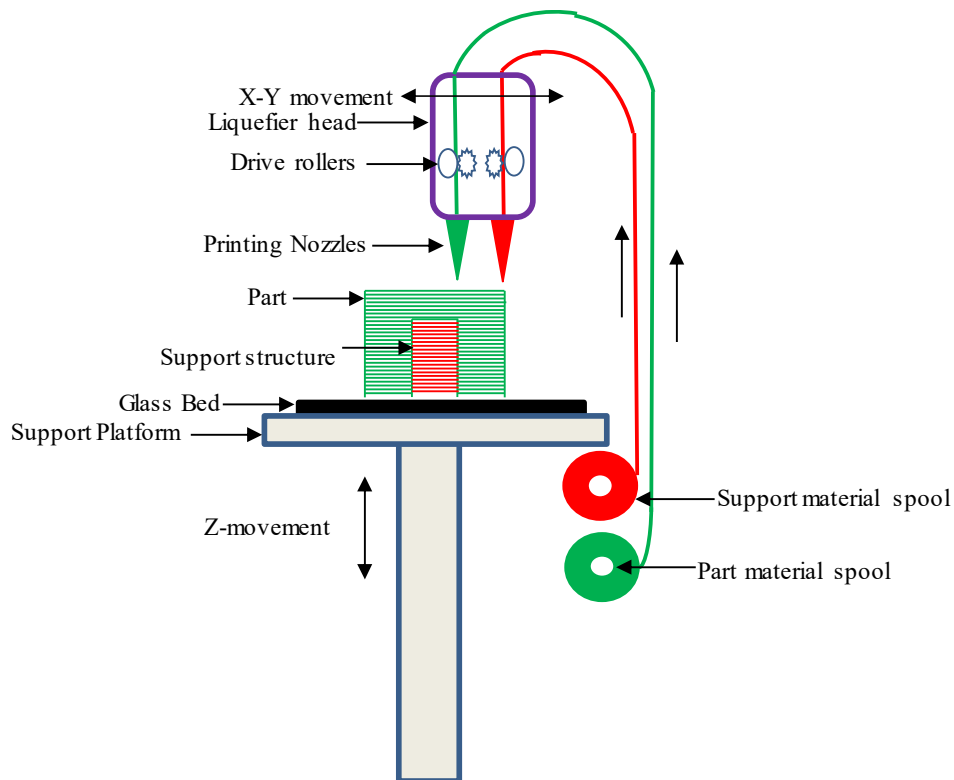


Figure 1.8 Schematic of FFF process.

Polymer additive manufacturing can enable the rapid manufacture of lightweight, complex components and impact a broad spectrum of manufacturing industries. Examples include the tool and die industry (rapid, low-cost tooling), lightweight components for the transportation industry (automotive and aerospace), low-cost components for the energy industry etc. The largest portion of additive manufacturing systems use polymers as the feedstock material, thereby advancements in polymer additive manufacturing can have a rapid impact on applications due to the large number of systems in the marketplace. To date, the primary market for additive manufacturing with polymers has been prototyping. There are three fundamental R&D challenges that are limiting use of polymer additive manufacturing for end use products. First, the material properties (strength and stiffness) are significantly lower than conventional materials. By doubling the specific strength of the polymer feedstock materials through the development of new polymers or adding hollow spherical fillers such as microspheres (glass, cenospheres, silica etc.), the material properties can approach those of medium strength aluminum alloys, opening up numerous end use applications. Second, the layer-wise deposition lowers the effective strength in the vertical build direction (Z-direction). Detailed thermal analysis and several process modifications are being pursued to increase Z-direction strength. Finally, all polymer additive systems run open loop. If something goes wrong during the build, the system has no knowledge and continues without correcting or stopping the build. Efforts are underway to address in-situ feedback and control to ensure part quality and fault detection. In summary the availability of a wider range of material properties in additive manufacturing may both allow for more design freedom in manufacturing and may better represent the physical properties of the end component that a prototype is designed for. AM of plastic parts is significantly more economical than injection/compression molded parts requiring expensive tooling and higher lead times alongside other materials such as metals and ceramics. Today many challenges lie ahead of the manufacturing industry. The increasing competition and shortage of resources raise a challenge for future manufacturing technologies and lightweight design. A possibility to cope with these circumstances is the manufacturing technology of 3D printing. However, there are still challenges to cope with due to the process novelty, such as the development of lightweight materials like Syntactic Foams and new design approaches. Innovative approach for material development and lightweight design are proposed in order to fully exploit the processes potentials in the present work. Additive

manufacturing approaches like 3D printing could provide a cost-effective production route and further speed-up the implementation of these enabling materials. However, majority of additive manufacturing efforts are focused on polymers and metallic systems as an input feed material and syntactic foam filaments are still in infancy due to numerous material and processing challenges. There has not been much research and development activity on additive manufacturing of syntactic foam composites (closed cell foams) and no data has been reported in the literature. For additive manufacturing of lightweight components using 3D printing approach, new prepared compositions with desirable properties and processing conditions need to be developed and optimized. The current effort addresses these challenges and provides the pathway for the application of additive manufacturing technologies for syntactic foam composites.

Proposed methodology in the present work can directly be implemented or used by 3D printing industry. Work has been undertaken to capture opportunities for decreasing the cost and increasing the efficiency through large scale additive manufacturing systems. The focus of this work is the development of novel lightweight feedstock material (syntactic foam composite filament) that enables the manufacture of lightweight components. Conventional manufacturing processes used for syntactic foams, limits the complexity of the component. Present work is focused towards POLYMER INDUSTRIES which are using HDPE components cast using injection molding machines involving expensive tooling. HDPE is reinforced with fly ash cenospheres. Replacing HDPE by fly ash cenospheres results in cost saving of relatively expensive matrix to develop syntactic foam filament to feed the 3D printer.

Present work deals with developing and synthesizing eco-friendly lightweight filament for 3DP. This work also addresses the recyclability potential of the developed filaments. Usage of environmentally pollutant fly ash cenosphere in replacing relatively expensive HDPE matrix renders eco-friendly solution alongside augmenting the possibility of wide material choices availability for 3D printing industry.

1.4 Literature review

Syntactic foams are lightweight composites and are used prominently in weight saving applications. However, the extent to which these can be tailored to yield a target mechanical performance strongly depends on the resultant effective properties and more importantly relating these properties to its microstructure. Therefore investigating mechanical, thermal and other relevant properties for a given microstructure and its spatial distribution plays an important role in the design and development of syntactic foam composites. A number of reviews dealing with various types of composites 3D printed using FDM process are presented in the tabular form herewith.

Table 1.2 Literature survey of thermoplastic materials/composites for FFF/FDM process.

| Author | Process | Parameters | Materials Used | Property Studied | Remarks |
|---------------------|----------------------------------|--|----------------|---|--|
| Yao et al. (2019) | FDM | Printing angle (0,15,30,45,60,75 and 90°) and layer thickness (0.1,0.2 and 0.3 mm) | PLA | UTS | <ul style="list-style-type: none"> • UTS changes significantly with the printing angle. • Both theoretical and experimental results showed UTS decrease as layer thickness increases (0.1 - 0.3 mm). • Theoretical models based on two types of shear formula have equivalent capacity in predicting the UTS of FDM 3D printed materials with different printing orientation. |
| Daver et al. (2018) | Compression molding (CM) and FDM | Filler (cork) percentage | PLA, PLA/Cork | CM: Tensile, DMA, impact. 3DP: Tensile | <ul style="list-style-type: none"> • CM showed lower tensile strength and improved impact strength relative to cork percentage. • Cork incorporation caused improvement in specific modulus and specific tensile strength of CM parts. |

| | | | | | |
|----------------------|-----|--|------------|-----------------------------------|--|
| | | | | | <ul style="list-style-type: none"> • Decrease in DMA (storage modulus, loss modulus and Tan δ) parameters is observed with increase of cork content. • Addition of cork showed reduction in impact strength. • 3DP PLA/Cork showed slightly lower elastic modulus and yield strength and higher elongation at break compared to CM. |
| Byberg et al. (2018) | FDM | Layer orientation ($0^\circ, 90^\circ, \pm 45^\circ$) and build direction (flat, edge and upright) | ULTEM 9085 | Tensile, Compression and flexural | <ul style="list-style-type: none"> • 0° layer orientation and edge build direction registered maximum tensile stress. • 90° layer orientation and flat build direction registered maximum compressive stress. • 0° layer orientation and flat build direction combination registered maximum flexural stress. |

| | | | | | |
|----------------------------------|-----|---|----------------------------------|-----------------------------|---|
| Dakshina murthy and Gupta (2018) | FDM | Slice height, Raster angle, Raster width | ABS | DMA (Viscoelastic property) | <ul style="list-style-type: none"> Percentage contribution of slice height and raster width is 55 and 31% respectively on the viscoelastic properties of the FDM-RP components. |
| Ning et al. (2017) | FDM | Raster angle, Infill speed, Nozzle temperature, Layer thickness | CFRP (ABS+ 5 wt. % Carbon fiber) | Tensile | <ul style="list-style-type: none"> 0 and 90° raster angle has more significant effect on tensile strength, Young's modulus and yield strength compared to -45 and 45°. Highest average tensile properties observed in parts printed at 25 mm/s. All the tensile properties first increased and then decreased with an inflection point at the nozzle temperature of 220°C. 0.15 mm layer thickness gave largest mean values for tensile strength, Young's modulus and yield strength. |

| | | | | | |
|----------------------|-----|--|--------------------------------|---|--|
| | | | | | <ul style="list-style-type: none"> • Toughness and ductility reached largest mean values at 0.25 mm layer thickness. |
| Porter et al. (2017) | FFF | Infill angle, Number of outside perimeters, Sample thickness, Nozzle temperature | Polyvinylidene fluoride (PVDF) | Young's Modulus, Yield strength, β -phase | <ul style="list-style-type: none"> • Young's modulus is highest and lowest for 0° (484 MPa) and 90° (419 MPa) respectively. • Yield strength is highest when the infill pattern is parallel to the loading axis and reduces with reducing infill angle. • Poisson's ratio is highest for 45° (0.361) and least for 0° (0.243). • Small but consistent piezoelectric response is observed in PVDF films printed with high β-phase content and is subjected to a post-printing corona poling procedure. • High β-phase belongs to lower extrusion temperature, faster |

| | | | | | |
|------------------------|-----|---|---|--|--|
| | | | | | extrusion rates and higher hot end voltages. |
| Yao et al. (2017) | FDM | Fill density (%), Carbon fiber (no of filaments) | PLA+Polyacrylonitrile (PAN) based continuous carbon fiber | Tensile, Three-Point Bending | <ul style="list-style-type: none"> • 70 and 18.7% improvement observed in tensile and flexural strength with fiber reinforcement. • 26.01% weight reduction and 11.41% print time reduction observed by reducing fill density without compromising tensile strength. |
| Ferreira et al. (2017) | FDM | Printing orientation (0°,90°,±45°) | PLA/short carbon fiber | Tensile modulus, shear modulus, Poisson's ratio, and related strengths | <ul style="list-style-type: none"> • Tensile modulus of PLA/CF is 2.2 and 1.25 times higher compared to neat PLA at 0° and 90° orientations respectively. • Shear modulus of PLA/CF is 1.16 times higher than neat PLA at ±45°. • Poisson's coefficient is same for neat PLA in both orientation (±45°). • PLA and PLA/CF strengths are almost same. |

| | | | | | |
|-------------------------|------------------------------|--|-------------------------|-------------------------------|---|
| Wang and Gardner (2017) | FDM (Makerbot Replicator 2X) | Layer height (0.1 and 0.3 mm), Extrusion temperature (200 and 250°C) | Polypropylene (PP) | Izod impact strength | <ul style="list-style-type: none"> • Izod impact strength of PP printed at 200°C of layer thickness 0.1 and 0.3 mm is comparable with injection molded PP. • Parts printed at 250°C and layer thickness of 0.1 and 0.3 mm shown lower impact strength compared to parts of same layer thickness printed at 200°C. |
| Zaldivar et al. (2017) | FDM (Stratasys FDM 400 mc) | Print orientation | ULTEM [®] 9085 | DMA, Poisson's ratio, Tensile | <ul style="list-style-type: none"> • Small overall variation in glass transition temperature (174.4-170.9°C) of all specimen sets is observed with no correlation between strength and glass transition temperature. • Highest Poisson's ratio (0.39) is observed for specimen printed on edge in X- direction. |

| | | | | | |
|----------------------|-----------------|---|-----|-------------------------|---|
| | | | | | <ul style="list-style-type: none"> • Tensile strength of 3D printed parts varied from 46-85% of reported IM ULTEM parts. • Parts printed with print orientation along load direction exhibited higher strength. • Failure strain for FDM parts varied from 2-7% and is considerably lower than the failure strain attained by injection molded ULTEM® parts (75%). |
| Alaimo et al. (2017) | FDM (3NTR A4v3) | Filament cross-section, material (ABS and chemically additivated ABS) | ABS | Tensile, Shear strength | <ul style="list-style-type: none"> • Increase in elastic modulus with filament cross-section (0° and 90°) is observed. • Tensile strength and ultimate strain increased at 90° and decreased at 0° with rise in filament cross-section. • Shear modulus increases with increasing cross-section, while strength increased at 90° and |

| | | | | | |
|--------------------|-----|--|---|------------------------------------|---|
| | | | | | <p>decreased at 0° with rise in filament cross-section.</p> <ul style="list-style-type: none"> Chemically additivated ABS shown ductile failure mode compared to ABS. |
| Tian et al. (2017) | FDM | Material states (Pure, originally printed and Re-manufactured) | Poly lactide (PLA) + Carbon Fibres (Carbon Fibre Reinforced Thermoplastics (CFRTPCs)) | Tensile, Flexural, Impact (Charpy) | <ul style="list-style-type: none"> Pure PLA sample shown 62 MPa tensile strength and 4.2 GPa modulus, while CFRTPCs originally printed and re-manufactured samples shown nearly equal strength (~ 256 MPa) and modulus (~ 20.6 GPa). Flexural strength and modulus is observed for pure sample: ~ 100 MPa and ~ 4.5 GPa, CFRTPCs originally printed: ~ 225 MPa and 14.5 GPa and re-manufactured sample: 263 MPa and 13.3 GPa. Impact strength for pure PLA, CFRTPCs originally printed and re- |

| | | | | | |
|------------------------|-----------|--|---|---|---|
| | | | | | manufactured samples is 20, 34.5 and 38.7 kJ/m ² respectively. |
| Singh et al. (2017) | Extrusion | Barrel temperature, Die temperature, Screw speed, Wt. % of Fe. | HDPE, HDPE + Fe, LDPE, LDPE + Fe. | Peak elongation, break strength, and shore D hardness, Porosity | <ul style="list-style-type: none"> • Better properties (peak elongation (3.63 mm), break strength (15.02 N/mm²) and shore D hardness (34.35) observed in case of 10% Fe reinforced HDPE. • Lowest porosity is observed in 100% HDPE sample. • Better peak elongation (166.14 mm) and shore D hardness (8.68) observed in case of 100% LDPE. • Better, break strength (8.75 N/mm²) is observed in case of reinforced LDPE. |
| Abdullah et al. (2017) | FDM | Filler wt. % | Polyamide 12 (PA 12) and ceramic filler (30, 35 and 40 wt. %) | Tensile, flexural and surface roughness | <ul style="list-style-type: none"> • Tensile (33.98 MPa) and flexural (47.53 MPa) strength of neat PA 12 (PA100) is better than the composites (PA70F30, PA65F35, PA60F40). |

| | | | | | |
|-----------------------|-----|---|-----------------|------|---|
| | | | | | <ul style="list-style-type: none"> • Tensile modulus of PA 100 (905.94 MPa) is higher than PA70F30 (873.44 MPa) but lower than PA65F35, PA60F40). • PA 100 registered highest flexural modulus (1083.14 MPa) than composites. • Composites registered 6μm average surface roughness. |
| Garg and Singh (2017) | FDM | Composition (Wt. % of Iron (Fe) and Nylon). | ABS, Fe-Nylon6. | Wear | <ul style="list-style-type: none"> • Wear resistance improved with Fe content in Nylon6. • 60% Fe and 40% nylon6 composition showed higher wear resistance value compared to ABS. • Coefficient of friction (μ) for Fe-nylon6 composite is less than ABS. • μ is highest for 60% Fe and 40% nylon6 composition. |

| | | | | | |
|-----------------------|-------------------------|--|---|---|---|
| Gardner et al. (2016) | FFF (Aleph Object, Co.) | Printing methods (Continuous and selective compaction), CNT content, Spacing between the filament lines. | Continuous carbon nanotube (CNT) infused with ULTEM®. | Tensile, Electrical characterization for conductivity | <ul style="list-style-type: none"> • Continuous compaction produced specimens with higher mechanical performance and tighter tolerances than those from selective compaction. • Increasing the number of printed CNT yarn filament layers (and thus the CNT to polymer ratio) leads to an even higher increase in specific mechanical properties. • CNT reinforcement led specific tensile strength of 317 MPa and specific modulus of 19.5 GPa. 287% improvement in the specific strength and 1850% increase in specific modulus over neat ULTEM® Sheet is observed. • The resistance of the specimen with the 350 μm spacing is less (11 Ω) |
|-----------------------|-------------------------|--|---|---|---|

| | | | | | |
|---------------------|------------------------|---|--|----------------------|---|
| | | | | | than that for the one with the 1 mm spacing (16 Ω). |
| Wang et al. (2016) | FDM | Heating time, Heating temperature, Microsphere percentage | Filament of poly wax mixed with hydrocarbon filled microspheres (Expancel 930DU120). | Tensile, Compressive | <ul style="list-style-type: none"> Tensile strength and compressive strength of 2 wt.% filled samples heated at 140° C for 120 s, increased by 25.4% and 52.2% respectively compared to untreated samples. |
| Singh et al. (2016) | FDM (uPrint SE system) | MFI, Filler matrix proportion | Matrix: Nylon-6, Filler: Al ₂ O ₃ | MFI, Wear | <ul style="list-style-type: none"> MFI of composite decreased with Al₂O₃ Content. Based on standard filament MFI alternative filament is developed with suitable filler-matrix proportion (50:50 by wt. %). Filler reinforcement caused significant increase in wear resistance. |

| | | | | | |
|-----------------------|--------------------|---|------------------------------------|---------|---|
| Singh et al. (2016) | FDM | Barrel temperature, Screw speed, Take up speed | ABS-EG (Extrusion Grade) | Tensile | <ul style="list-style-type: none"> • Tensile strength increases with increase in screw speed and barrel temperature (up to 145°C). • Take up speed has no effect on tensile strength and Young's modulus. • Young's modulus decreases with increase in barrel temperature and increases with screw speed (up to 35 rpm). • Fabrication cost of one cartridge is 16.27\$ which saves around 93% on part of FDM filament. |
| Mohamed et al. (2016) | FDM (Fortus 400mc) | Layer thickness, Air gap, Raster angle, Build orientation, Road width, Number of contours | PC-ABS (Polycarbonate - ABS) blend | DMA | <ul style="list-style-type: none"> • Air gap, number of contours, layer thickness, raster angle, build orientation and road width showed significant impact on the storage and loss moduli. • Optimum parameters for maximum dynamic mechanical properties are: |

| | | | | | |
|-----------------------|------------------------|--|---|--|--|
| | | | | | 0.3302 mm layer height, zero air gap, zero raster angle, 0.4572 mm raster width and 10 contours. |
| Singh et al. (2016) | FDM (uPrint SE system) | Wt.% of Nylon-6, Size of Al ₂ O ₃ , Wt.% of Al ₂ O ₃ SPS: single particle size, TPS: three particle size, DPS: Double particle size | Nylon-6 with Al ₂ O ₃ reinforced filament | Tensile strength, Percentage elongation, Young's modulus, Yield strength | <ul style="list-style-type: none"> Percentage elongation decreases as the particle size changes from SPS (100 μm) to TPS (100, 120 and 150 μm) in equal proportion. Maximum tensile strength is observed for DPS (100 and 120 μm) in equal proportion and reaches minimum value for TPS. Yield strength and Young's modulus is maximum for DPS. |
| Riddick et al. (2016) | FDM (Fortus 400 mc) | Build Direction, Orientation. | ABS | Tensile | <ul style="list-style-type: none"> Build Direction - Horizontal (max. strength-32.60 MPa and modulus-2.69 GPa, raster angle 0°, min. strength-15.26 MPa, raster angle 90°). Build Direction - Side (Max. strength-34.17 MPa and modulus- |

| | | | | | |
|--------------------|----------------------------|--|----------|------------------|--|
| | | | | | <p>2.79 GPa, raster angle 0°, min. strength-24.24 MPa, raster angle 90°).</p> <ul style="list-style-type: none"> • Build Direction - Vertical (Max. strength - 19.80 MPa, raster angle $\pm 45^\circ$, min. strength-12.42 MPa raster angle 90°, max. modulus-2.77 GPa and raster angle 0°). |
| Faes et al. (2016) | FDM (Dimension SST 1200es) | Inter layer-cooling time, Build orientation. | ABS -m30 | Tensile strength | <ul style="list-style-type: none"> • Upright sample strength decreases from 20.5 to 13.3 MPa and elongation decreases from 1.24 to 0.86 % when interlayer cooling time increases from 3.59 to 45.27 s. • Flat sample strength remains constant at 19 MPa when interlayer cooling time varies from 54.92 to 282.71 s. • Flat sample elongation and modulus remain constant when interlayer |

| | | | | | |
|-----------------------|--|--|--|--|--|
| | | | | | cooling time increases from 3.59 to 45.27 s. |
| Zou et al. (2016) | FDM (Dimension SST 1200es) | Build angle | ABS plus | Tensile | <ul style="list-style-type: none"> • Isotropic model results for Young's modulus, Poisson's ratio and yielding stress are 2400 MPa, 0.37 and 26.84 MPa respectively. • Transversely isotropic model results in transvers and principal axis are, Youngs modulus: 2432.29 MPa and 2367.10 MPa, Poisson's ratio: 0.24 and 0.34 and shear modulus 830.47 MPa. |
| Weng et al. (2016) | FDM (creator, flash forge, china) | Organic Modified Montmorillonite (OMMT) wt.% | ABS and Organic Modified Montmorillonite (OMMT). | Tensile, Flexural, DMA, Thermal expansion | <ul style="list-style-type: none"> • Addition of 5 wt. % OMMT in ABS samples improved tensile strength and modulus of 3D printed (43%, 200%) and IM (28.96%, 68.42%) respectively. • Flexural strength increased from 42.69 to 56.92 MPa (5 wt. % OMMT). |

| | | | | | |
|---------------------|--------------------------|---|--|------------------------|---|
| | | | | | <ul style="list-style-type: none"> • Storage modulus of neat ABS increased from 1.1 to 1.6 GPa. (5 wt. % OMMT). • Upon OMMT addition thermal stability improved and thermal expansion coefficient dropped. |
| Singh et al. (2016) | FDM | Particle size in equal proportion in weight (SPS, DPS, TPS) | Al ₂ O ₃ and SiC-Al ₂ O ₃ in Nylon 6 matrix. | Wear, MFI, Tensile | <ul style="list-style-type: none"> • Wear rate decreases as the particle concentration increases. • MFI decreases relative to particle concentration. • Percentage elongation, tensile strength, yield strength and Young's modulus decreases with particle concentration. |
| Dul et al. (2016) | FFF (Sharebot NG, Italy) | Build orientation, Processing condition, Composition | ABS and Graphene nanoplatelets (xGnP) | Tensile, MFI, DMA, CTE | <ul style="list-style-type: none"> • 4 Wt. % of xGnP into ABS caused about 30% improvement in modulus compared to neat ABS for all processing conditions (CM, 3DP, extrusion) and decrease in stress and strain at break. |

| | | | | | |
|-----------------------------|--------------------|-----------------------|--------------------------|-------------------|--|
| | | | | | <ul style="list-style-type: none"> • MFI of neat ABS decreases with xGnP addition. • Addition of 4 Wt. % of xGnP increased storage modulus and lowers CTE. |
| Garg and Singh (2015) | FDM | Nylon6-Fe Composition | Nylon6-Fe composite, ABS | Wear | <ul style="list-style-type: none"> • Nylon6-Fe (40 and 60% by mass) composite has very high wear resistance. • Wear rate reduced with higher volume content of reinforcement. • μ of ABS is higher than Nylon6-Fe composite and decreases with higher load for both the materials. |
| Domingo Espin et al. (2015) | FDM (fortus 400mc) | Build orientation | Polycarbonate | Tensile, Flexural | <ul style="list-style-type: none"> • Similar tensile strength is observed for sample printed in X (45.9 MPa) and Z (45.6 MPa) orientation, sample printed in Z+45 (36.0 MPa) shown least strength whereas sample printed in Y (54.6 MPa) |

| | | | | | |
|---------------------|-----|--|------------------------------|-------------------------------|---|
| | | | | | <p>orientation registered highest tensile strength.</p> <ul style="list-style-type: none"> • Sample printed in Y (2.41 GPa) and X (2.10 GPa) orientation registered highest and lowest Young's modulus respectively. • X and Y orientation registered highest (1.43) and lowest (1.33) flexural stiffness coefficient. |
| Hwang et al. (2015) | FDM | Proportion of Cu and Fe particles, Temperature, Fill density | ABS with Cu and Fe particles | Tensile, Thermal conductivity | <ul style="list-style-type: none"> • Inclusion of Cu (10-30%) lowered tensile stress of ABS (45.7 to 26.5 MPa). • Inclusion of Fe particles lowered the tensile stress of ABS from 45.7 to 36.2 MPa. • 50 wt. % of Cu particle into ABS lowered CTE (29.50%) and improved conductivity from 0.646 to 0.912 W/Mk. |

| | | | | | |
|--------------------------|------------------------------|----------------------------|---|--------------------------------|--|
| | | | | | <ul style="list-style-type: none"> • Inclusion of metal powder into neat ABS lowered printed part distortion. |
| Tuan Rahim et al. (2015) | 3DP (MakerBot Replicator 2X) | Material (neat, composite) | Polyamide(PA 12) + 5 wt.% Hydroxyapatite (HA) + 15 wt.% zirconium oxide (ZrO ₂) fillers, Pure polyamide 12, Commercial polyamide, Taulman 618, ABS with Cu and Fe particles | MFI, Thermal analysis, Tensile | <ul style="list-style-type: none"> • MFI of PA12 dropped from 13.5 to 2.7 g/10 min with addition of 15 wt. % of ZrO₂ and 5wt. % HA. • Presence of filler increased crystallization temperature (~4°C) and lowered melting temperature (~1°C). • Tensile strength of new developed composite (PA12/ZrO₂/HA) is 22.78 MPa, which is lower than unfilled PA12 (26.54 MPa) and nearly equal to commercial PA and Taulman 618 (21.49 MPa). • Filler incorporation caused porosity in the printed parts. |

| | | | | | |
|------------------------------|--------------------|---|---------------------------------|--------------------------------------|--|
| Tekinalp et al. (2014) | FDM (solidoodle 3) | Method (CM, FDM), carbon fiber wt. %. | ABS, Carbon fiber (short fiber) | Tensile, Comparison with CM specimen | <ul style="list-style-type: none"> • FDM composite registered ~115% and ~700% higher tensile strength and modulus compared to neat ABS. • High porosity in printed samples is observed compared to CM sample. • FDM and CM sample exhibited comparable tensile modulus and strength. |
| Rayegani and Onwubolu (2014) | FDM (Fortus 400mc) | Part orientation, Raster angle, Raster width, Air gap | ABS | Tensile | <ul style="list-style-type: none"> • Functional relationship between process parameters and tensile strength is developed. • Variation in part orientation and raster angle affects the tensile strength. • Tensile strength improvement observed with negative air gap and smaller raster width. |

| | | | | | |
|----------------------|--------------------|--------------------------------|---|---|---|
| Lee and Huang (2013) | FDM | Print orientation | ABS, ABS plus | Tensile | <ul style="list-style-type: none"> • Ultimate stress of ABS printed sample ranges from 50-80% of the ABS wire data. • Ultimate stress of ABS plus printed sample ranges from 75-80% of the ABS plus wire data. • Strain energy of ABS printed sample ranges from 3.4-19.7% of the ABS material. • Strain energy of ABS plus printed sample ranges from 1.8-7.4% of the ABS plus material. |
| Nikzad et al. (2011) | FDM (3000 machine) | Composition, Filler percentage | ABS (P400) - Iron Filler, ABS (P400) - Copper filler. | Thermal conductivity, Heat capacity, DMA, Tensile | <ul style="list-style-type: none"> • Copper-ABS composite (30 vol. % of Cu (45μm)) shown noticeable increase in conductivity. • Fe addition lowers the heat capacity of ABS composites. • Fe-ABS composite (30 vol. % of Fe (45μm)) shown remarkable increase in conductivity. |

| | | | | | |
|--|--|--|--|--|---|
| | | | | | <ul style="list-style-type: none">• 3.5-4 GPa increase in storage modulus of composite (30 vol. % Cu (10 μm)) is observed, upon further addition lowered the value significantly.• 2.5-3 GPa increases in storage modulus of composite (30 vol. % Fe (45μm)) is observed, upon further addition values lowered significantly.• Storage modulus dropped significantly beyond 10 vol.% of Cu (45μm) in ABS composite.• Iron-ABS (10 vol. % of Fe) composite tensile strength dropped suddenly compared to neat ABS. |
|--|--|--|--|--|---|

Majority of the additive manufacturing efforts regarding thermoplastics are focused on printing only selected few polymers/composites restricting their applications in weight sensitive structures and buoyancy modules as seen from Table 1.2. From the existing literature, it is very clear that environmental pollutant like fly ash has not exploited well to synthesize and develop thermoplastic based syntactic foams using 3D printing. Hence, present work deals with development and characterization of eco-friendly and lightweight cenosphere/HDPE syntactic foam filaments, recyclability potential and their feasibility for printing through commercially available 3D printers.

1.5 Motivation of work

Fly ash is a waste by-product produced in abundance by combustion of coal in thermal power stations. The main constituents of fly ash are silicon dioxide, iron oxide and aluminium oxide. Fly ash possesses severe environmental threat by polluting the surrounding atmosphere and increasing land fill burden for its disposal. Increase in the production of fly ash year by year from coal thermal power plants poses a serious problem in terms of its safe dumping and utilization. Use of fly ash as fillers in polymer composites is appreciated from both economic and commercial point of view. Some studies have pointed to the excellent compatibility between fly ash and polymers. Few researchers have also shown the advantageous of utilizing treated fly ash in a wide variety of polymer matrices. The present work is focused on studying the possibility of developing lightweight syntactic foam feedstock filament for FFF based 3D printers and characterization of 3D printed syntactic foam composites. Fly-ash/polymer composites provide a significant opportunity to science and technology and pose significant challenges for future work in polymer composite field. Such fly ash filled polymer composites possess attractive mechanical, thermal, electrical properties, better dimensional stability and are cost effective. Motivation for pursuing this topic is summarized as below.

- Waste utilization
- Lower environmental pollution
- Reduction in consumption of polymers
- Eco friendly processing

- Durable components

Based on the above points, objectives are laid down and are presented in the following sections.

1.6 Objectives and scope of the work

From the foregoing literature survey, it is evident that, the literature on development of thermoplastic-based syntactic foam filament are scarce. Hence, development and suitability of syntactic foam feedstock material, recyclability potential and their 3D prints is proposed in the present investigation.

Therefore the work undertaken pursues the following objectives

- Preparations of cenosphere/HDPE blend using brabender and understanding its flow, thermal, rheological behaviour through conducting melt flow index (MFI), thermogravimetric analysis (TGA) and rheological tests respectively.
- Development of syntactic foam feedstock filament by optimising extrusion process parameters.
- Extensive micrography, thermal (DSC, XRD) and mechanical (tensile) characterization of syntactic foam filaments.
- Investigate effect of filler volume fraction on physical (density and void content), thermal (DSC, XRD and CTE) and mechanical properties (tensile, flexural, compression and DMA) of filament and 3D printed syntactic foams.
- To study the micrographs of as printed and fractured samples for structure-property correlations followed by several industrial components to show the feasibility of 3DP technique to synthesize cenosphere/HDPE syntactic foam composite products.

The available studies on thermoplastic syntactic foams, process materials under controlled conditions at laboratory scale, which usually provides foams with high quality. Nonetheless, syntactic foams have been processed using injection and compression molding routes involving expensive tooling. However studies on AM of syntactic foams are not yet available due to the challenges associated with manufacturing quality filaments, which include particle breakage during blending and filament extrusion. Rapid manufacturing with zero lead-time is the key to satisfy ever-

growing demands of complex and durable products. Thus present work deals with utilization of one such technique known by name 3D printing.

Scope of the present work includes, preparation and characterization of cenosphere /HDPE blend for their thermal (TGA/DTG) and rheological properties. Hollow fly ash cenospheres as fillers are reinforced (20, 40 and 60 vol.%) in HDPE matrix. Extrusion parameters are optimized to get desired feedstock filament diameter that can be easily fed into commercial 3D printer. Thermal and mechanical characterization of novel syntactic foam filament is further carried out to understand filler-matrix behavior using DSC, XRD and tensile test respectively. Finally using optimized printing parameters samples are printed and tested for tensile, flexural, compressive and DMA. Exhaustive micrography is carried out to establish structure-property correlations. Property maps for selected properties is presented for comparative analysis between other thermoplastic processing and 3D printing routes. Finally, potential for using the optimized 3D printing process parameters is demonstrated by printing eco-friendly lightweight industrial scale components.

1.7 Outline of the thesis

The systematic study carried out with respect to above objectives is presented in the thesis. A brief skeletal structure of the thesis is,

Chapter 1. Intends to provide exhaustive literature survey on FFF method followed by objective and scope of the work.

Chapter 2. Focuses on the constituents used for thermoplastic syntactic foam composites, fabrication route adopted and testing methodology.

Chapter 3. Deals with basic material characterization and processing aspects.

Chapter 4. Tensile behavior of filament and 3D prints is dealt in this chapter.

Chapter 5. Flexural response of 3D prints is reported.

Chapter 6. Deals with compressive behavior of 3D prints.

Chapter 7. DMA of 3D prints is discussed in this chapter.

Chapter 8. 3D printed industrial components.

Highlights of the significant conclusions drawn from the results are presented finally.

2 MATERIALS AND METHODS

2.1 Constituents

In the present work, hollow fly ash cenospheres (filler) and HDPE (matrix) is used to prepare lightweight thermoplastic syntactic foam composites. Details about these constituents are dealt with in the sections to follow.

2.1.1 Fly ash cenospheres

Fly ash cenospheres of CIL 150 grade used as filler is procured from M/S Cenosphere India Ltd., Kolkata, West Bengal, India. Cenospheres are used in as received condition (Figure 2.1a), without any surface treatment. Table 2.1 presents the physical, chemical and sieve analysis details of fly ash cenospheres in as received condition. These cenospheres are primarily made up of alumina, silica, calcium oxide and iron oxides as observed from this table.

Table 2.1 Physical, chemical and sieve analysis details of cenospheres*.

| Physical properties | | Chemical analysis | | Sieve analysis | |
|-----------------------|--------------------------------|--------------------------------|----------|-------------------|--------|
| True particle density | 920 kg/m ³ | SiO ₂ | 52-62% | + 30 # (500µm) | Nil |
| Bulk density | 400 - 450 kg/m ³ | Al ₂ O ₃ | 32-36% | + 60 # (250µm) | Nil |
| Hardness (MOH) | 5 - 6 | CaO | 0.1-0.5% | +100 # (150µm) | Nil |
| Compressive strength | 0.00176 - 0.00274 MPa | Fe ₂ O ₃ | 1-3% | +150 # (106µm) | 0-6% |
| Shape | Spherical | TiO ₂ | 0.8-1.3% | + 240 # (63µm) | 70-95% |
| Packing factor | 60-65% | MgO | 1-2.5% | + 240 # | 0-30% |
| Wall thickness | 5-10% of shell dia. | Na ₂ O | 0.2-0.6% | | |
| Color | Light grey - light buff | K ₂ O | 1.2-3.2% | | |
| Melting point | 1200 - 1300 °C | CO ₂ | 70% | | |
| pH in water | 6 - 7 | N ₂ | 30% | | |
| Moisture | 0.5% max. | | | | |
| Loss on ignition | 2% max. | | | | |
| Sinkers | 5% max. | | | | |
| Oil absorption | 16 - 18 g/100g | | | | |

*As provided by the supplier.

2.1.2 Matrix

HDPE of grade HD50MA180 supplied by Reliance Polymers, Mumbai, India is used as the matrix material. The resin is in granular form (~3 mm diameter). Table 2.2 presents the details about the matrix used. HDPE (Figure 2.1b) is also used in as received condition.

Table 2.2 Characteristics of HDPE grade HD50MA180*.

| Property | Test Method | Typical Value | Unit |
|--|-------------|---------------|------------|
| Melt Flow Index (190 ⁰ C/2.16 kg) | ASTM D1238 | 20.0 | gm/10 min. |
| Tensile Strength at Yield | ASTM D638 | 22 | MPa |
| Elongation at Yield | ASTM D638 | 12 | % |
| Flexural Modulus | ASTM D790 | 900 | MPa |
| Notched Izod Impact Strength | ASTM D256 | 30 | J/m |
| Vicat Softening Point | ASTM D1525 | 123 | °C |

*As specified by supplier

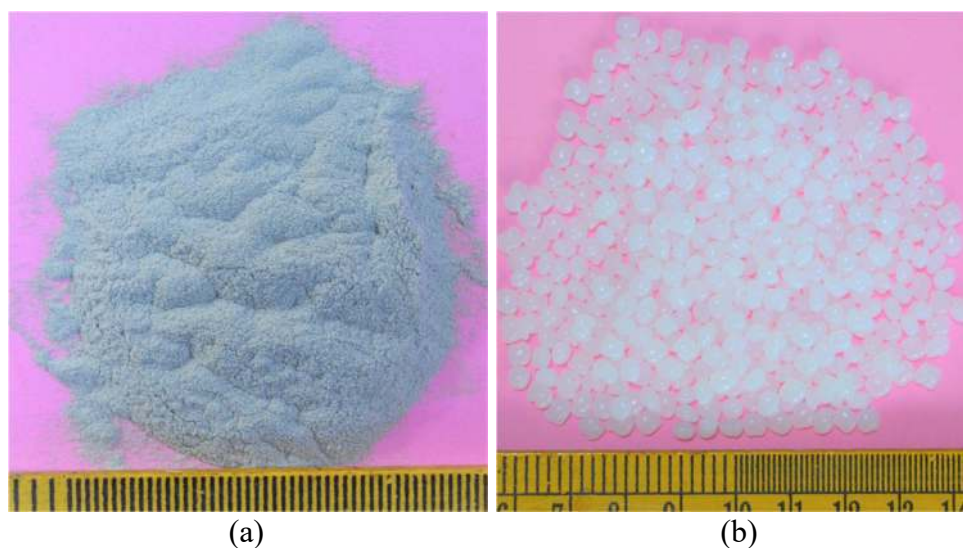


Figure 2.1 (a) Cenospheres and (b) HDPE matrix used in the present work.

2.2 Blend preparation

Blending of HDPE with cenosphere (20, 40 and 60 vol. %) is carried out using Brabender (16CME SPL) at 210°C (Bharath Kumar et al. 2016). Figure 2.2a shows the image of brabender used for blending while blending mechanism is presented in Figure 2.2b. Material is fed through feeder which melts in the heating zone and later

carried to twin screws/lobes (Figure 2.2b) rotating at 30 rpm. Blend of cenosphere/HDPE from brabender in the granular form having average mean diameter of 7 mm is shown in Figure 2.2c. Blend compositions and specimen convention of 20, 40 and 60 vol. % cenospheres in HDPE (H) are represented as H20, H40, and H60 respectively.

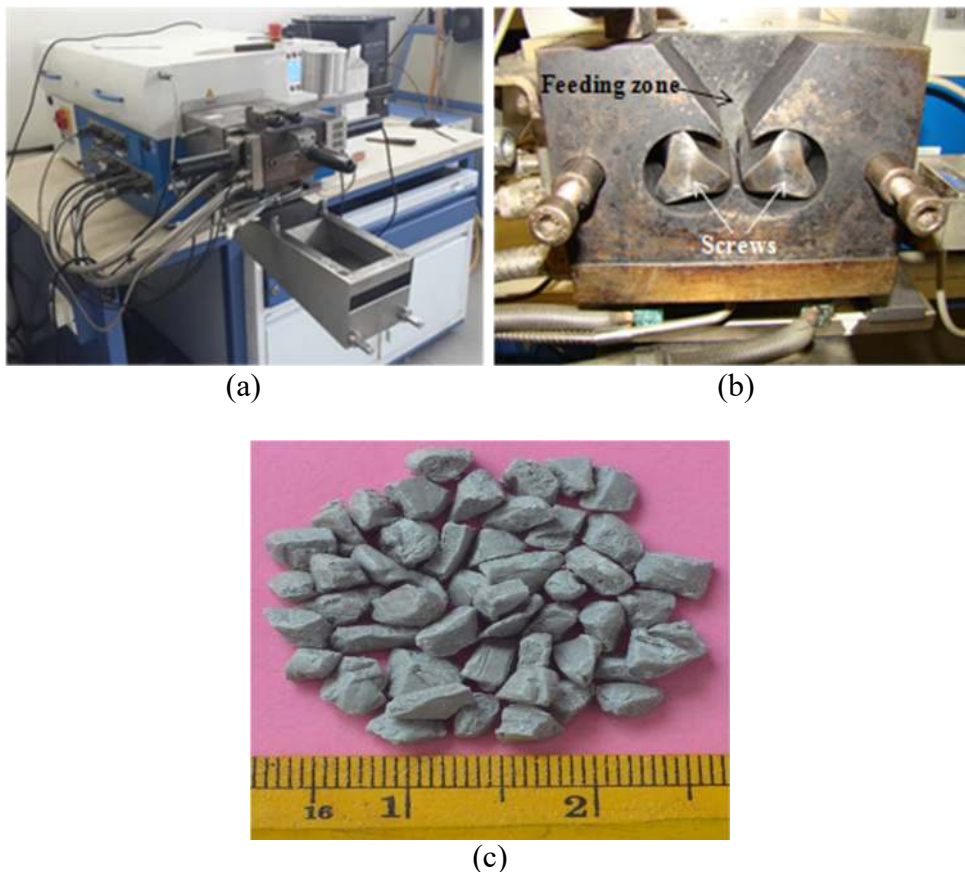


Figure 2.2 (a) Brabender (b) blending mechanism and (c) cenosphere/HDPE blend from brabender.

An overview of filament development and 3D printing of syntactic foam in the form of flow chart is presented in Figure 2.3 and is discussed in section 3.2

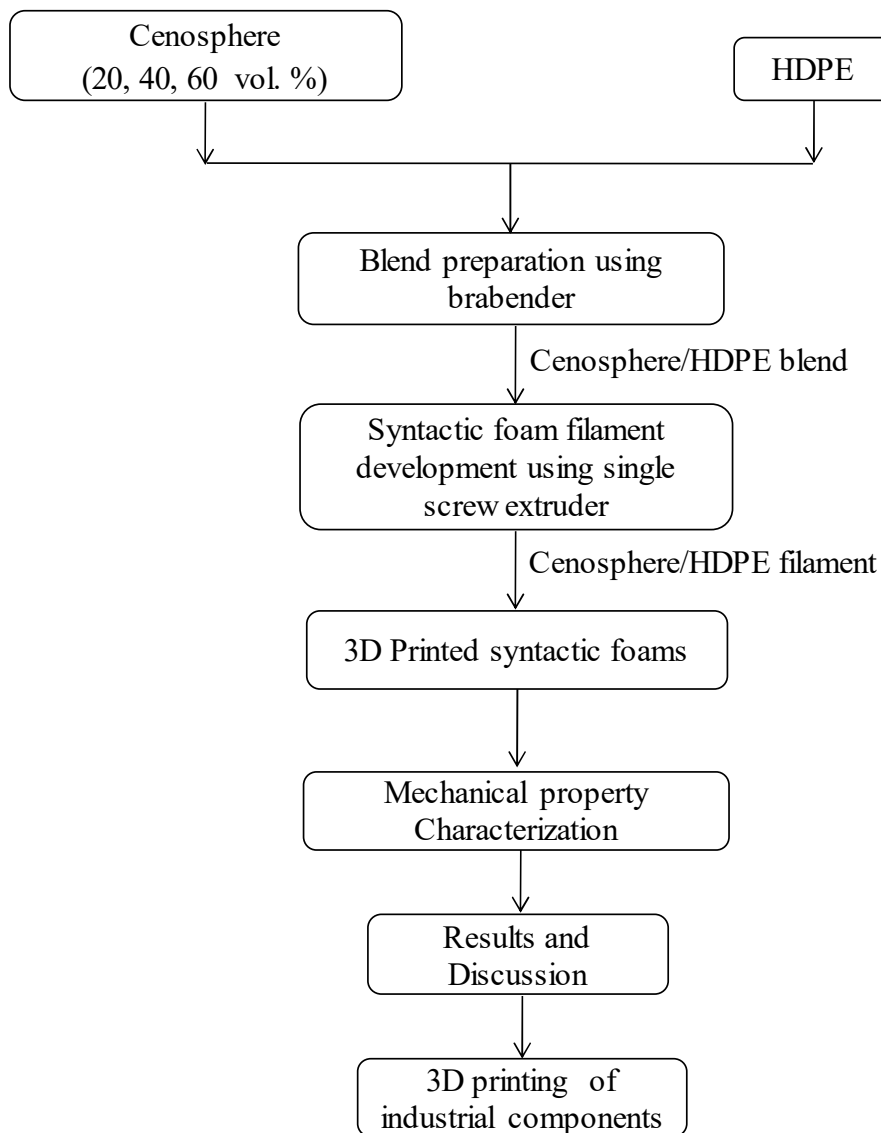


Figure 2.3 Flow chart of the present study.

2.3 Thermogravimetric analysis (TGA)

TGA of HDPE and their blend is carried out to estimate effect of cenosphere content on the degradation temperature. TGA measurements compute the thermal stability of polymer and their composite when heated at higher temperatures. In general, degradation mechanism of polymer comprises loss of mass and its molecular weight reduction due to molecular chain degradation. TGA of HDPE and their foam blends is computed using Perkin Elmer (STA 8000, USA) TGA/DTA analyzer. The sample heating is carried out with 10 °C/min heating rate within a temperature range of 40-600°C under nitrogen atmosphere.

2.4 Melt Flow Index (MFI)

MFI estimates material flowability. Melt flow rate measures the rate of extrusion of thermoplastics through an orifice at a prescribed temperature and load. MFI helps in setting appropriate multiplier in the 3D printer for printing foam samples. As received HDPE and cenosphere/HDPE blends MFI is determined by using Dynisco LMI5000 laboratory melt flow indexer (Figure 2.4).

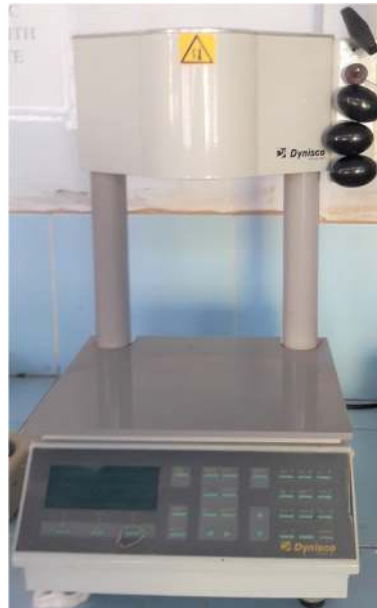


Figure 2.4 Melt flow indexer (Dynisco LMI5000).

2.5 Rheological study of cenosphere/HDPE blend

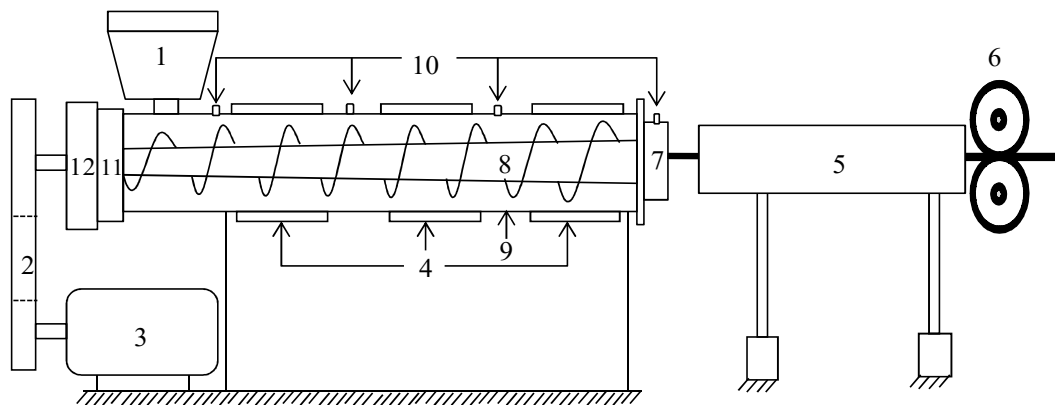
Rheological properties are important to understand the filler influence on processing conditions. Relative interaction between constituents and rheological behavior of HDPE and their foams is carried out using rotational rheometer (Anton Paar rheometer, MCR 502). Frequency sweep and temperature sweep test is carried out on a specimen having a dimension of $\phi 25 \times 1$ mm at a constant strain rate of 5%. The frequency sweep is conducted at 150°C in the range of 0.1 to 10 Hz. Change in complex viscosity (η^*), storage (G') and loss modulus (G'') against frequency and cenospheres content is investigated. Similarly temperature sweep is conducted at 1 Hz in temperature range of 130-150°C. For all the tests average of five replicates is presented.

2.6 Filament development and 3D printing

Extrusion is most commonly used method for shaping polymer. It is a continuous process based on a screw/barrel system and used to produce finished or semi-finished products (films, plates, pipes, profiles, tubes and cable insulation) by forcing the polymer melt through a die. It can be used for palletizing polymerization or compounding. An extruder consists of an Archimedean screw rotating within a heated barrel, gradually melting polymeric granules or powder and conveying this melt to a die where it is formed into shape. Polymer is melted by combined heating action of electrical heaters along the length of the barrel and frictional heat generated due to shearing of melt by rotation of the screw. The screw is the heart of an extruder and it has three main functional/geometrical zones (i.e., solids conveying or feeding, melting or transition and metering or pumping).

Challenges of particle fracture, porosity entrapment and incomplete mixing needs to be carefully looked into in developing a cenosphere/HDPE syntactic foam filament. The schematic representation (Figure 2.5a) and photograph (Figure 2.5b) of single screw extruder used to fabricate HDPE and foam filament is shown for clarity. The specifications of the single screw extruder are listed in Table 2.3.

The schematic representation (Figure 2.6a) and photograph (Figure 2.6b) of industrial-scale FFF 3D printer is shown for clarity. The printer is equipped with dual brass nozzles and has overhead gantry which carries an extrusion/printing head comprising of melting unit and pair of nozzle, one for part material and one for support material. The heating block situated over nozzle supplies necessary heat for filament melting. The temperature of enclosed printing chamber can be maintained by appropriate built-in heating elements. The chamber has stationery glass bed with embedded heating elements, over which material from nozzle is dispensed to form layers. Hanger arrangement is provided to load spools of part material and support material. The movement of printing head in X, Y and Z direction are controlled by machine control unit using individual stepper motor. The specifications of the 3D printer utilized for the present work are listed in Table 2.4.



1.Hopper 2.Power transmission 3. Motor 4.Heater 5.Water trough 6.Take-up unit
7.Die 8.Screw 9.Barrel 10.Thermocouple 11.Thrust bearing 12.Gear reducer

(a)



(b)

Figure 2.5 (a) Schematic representation of the industrial scale single screw extruder and (b) experimental set up.

Table 2.3 Single screw extruder specifications.

| Specification | Details |
|-----------------------|--|
| Hopper | Min. 3 Kg, SS sheet with discharge chute. |
| Die sizes | 1.75, 2.5 and 3 mm. |
| Screw | High tensile nitride hardened alloy steel to sustainable up to 450°C, Dia. 25 mm with length 26D having uniform discharge. |
| Heaters | Ceramic in SS cover, 4 nos. with load up to 5 Kw. |
| Heating control panel | PID controllers with 5 zones, Accuracy $\pm 1^\circ\text{C}$, Max. Temp. 450°C. |
| Drive | 3 HP ACVF Drive, Max. RPM 60. |
| Cooling | Water cooling |
| Spooling arrangement | Take up rollers with 0.5 HP ACVF drive with height adjustments and castor wheels |
| Pelletizer | Helical type, minimum 4" dia \times 4" L with 0.5HP ACVF drive. |
| Make and Model | Aasabi Machinery (P) Ltd. Dombivli, Mumbai, India. (25SS/MF/26, L/D ratio of 25:1) |

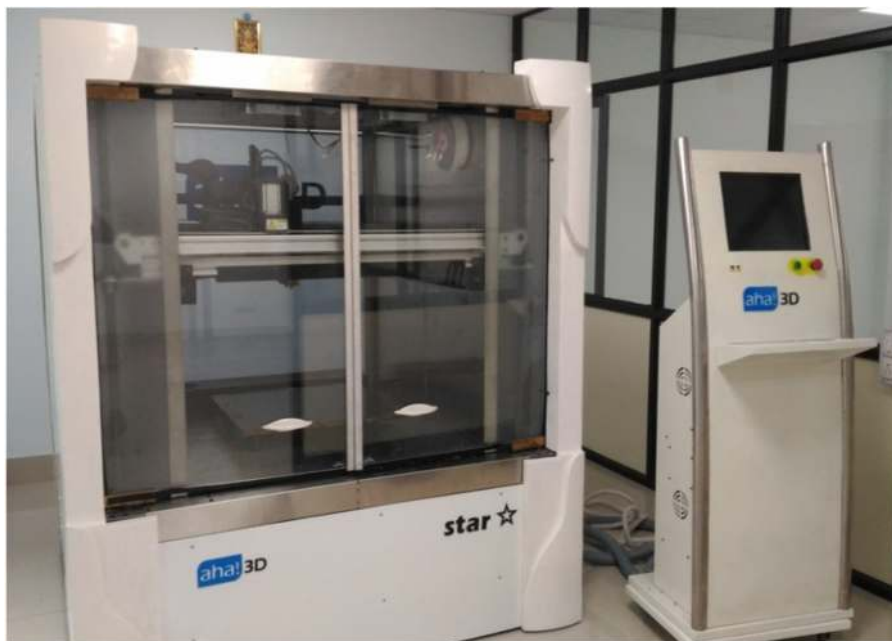
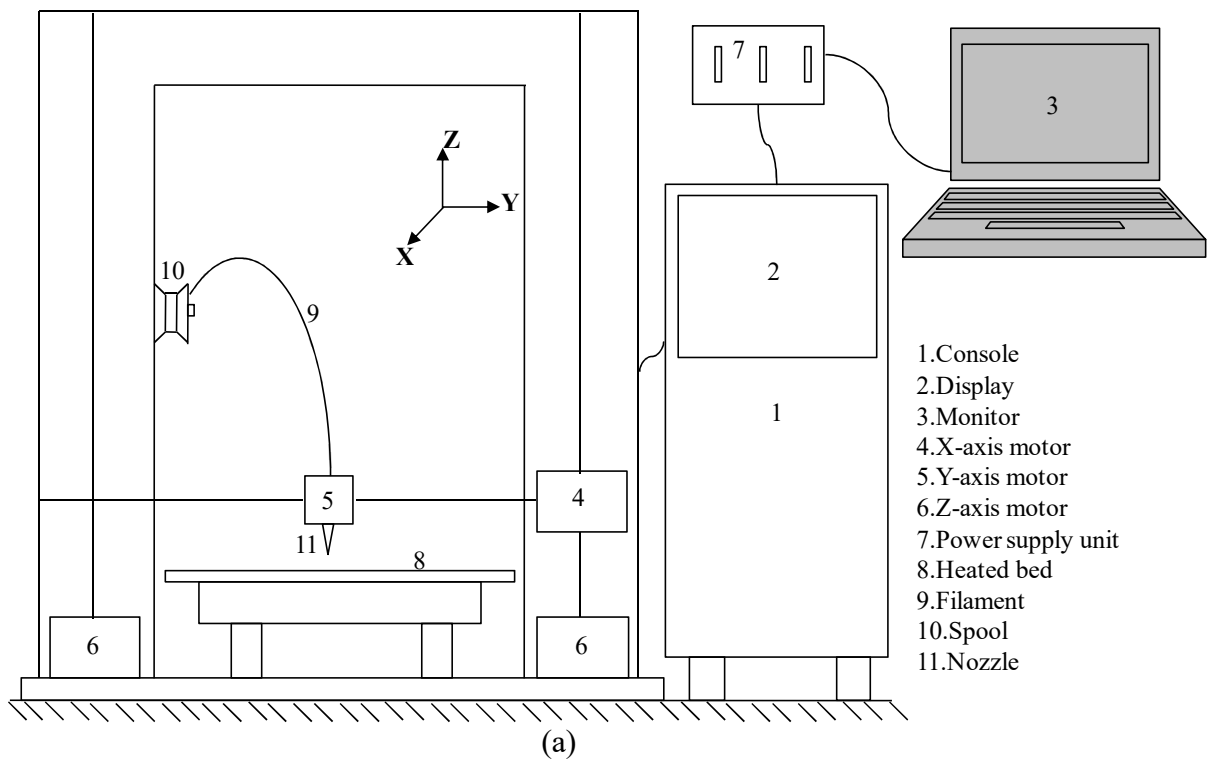


Figure 2.6 (a) Schematic representation of FFF printer and (b) FFF printer utilized in the present work.

Table 2.4 Specifications of FFF based 3D printer.

| Specification | Details |
|---------------------------|--|
| Technology | Fused Filament Fabrication (FFF) |
| Build volume | 500×500×500 mm ³ |
| Screw | High tensile nitride hardened alloy steel to sustainable up to 450°C. Suitable compression ratio (at least Dia. 25 mm with length 26D) uniform discharge is a must at metering zone. |
| Printing materials | All engineering thermoplastic and Plastic Composites, ABS, HIPS, PC, Nylon, TPU, TPE, Carbon fiber composite, etc. |
| Filament diameter | 3 mm (Standard) |
| Number of extruders | 2 |
| Layer height | 100 to 500 microns |
| Rate of production | Basic tool head: up to 15 cm ³ /hr., Standard tool head: Up to 150 cm ³ /hr. |
| Max. extrusion temp. | Basic tool head: 300°C, Standard tool head: 500°C |
| Tool head cooling | Basic tool head: air cooled, Standard tool head: liquid cooled. |
| Build platform | Up to 150°C |
| Build chamber | Up to 100°C |
| Positional accuracy | 50 micron (stepper), 20 microns (servo), 4 microns (dual servo) |
| Power requirement | 220V AC, three phase |
| Data import format | STL, AMF, OBJ. |
| Workstation compatibility | Windows XP, Windows 7, Linux |
| Make and model | Aha 3D, Jaipur, Rajasthan India; Model: Star |

2.7 Differential scanning calorimetry (DSC)

Melting and crystallization behavior of the filaments, 3D printed HDPE and their foams are analyzed using DSC (Perkin Elmer DSC-6000, USA). Sample weighing about 10 mg in 30 µl Al standard crucible is heated from 0-200°C with isothermal curing for 3 min at 200°C and subsequent cooling to 0°C at a rate of 10 °C/min. Second heating is performed from 0-200°C after cooling the sample at 0°C for 3 min. First heating is carried out to nullify the thermal history creped in because of earlier processing steps. DSC curve typically represents endothermic, exothermic (T_g) and cold crystallization melting enthalpy peak. Crystallinity % (α_{Cryst}) is estimated as,

$$\alpha_{\text{Cryst}} = \frac{\Delta H_m}{\Delta H_m^*} \times 100 \quad (2.1)$$

where, ΔH_m is fusion heat in J/g and ΔH_m^* is fusion heat per gram for crystalline HDPE, 293 J/g (Divya et al. 2013).

2.8 X-ray diffraction (XRD)

The percentage of crystallinity of filament and 3D printed samples is calculated using XRD measurement. XRD measurements are performed using Rigaku 5th miniflex, USA, XRD system equipped with a Cu $k\alpha$ radiation source ($\lambda=15406\text{\AA}$) at 40 kV and 15 mA with Nickel filter. Sample scanning is done from 10-80° (2 θ) range at a speed of 2°/min. The percentage of crystallinity (α_{Cryst}) is estimated as,

$$\alpha_{\text{Cryst}} = \frac{A_{\text{cr}}}{\frac{A_{\text{cr}}}{A_{\text{am}}}} \times 100 \quad (2.2)$$

Where A_{cr} and A_{am} corresponds to the area of the crystalline and amorphous phase of HDPE respectively.

2.9 Coefficient of thermal expansion (CTE)

CTE is the most crucial parameter as far as dimensional stability and part warpage in the FFF process is concerned. CTE of 3D printed specimens is estimated (ASTM D696-13) using Dilatometer (CIPET, Chennai) and are utilized to correlate the filler loading effect on dimensional stability and microstructural analysis. HDPE and their foams are 3D printed to 75×12.7×3 mm dimension and CTE is performed in the temperature range of 20-90°C. Average of five samples are reported for analysis.

2.10 Density

Densities of filaments and printed specimens are measured using the procedure outlined in ASTM D792-13 . Theoretical density is computed using the rule of mixture and is given by,

$$\rho = \rho_f V_f + \rho_m V_m \quad (2.3)$$

where, ρ and V are density and volume fraction, respectively. Subscripts f and m denote filler and matrix, respectively. Furthermore, the void content (Φ_V) is estimated using theoretical (ρ^{th}) and experimental (ρ^{exp}) densities and is given by (Gupta et al. 2004, Tagliavia et al. 2010),

$$\Phi_V = \frac{\rho^{th} - \rho^{exp}}{\rho^{th}} \quad (2.4)$$

2.11 Tensile testing

Tensile tests are performed on filament and 3D prints using Z020 Zwick Roell (USA) UTM (20 kN load cell). Zwick Roell gauge length extensometer (2 inch) is used to record the elongation with 0.1 MPa initial load. Tensile tests on pilot basis is performed on filament and printed sample at 10^{-4} s^{-1} , 10^{-3} s^{-1} , 10^{-2} s^{-1} and 10^{-3} s^{-1} strain rates. Later, constant crosshead displacement rate is maintained at 5 mm/min (ASTM D638-14). The acquired load and displacement data are used to calculate the stress and strain, respectively. Average modulus and strength values of five specimens for each sample are reported.

2.12 Flexural test

The flexural testing (ASTM D790-17) is performed in three-point bend configuration using a computer controlled Zwick (Zwick Roell Z020, ZHU) machine having a load cell capacity of 20 kN. A pre-load of 0.1 MPa is set and crosshead displacement rate is maintained at 1.54 mm/min. All specimens have span length of 52 mm to maintain 16:1 span length/thickness ratio. Five replicates of each volume fraction are tested and average values are reported for analysis. Tests are terminated at 10% strain if the specimen does not fracture. The flexural modulus is calculated by,

$$E_{fM} = \frac{L^3 m}{4bd^3} \quad (2.5)$$

where L is the support span (mm), b is the width of beam (mm), d is the thickness of beam (mm) and m is the slope of the tangent to the initial straight-line portion of the load-deflection curve. The flexural stress is estimated by,

$$\sigma_{fS} = \frac{3PL}{2bd^2} \quad (2.6)$$

where P is the load (N) at a given point on the load-deflection curve.

2.13 Compression test

The compression tests are conducted using a Zwick (Zwick Roell Z020, ZHU) computer controlled universal test system with 20 kN load cell. The test is conducted in quasi-static mode (10^{-3} , 10^{-2} and 10^{-1} s^{-1} strain rate corresponding to cross-head displacement velocity of 0.001, 0.01 and 0.1 mm/min). The criteria for end of the test

is set at 20 kN load. The data is analyzed using an in-house developed MATLAB code. Compressive modulus and strength are calculated for all the specimens. The compressive strength is defined by the peak stress at the end of the elastic region. At least five samples of each volume fraction are tested to check for repeatability.

2.14 Dynamic Mechanical Analysis

Dynamic mechanical analysis is carried out using TA Instruments (New Castle, DE) Q800 DMA. Specimens of recommended dimensions $50 \times 10 \times 3.2 \text{ mm}^3$ are tested in the dual cantilever configuration with a span length of 35 mm. The testing is conducted in the strain control mode with a maximum displacement of 25 μm . DMA is conducted to study the behavior of the syntactic foams at high temperature using the temperature sweep mode at constant frequency. Temperature is ramped from 30 to 125°C at a rate of 1°C/min with the deformation occurring at a constant frequency of 1 Hz. Testing is stopped once the storage modulus reaches a value of 20 MPa to prevent total melting of the specimen. Average of five samples are reported for analysis.

2.15 Imaging

Scanning electron microscope (JSM 6380LA, JEOL, Japan) is used for micro structural analysis. All the samples are sputter coated using JFC-1600 auto fine coater (JEOL, Japan). Nikon D7000 camera with Nikkor 35 mm F1.8G lens is used for optical imaging. Tokina AT-X pro 100 mm F2.8D macro lens is used for imaging fractured features.

The internal structure of filaments is studied by using a Bruker Skyscan 1172 micro-CT scanner equipped with a digital X-ray camera having 4000×2664 -pixel array (corresponding to 4K resolution). The specimens are placed at 36.55 and 308.36 mm from the source and camera, respectively, resulting in a pixel size of 0.95 μm . A rotation step of 0.2° is used in scanning. Samples are exposed for 1420 ms at a source voltage of 50 kV.

3 MATERIAL CHARACTERIZATION AND PROCESSING ASPECTS

3.1 Blend characterization

Cenosphere/HDPE blends are characterized for TGA, MFI and rheology.

3.1.1 Thermogravimetric analysis (TGA)

Figure 3.1a and Figure 3.1b shows TGA and differential thermograms (DTG) of neat HDPE and cenosphere/HDPE blends respectively and the result are presented in the Table 3.1. Neat HDPE and syntactic foam exhibit single decomposition step with maximum weight loss rate appearing at 478°C (Figure 3.1b). Neat HDPE and their syntactic foams exhibit similar trend as seen from of TGA/DTG plots. TGA analysis reveal that there is no significant change in initial degradation temperature of foams relative to neat HDPE. The shift is marginal ($\sim 3\text{-}7^\circ\text{C}$) signifying the absence of surface/physical interactions between filler and polymer chains if any. Final degradation of neat HDPE occurs at 500°C (Figure 3.1a) due to the thermal cracking of the hydrocarbon chain (Banat and Fares 2015).

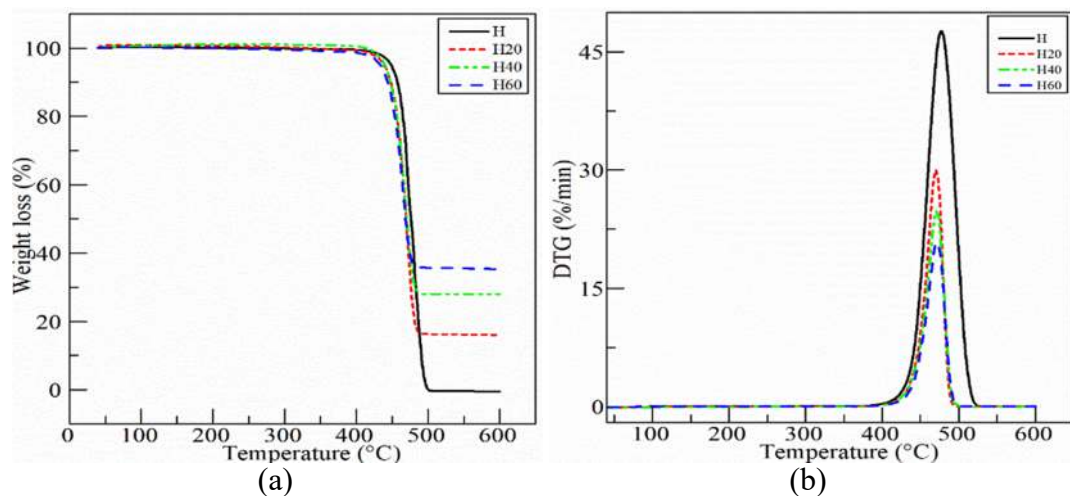


Figure 3.1 (a) TGA and (b) DTG thermograms of HDPE and cenosphere/HDPE blend.

It is observed that 20, 40 and 60 vol.% of cenosphere lowered the final degradation temperature of HDPE indicating cenospheres effective role as a good thermal conductor of heat. TGA and DTG curve reveal that, there is no much variation among final degradation and decomposition peak temperatures of foams. The percentage residual weight in TGA indicate the undecomposed inorganic filler and ash (char

content). HDPE decomposed completely with no char, whereas char content increased by 15.3, 27.91 and 35.33% with increasing cenospheres content of 20, 40 and 60 vol.% respectively as seen from Table 3.1. TGA/ DTG results affirm syntactic foams better thermal stability as compared to neat HDPE (Deepthi M V et al. 2010). Maximum weight loss rate at decomposition peak temperature decreases with increasing cenosphere content indicates better thermal stability of foams making them suitable material in high temperature applications (upto 485 °C).

Table 3.1 TGA and DTG thermograms of HDPE and their foams.

| Material | Onset degradation temp. (°C) | Final degradation temp. (°C) | % residue at 600°C | Decomposition peak temp. (°C) | Max. weight loss rate at decomposition peak temp. (%/min) |
|----------|------------------------------|------------------------------|--------------------|-------------------------------|---|
| H | 457.86 | 500 | 0 | 478 | 47.59 |
| H20 | 453.55 | 487 | 15.30 | 470 | 30.01 |
| H40 | 449.82 | 484 | 27.91 | 468 | 24.75 |
| H60 | 450.95 | 485 | 35.33 | 469 | 20.83 |

3.1.2 MFI of HDPE and cenosphere/HDPE blends

Flowability of polymer in the molten state is measured using MFI and is inversely proportional to the viscosity. MFI decreases with increasing filler content because of the particles resistance to the polymer flow (Viviane Alves Escocio et al. 2015). Neat HDPE has registered highest MFI (23.06 gm/10 min) as compared to H20 (14), H40 (9.1) and H60 (6.80). MFI decreases by 39.29, 60.54 and 70.51% with increasing cenospheres content of 20, 40 and 60 vol. % respectively (Mohanty and Nayak 2010, Viviane Alves Escocio et al. 2015).

For 3D printing of cenosphere/HDPE foams, reduction in MFI values needs to be compensated either by increasing printing temperature or setting appropriate multiplier factor. The latter option is viable to isolate temperature effects and hence printing temperature is kept constant and the multiplier factor is changed while printing.

3.1.3 Rheology of HDPE and cenosphere/HDPE blend

Frequency sweep

Figure 3.2a present complex viscosity (η') versus frequency for all the samples. Polymer melt viscosity increases with filler infusion (Shaikh et al. 2016) and is observed in the complete frequency range. HDPE shows Newtonian-Plateau at a lower angular frequency and the shear thinning region at a higher frequency. H20 exhibit similar behavior with a moderate increase in η' . Whereas for H40 and H60, Newtonian-plateau region is disappeared and only shear thinning is seen for the entire frequency range which is due to more number of polymeric chain entanglements getting divided than reformed (Shaikh et al. 2016).

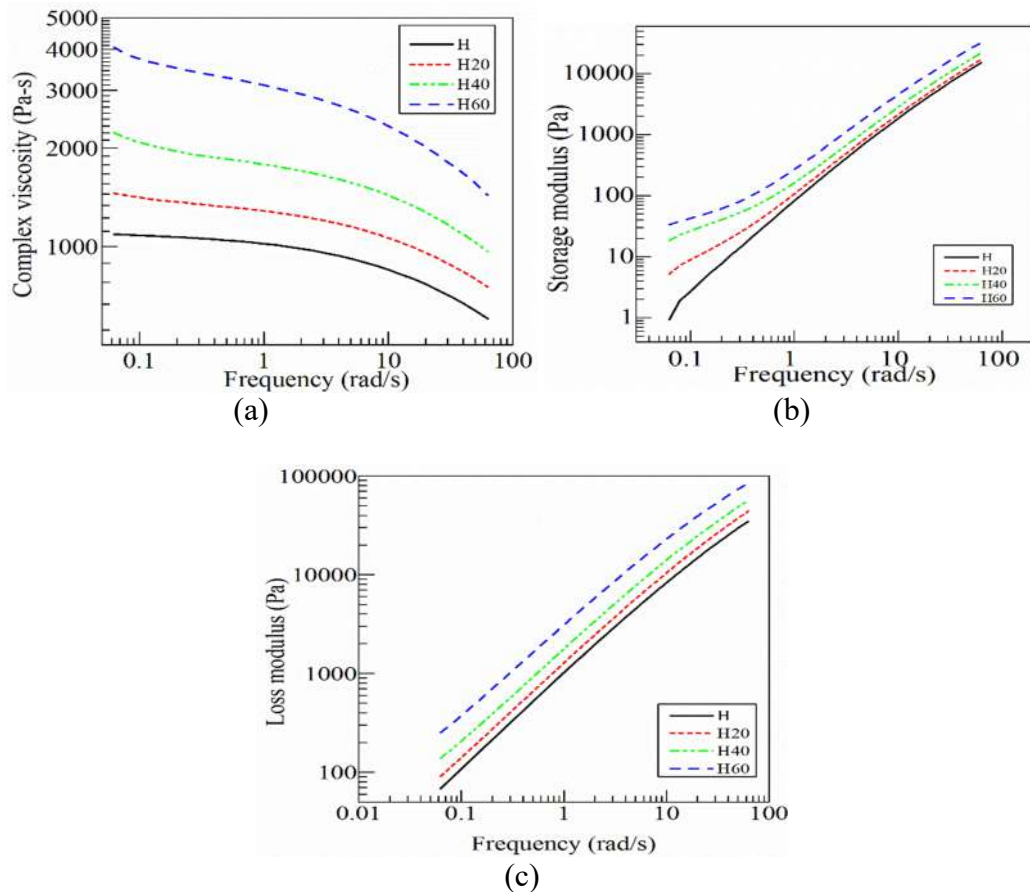


Figure 3.2 (a) Complex viscosity (b) storage modulus and (c) loss modulus as a function of frequency for HDPE and their blends.

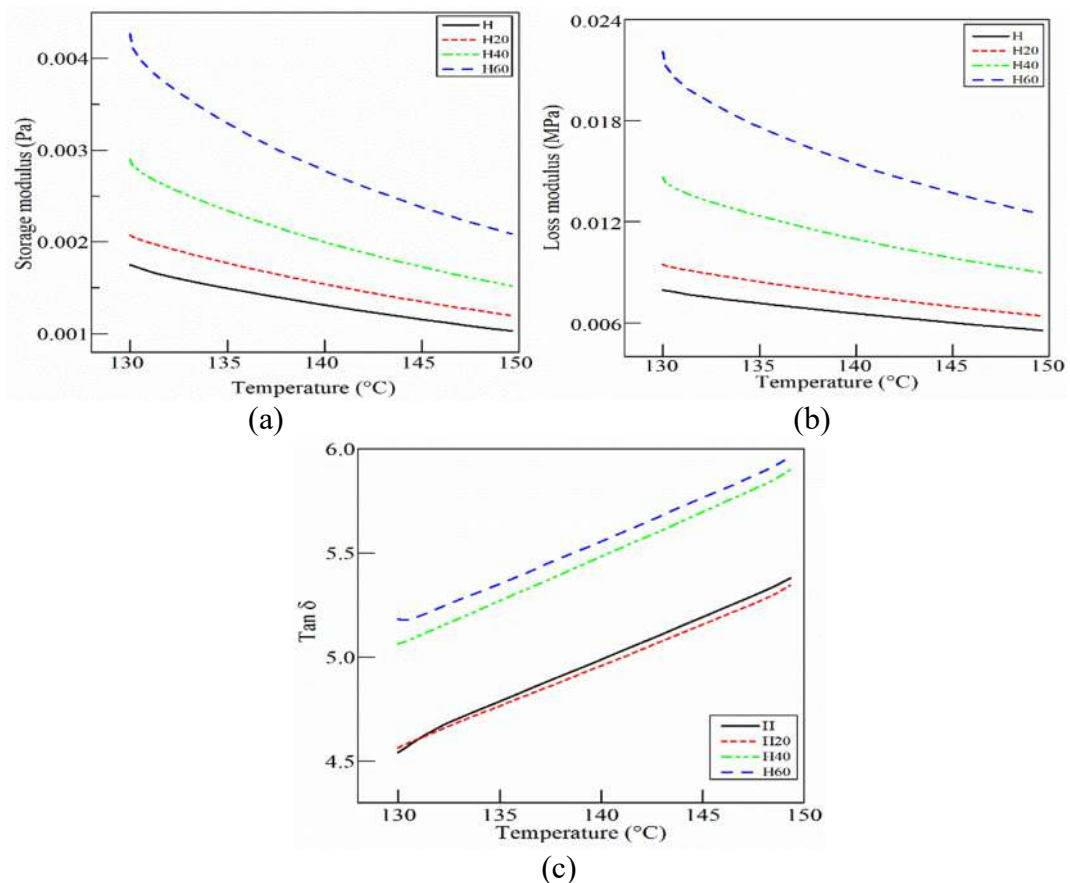
H60 composition has registered highest η' implying increased viscosity. Cenospheres hinders polymer chain segments mobility making the flow more viscous. Compared to

neat HDPE (1080.52 Pa.s), viscosity at 0.1 rad/s for H20, H40 and H60 is 1412.42, 2082.10 and 3739.50 Pa.s respectively. However, the decrease in η' with frequency is observed for all the samples. At 50 rad/s, the η' of HDPE is about 636.75 Pa.s while it's 794.92, 1029.31 and 1558.81 Pa.s respectively for H20, H40 and H60. Foams exhibit shear thinning (pseudo plasticity) behavior and are similar to polypropylene-fly ash blend as reported in Ref. Pardo et al. (2010). Storage modulus (G') of foams is higher compared to HDPE (Figure 3.2b) indicating cenospheres constrain matrix deformation. Storage modulus increases with increasing filler loading leading to foam stiffness enhancement. At lower frequency, neat HDPE and H20 show typical homopolymer-like terminal behavior as HDPE chains are fully relaxed (El Achaby et al. 2013). H20 shows slightly higher modulus compared to neat HDPE. In the case of H40 and H60, a plateau at lower frequency is observed indicating viscoelastic behavior (liquid to solid-like). Also, as frequency increases, the G' difference between the foams reduces. Loss modulus (G'') is noted to increase with frequency for all samples (Figure 3.2c). Further, addition of cenospheres increases G'' . The G'' at 0.1 rad/s is 107.56, 140.37, 205.66 and 370.02 Pa for neat HDPE, H20, H40 and H60 respectively. This behavior is due to deformation restrictions caused by the cenospheres addition.

Temperature sweep

Figure 3.3 shows temperature sweep plots of HDPE and their foams at 1 Hz. From Figure 3.3a it is clear that, as the temperature increases G' decreases for neat HDPE and foams throughout the temperature range. At higher temperature, the gap between G' curves tend to reduce. This signifies that, the cenosphere content has lower effect on G' at higher temperature than at lower temperature. At low temperature, the gap between G' curves is more and all curves are significantly separated. Since G' represents molecular elastic response in viscoelastic material, its effect gets reduced at higher temperature. This reduction in G' at higher temperature may be well explained by increased polymer chain mobility and decreased bonding strength between HDPE and cenospheres. Similar observation is deduced from G'' as seen from Figure 3.3b. G'' is dominating over storage modulus signifying viscous segmental friction between

cenosphere and the polymer melt and increases viscous behaviour. Further, $\text{Tan } \delta$ results are plotted against temperature in Figure 3.3c. $\text{Tan } \delta$ is the ratio of viscous portion (loss modulus) to elastic portion (storage modulus). The value of $\text{Tan } \delta$ determines the melt behavior (liquid or solid). From the $\text{Tan } \delta$ curve it is clear that the viscous portion is contributing predominantly throughout the temperature range. Also it is clear from the prevailing discussions that as cenosphere content increases melt viscosity increases. $\text{Tan } \delta$ increases with temperature and cenosphere content. The difference in $\text{Tan } \delta$ value of HDPE and H20 is negligible. $\text{Tan } \delta$ of H20 is less as compared to HDPE indicating viscoelastic nature of HDPE dominates over viscous regime of H20.



MFI and rheological behavior results indicate differential parameter choices to be made pertaining to processing conditions and fabrication routes. Hence, processing

parameters need to be looked into carefully based on MFI and rheological investigations.

3.2 Filament development

During pilot study extruder design is finalized based on quality of the filament. Three heaters are controlled separately using solid-state relays that are switched on/off by an Arduino using the input from two K-type thermocouples attached to each heater. In single screw extruder, heaters (barrel temperature) are set at 160°C (Bharath Kumar et al. 2016), die temperature at 150°C with constant screw speed of 25 rpm and take-up unit speed of 12.5 rpm to obtain the filaments of diameter 2.85 ± 0.05 . In previous studies, H40 composition is found to be the highest filling level of cenospheres without substantial fracture (Bharath Kumar et al. 2016, Jayavardhan et al. 2017). After pre-heating of H40 pellets for 10 minutes, the material is extruded through a die with a 3 mm hole to obtain 1X (once extruded) filament. Recycling potential of syntactic foam filaments is studied by pelletizing and extruding them twice (2X) and three times (3X). The 1X filament is pelletized and fed into the hopper again to prepare 2X filament and the process is repeated one more time to obtain 3X filament. Success in recycling syntactic foam filaments would make them more environmental friendly even after printing the objects and using them in some applications.

H40-2X and 3X filaments are observed to have a uniform cross-section in SEM observations as seen from Figure 3.4. The average diameters of 2X and 3X filaments are measured to be 2.85 ± 0.01 mm, suggesting extrusion consistency. The blended H40 pellets and 1X, 2X and 3X filaments have densities of 0.807 ± 0.016 , 0.897 ± 0.029 , 0.966 ± 0.018 and 0.975 ± 0.022 g/cm³, respectively. The theoretical density of H40 pellets, estimated using rule of mixtures, is 0.938 g/cm³. The density of the foam increases after each extrusion pass, although the values are in a small range. The standard deviation is higher for H40-1X filament, suggesting entrapment of voids and breakage of cenospheres during extrusion process. The entrapped air porosity is expected to reduce with each pass, making the density more consistent. However, breakage of particles in each pass results in increase in density and is undesirable.

Density of syntactic foams does not show any significant change between the second and the third extrusion pass. Since the density of the cenosphere wall material is around 3.5 g/cm^3 , stabilization of density below 1 g/cm^3 shows that there is no additional particle fracture or void entrapment. Figure 3.4a shows a low magnification micrograph of the H40-1X filament. Cenospheres are observed to be uniformly distributed around the cross section of the filament. A close observation of the filament microstructure in Figure 3.4b suggests some broken fragments among mostly intact cenospheres. Figure 3.4c and Figure 3.4d show the microstructure of H40-2X and 3X specimens. Since the density of H40-2X and 3X filaments is the same, their microstructures also reflect that fact and appear to be very similar. The second and third extrusion passes under similar processing conditions do not lead to significant additional breakage of particles. This observation shows that the recycling of the syntactic foam filament is possible.

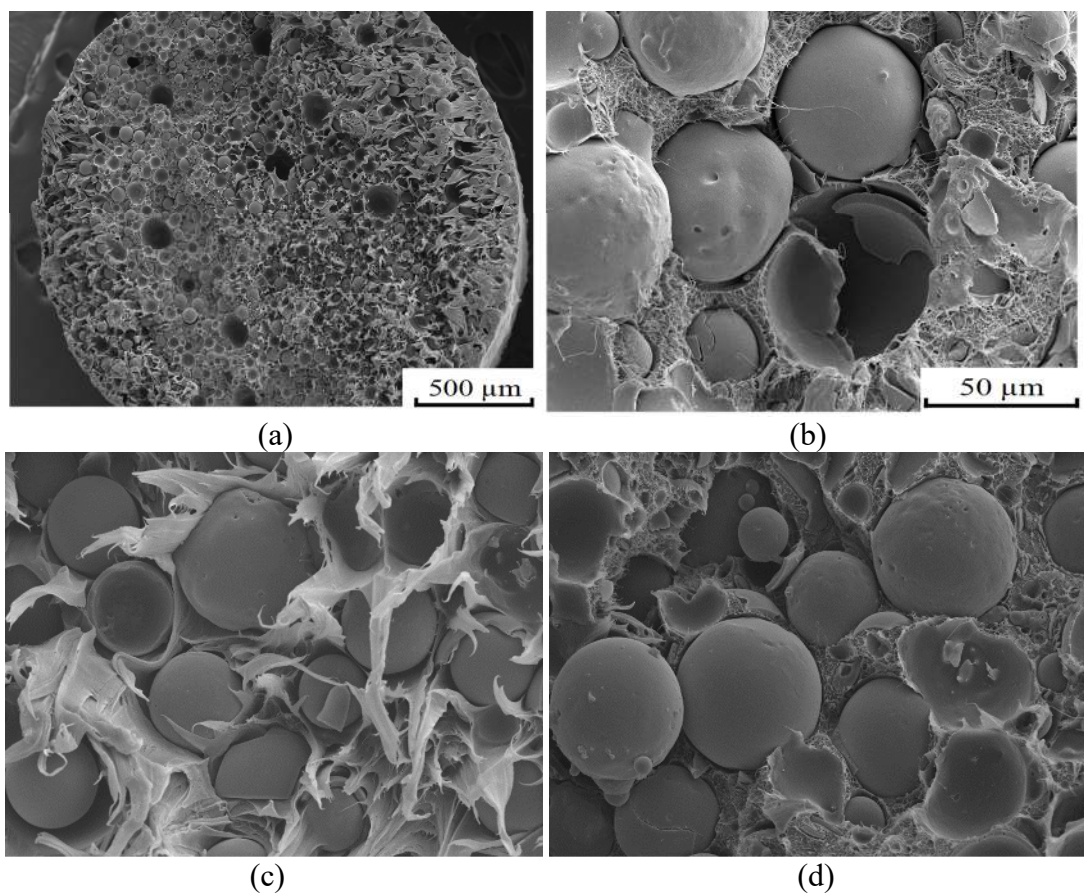
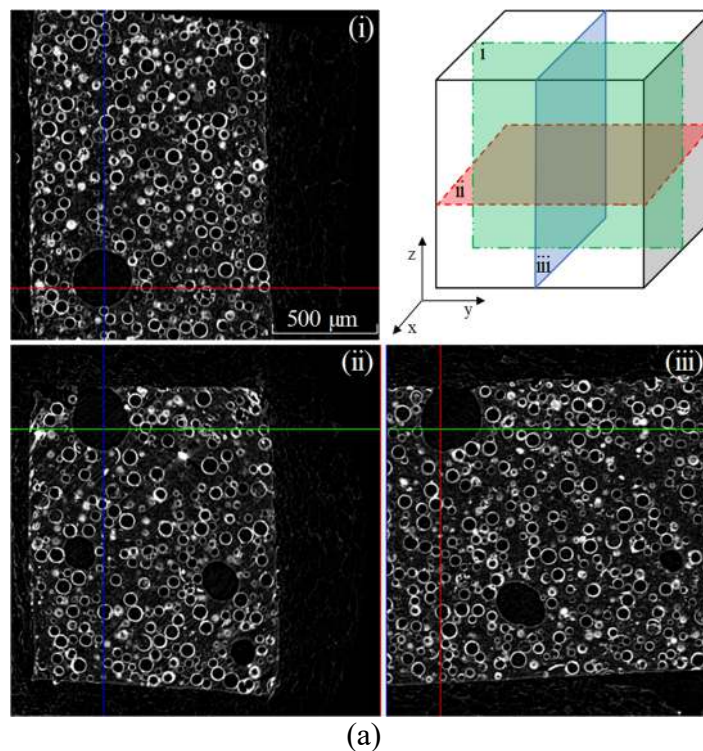


Figure 3.4 Micrograph of (a) H40-1X filament at low magnification (b) a higher magnification image (c) H40-2X and (d) H40-3X filaments.

Figure 3.5a-d exhibits micro-CT 3D reconstruction of one representative H40-1X specimen. The filament specimens are mounted with the length oriented along the z-axis. Cenospheres are observed to be uniformly distributed across all sections in the filament. There are a few limitations of the micro-CT scan analysis due to varying cenosphere wall thickness and wall porosity (Figure 3.5b-c). Figure 3.5d presents successive trans-axial images (i, ii, iii and iv) that are 2-pixel distance apart. Highlighted regions “a” and “b” in Figure 3.5b-c show defects on the cenosphere surface and wall porosities. The circles highlight a portion of the same cenosphere that appears to be broken in image (iii), and solid in image (iv). It is likely that this discontinuity is caused by one of the defects similar to those shown in Figure 3.5b-c. Some of these defective regions may make the walls appear broken in an intact cenosphere in micro-CT images, which makes it difficult to obtain reliable results from image analysis. Such deviations lead to erroneous data and thereby experimental density estimations to quantify hollow particle breakage is the relatively better approach in case of cenospheres.



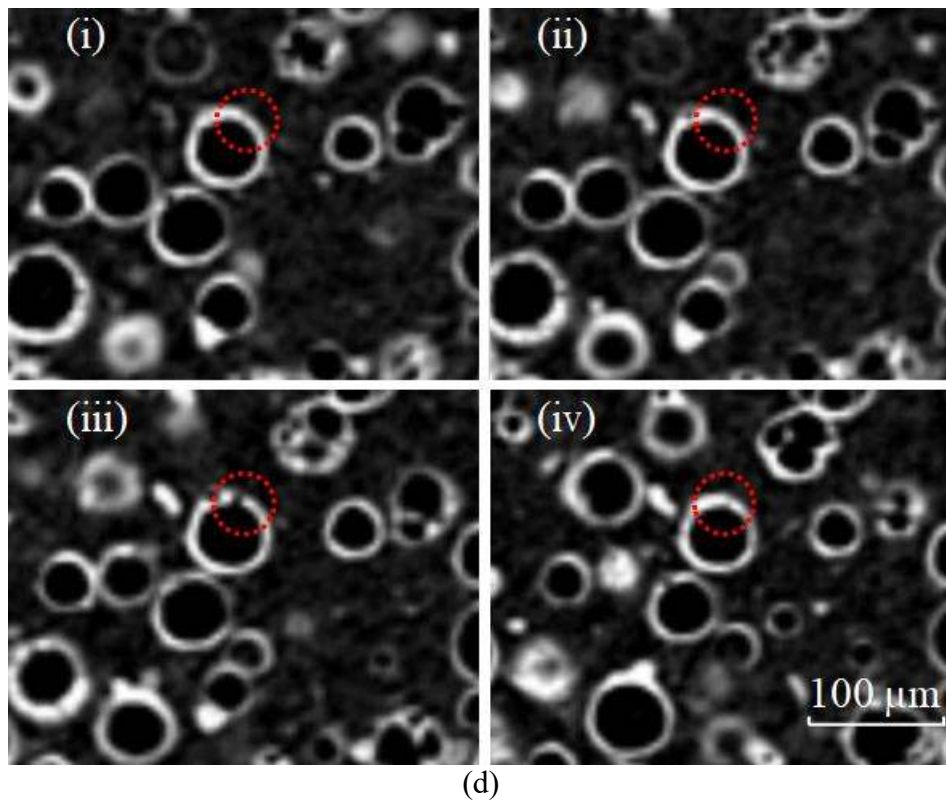
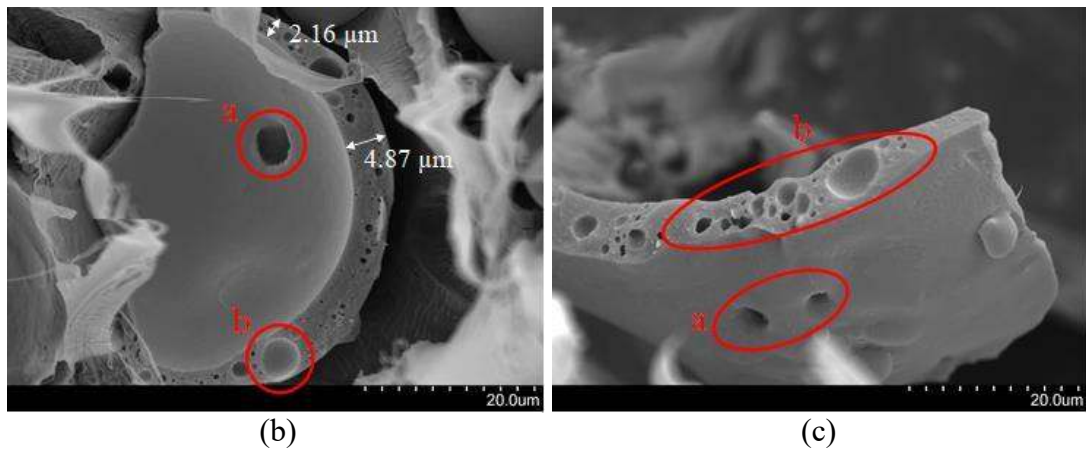


Figure 3.5 (a) Micro-CT scan image showing reconstructed (i) sagittal (y - z) (ii) transaxial (x - y) and (iii) coronal (z - x) views of H40-1X specimen (b) & (c) micrographs showing cenosphere walls with porosities and variable thickness and (d) voids present in cenosphere walls can appear to be discontinuities in some slices in the micro-CT scan images of H40.

Based on the pilot study extrusion parameters for single screw extruder using 3 mm die are finalized. Barrel temperature of 160°C, die temperature is set at 150°C, screw speed is maintained constant at 25 rpm and take-up unit speed is fixed at 12.5 rpm to obtain

the filaments of diameter 2.85 ± 0.05 mm (Figure 3.6). These developed filaments are used to feed the 3D printer for printing neat HDPE and foam samples.



Figure 3.6 Representative H60 filament.

Quality and behavior of eco-friendly foam feedstock filament is governed by filler-matrix interaction, intact filler and void formations. Sufficient stiffness for spooling and strength (avoid buckling and shearing between the feeding wheels and printer nozzle) are required for the filament to be useable on a 3D printer. Thereby, before using these filaments for 3D printing, their density, morphology (in this section) and tensile tests (chapter 4) are carried out. Table 3.2 presents densities, void % and weight saving potential data of filament and 3D printed specimens. There is a negligible difference in theoretical and experimental density of HDPE filament indicating the absence of voids. Voids formed during blending and extrusion (0.34-4.90%) of foams results in three-phase foam structure making them better energy absorbing materials. ***Hence, characterization of 1X filaments and their prints are investigated in the later part of this thesis.*** Void content increases with cenospheres content as seen in Table 3.2. Due to hydrophobic nature, HDPE did not show any voids post extrusion. Nonetheless, porosity is only observed in foam filament as cenospheres are hydrophilic in nature. Cenospheres primarily comprise of oxides (Al_2O_3 and SiO_2) which links with hydroxyl group resulting in void formation during processing though blends are preheated (90°C) for 24 hr. Figure 3.7a shows a circular cross-section of freeze-fractured H20 filament. Figure 3.7b shows higher magnification H20 wherein circular

pores are formed in the matrix whereas in H40 (Figure 3.7c) and H60 (Figure 3.7d) larger sized irregular shaped pores are observed. These pores might enhance the damping capabilities of the prints if gets retained in prints.

Table 3.2 Density, void content and weight saving potential of filament and 3D printed samples.

| Material | Φ_f (vol. %) | ρ^{th} (kg/m ³) | ρ^{exp} (kg/m ³) | | Φ_V (%) | | Weight saving potential (%) | |
|----------|----------------------|-------------------------------------|-----------------------------------|-----------|--------------|------|-----------------------------|------|
| | | | Filament | 3DP | Filament | 3DP | Filament | 3DP |
| H | --- | 950 | 949.32±15 | 948.93±23 | 0.07 | 0.11 | --- | --- |
| H20 | 20 | 944 | 940.73±21 | 938.32±30 | 0.34 | 0.60 | 0.90 | 1.12 |
| H40 | 40 | 938 | 897.41±29 | 892.14±37 | 4.32 | 4.89 | 5.47 | 5.98 |
| H60 | 60 | 932 | 886.28±38 | 872.11±42 | 4.90 | 6.43 | 6.64 | 8.10 |

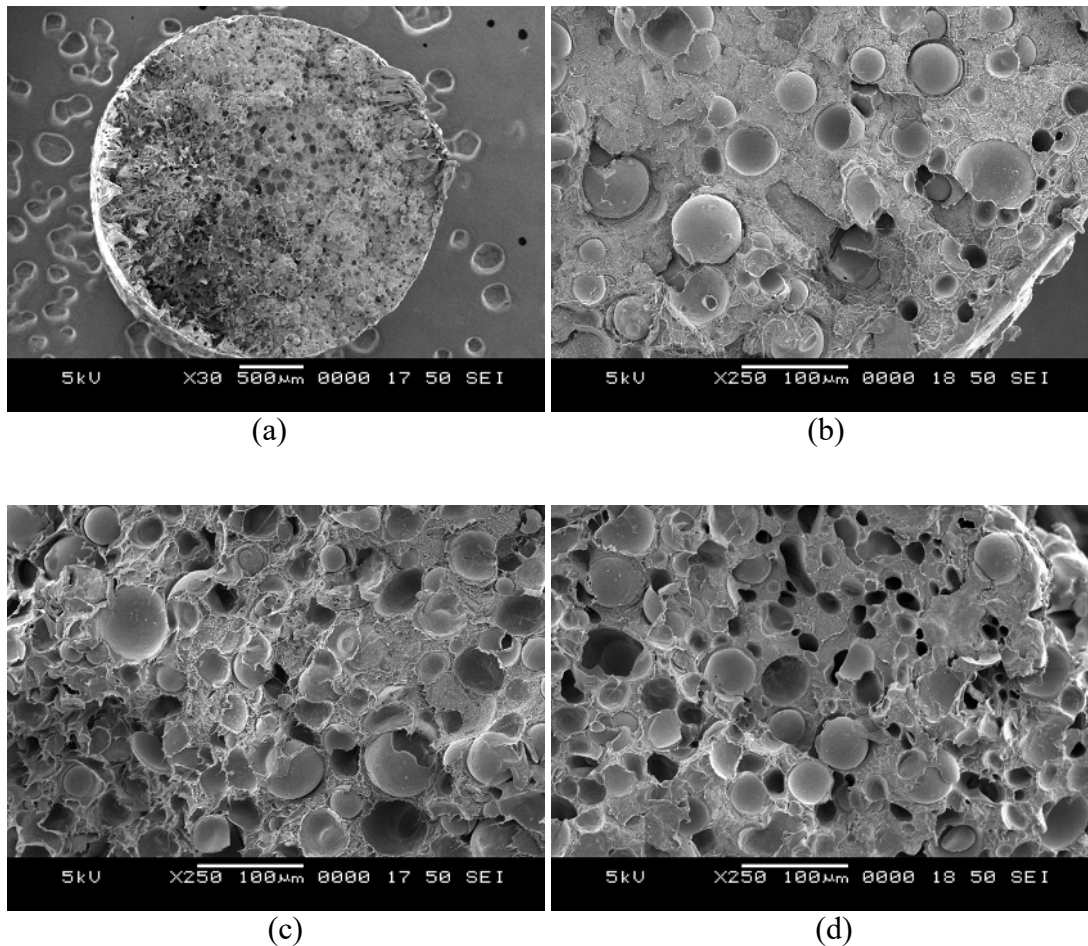


Figure 3.7 Freeze fractured micrographs of (a) filament cross section for H20 at lower magnification (b) H20 (c) H40 and (d) H60 at 250X.

3.3 3D printing of HDPE and their foams

Pilot studies are conducted to obtain the optimum settings for printing with H40 filament. Specimens of size 25×12×6 mm³ are printed using parameters listed in Table 3.3 for each trial setting. The presence of ceramic particles in syntactic foams has been shown to reduce their coefficient of thermal expansion (Shunmugasamy et al. 2012). Such materials would show less shrinkage upon cooling, making them useful in developing 3D printing methods to obtain parts with close dimensional tolerances. Several initial trials in the pilot study did not result in high quality specimens as seen from Figure 3.8. The most significant failure is the development of a bulge in the body of the printed part, which is the result of an excess volume of molten material constrained within the solidified shell which shrinks. The bulge grew as the printing continued and eventually started to interact with the print head. To minimize bulging, the layer height is increased from 0.27 mm to 0.35 mm to allow higher clearance above the part. This change significantly reduced bulging.

Subsequent trials resulted in reducing the feed rate and travel feed rate from 35 mm/s to 30 mm/s, which improved the surface finish, and reduced warpage in the specimens. Optimization of additional parameters such as increasing the print bed temperature from 110°C to 125°C reduced the warping effect at the face of the build that lies away from the cooling fan, but deforms the bottom of the part as more material is deposited on top. Infill percentage is lowered from 100 to 60% to further reduce the amount of extruded material within the solidified shell. These trials resulted in understanding of the effect of each parameter on the build quality.

Based on the initial tests, the build platform temperature is reduced from 125°C to 115°C to allow the cooling of bottom layer so that it can support the weight of layers above. The air cooling fan is disabled to allow slow and uniform cooling and printing surface is covered with a thin sheet of neat HDPE for better adhesion. The optimized print settings used for trial setting 4, listed in Table 3.3, are then used to print the tensile test specimens. Infill pattern is at ±45° to the x-axis (Domingo Espin et al. 2015).

Examples of two 3D printed HDPE and H40-2X tensile specimens are shown in Figure 3.9.

Table 3.3 Pilot study print settings.

| Parameter | Trial 1 | Trial 2 | Trial 3 | Trial 4 |
|-------------------------------|---------|---------|---------|---------|
| Infill (%) | 100 | 100 | 60 | 60 |
| Layer thickness (mm) | 0.27 | 0.35 | 0.35 | 0.35 |
| Feed rate (mm/s) | 35 | 35 | 30 | 30 |
| Print head travel rate (mm/s) | 35 | 35 | 30 | 30 |
| Print Temperature (°C) | 250 | 250 | 250 | 250 |
| Surface Temperature (°C) | 110 | 110 | 125 | 115 |
| Air cooling | on | on | on | off |

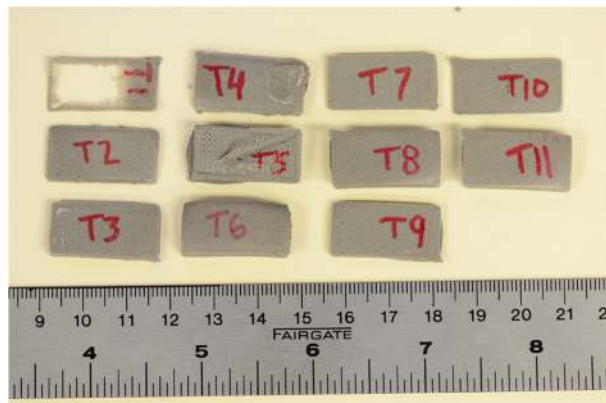


Figure 3.8 Print trials of H40.



Figure 3.9 3D printed (a) HDPE and (b) H40-2X tensile bar.

Density of 3D printed HDPE specimens is $0.855 \pm 0.012 \text{ g/cm}^3$ and H40-2X is 0.95 g/cm^3 , which is 6 and 2% lower than injection molded H40 and H40-2X filaments respectively. The decrease in density of 3D printed specimens is attributed to the presence of porosity between layers. Imaging studies on H40 specimens show a uniform distribution of cenospheres throughout the cross section of specimens printed with 2X (Figure 3.10a) and 3X (Figure 3.10b) filaments. Intact cenospheres are visible in high magnification micrograph (Figure 3.10c) indicating high survival rate through

two and three rounds of extrusion during filament manufacturing and the 3D printing process. Some of the specimens showed defects in the form of porosity in incompletely fused layers at certain locations (Figure 3.10d). However, the process optimization is successful in reducing these defects and providing specimens of density close to the predicted value.

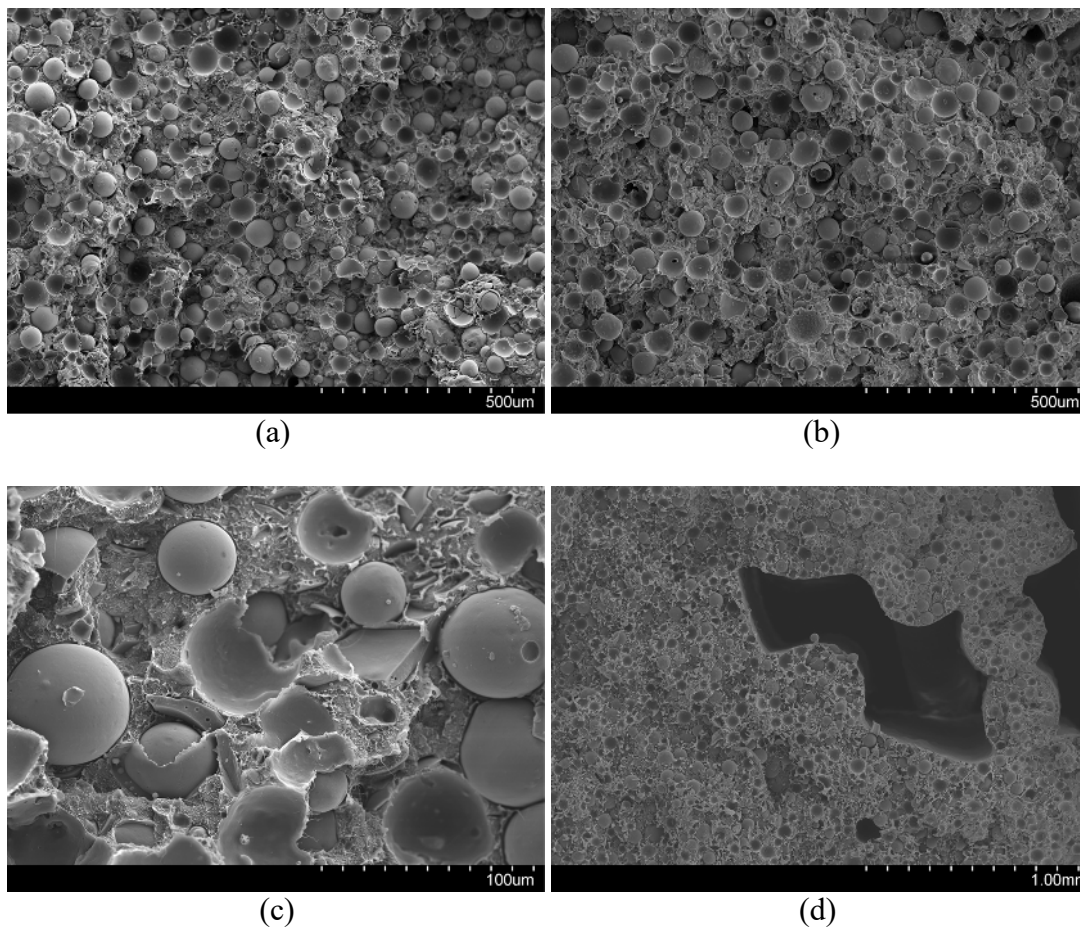


Figure 3.10 Micrographs showing uniform distribution of cenospheres in 3D printed (a) H40-2X (b) H40-3X (c) high magnification micrograph of H40-2X shows cenospheres that survived the filament manufacturing and 3D printing process and (d) a defect in H40-2X specimen where incomplete filling is observed.

Based on pilot experiments carried out using neat HDPE and H40 filament, optimized printing parameters for once extruded neat HDPE, H20, H40 and H60 (ϕ 2.85 ± 0.05 mm) are finalized and are listed in Table 3.4. H, H20, H40 and H60 printed representative sample are presented in Figure 3.11. Infill is fixed at 100% to print fully

dense foam samples to achieve targeted enhanced structural stability and to compare with fully dense injection/compression molded foams.

Table 3.4 Optimized printing parameters.

| Printing parameters | Typical Value |
|-------------------------------|--------------------------------------|
| Nozzle temperature (°C) | 250 |
| Printing bed temperature (°C) | 115 |
| Layer thickness (mm) | 0.35 |
| Multiplier | 1 for H, H20, H40 and 1.2 for H60 |
| Printing speed (mm/sec) | 30 |
| Printing pattern | Rectilinear |
| Part orientation | Y-axis |
| Infill (%) | 100 |

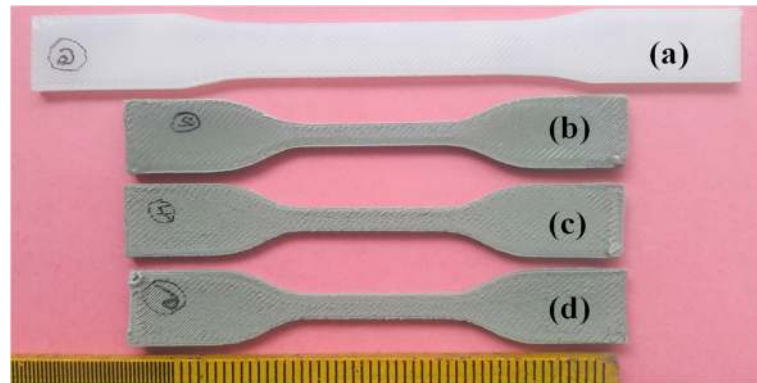


Figure 3.11 3D printed (a) HDPE (b) H20 (c) H40 (d) H60 tensile bar.

Parameters chosen for 3D printing (Table 3.4) exhibited seamless interface bonding between the layers (Figure 3.12a) and minimum warpage. Micrographs of freeze-fractured as 3D printed samples for neat HDPE and H60 is presented in Figure 3.12b-d. Voids are not seen in neat HDPE (Figure 3.12b) while H60 micrograph depicts the uniform distribution of intact cenospheres post printing and elongated voids (Figure 3.12c) as mentioned earlier. Density drop in prints compared to HDPE signifies the void content and particle survival post 3D printing process. Void content (Table 3.2) in printed samples are higher as against the filament owing to the air gaps between bonded adjacent raster (Figure 3.12d). These gaps are more prominent at higher filler loadings owing to higher melt viscosity and lower matrix phase. Such additional air gaps in these

3D printed closed cell foams as compared to their filament counterparts results in better weight saving potential (Table 3.2).

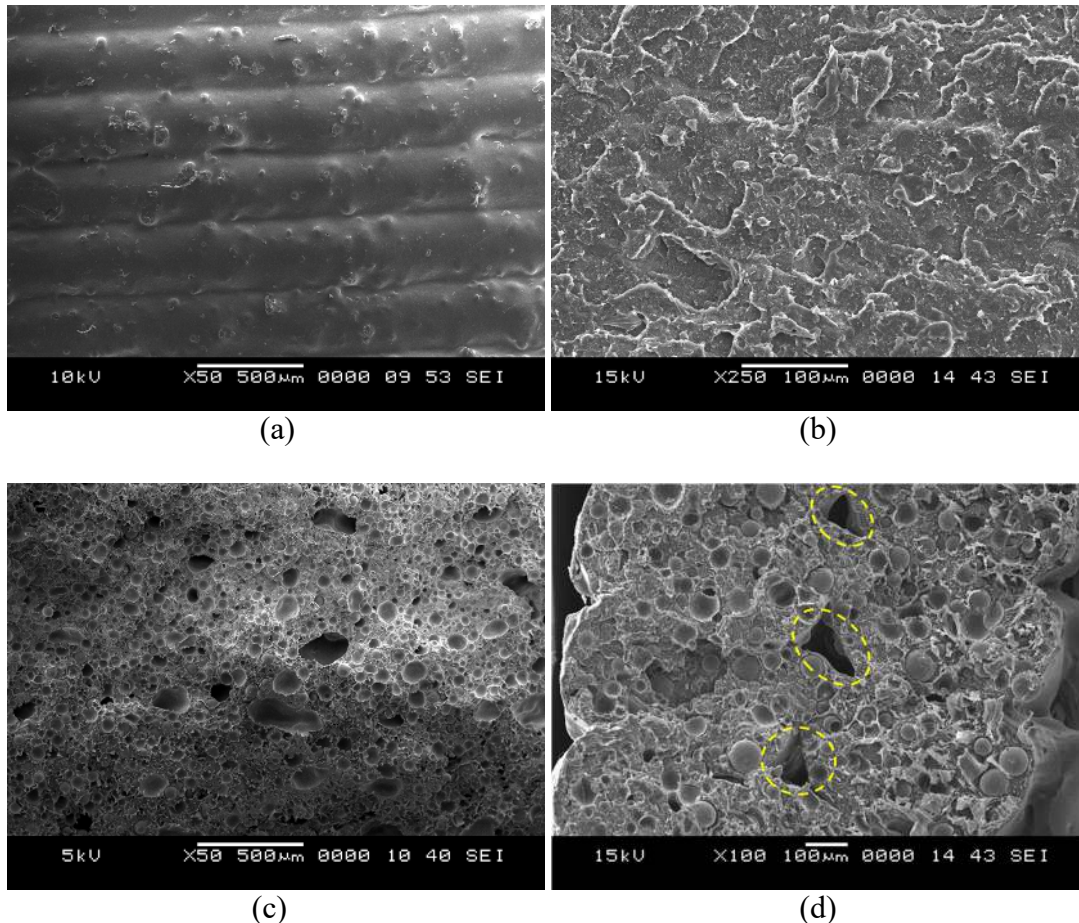


Figure 3.12 SEM of representative (a) 3D printed sample in thickness direction (b) freeze fractured HDPE (c) H60 and (d) air gap (marked area) between raster.

3.4 DSC of filament and 3D prints

Degree of crystallinity (α_{cryst}), melting peak temperature (T_{Melt}) and crystallization temperature (T_{Cryst}) are investigated for both filament and prints for analyzing thermal behavior (Table 3.5). Figure 3.13 presents the DSC thermograms of the samples. Compared to HDPE (108.2°C) all the foam filaments exhibited gradual increment in T_{Cryst} . Amid HDPE matrix cooling, at comparatively higher temperature melt nucleates on the cenosphere surface forming crystal lamellas of larger thickness resulting in higher T_{Cryst} (Shaikh et al. 2016). 3D prints follow a similar trend. It signifies that additional processing has no significant effect on the crystallization temperature. There

is no appreciable change observed in T_{Melt} of the filament and prints indicating the addition of filler and processing step do not influence T_{Melt} (Table 3.5). Degree of crystallinity α_{cryst} in foam filaments decreases as cenosphere content increases as compared to H (33.15%).

Table 3.5 T_{Cryst} , α_{cryst} and T_{Melt} of samples.

| Material | T_{Cryst} (°C) | | α_{Cryst} (%) | | T_{Melt} (°C) | |
|----------|------------------|-------|----------------------|------|-----------------|-------|
| | Filament | 3DP | Filament | 3DP | Filament | 3DP |
| H | 108.2 | 109.5 | 55.5 | 57.1 | 131.7 | 131.2 |
| H20 | 111.4 | 110.5 | 43.4 | 45.6 | 131.5 | 130.9 |
| H40 | 112.5 | 110.6 | 41.5 | 44.8 | 130.6 | 129.5 |
| H60 | 112.6 | 111.3 | 37.1 | 39.9 | 130.2 | 129.8 |

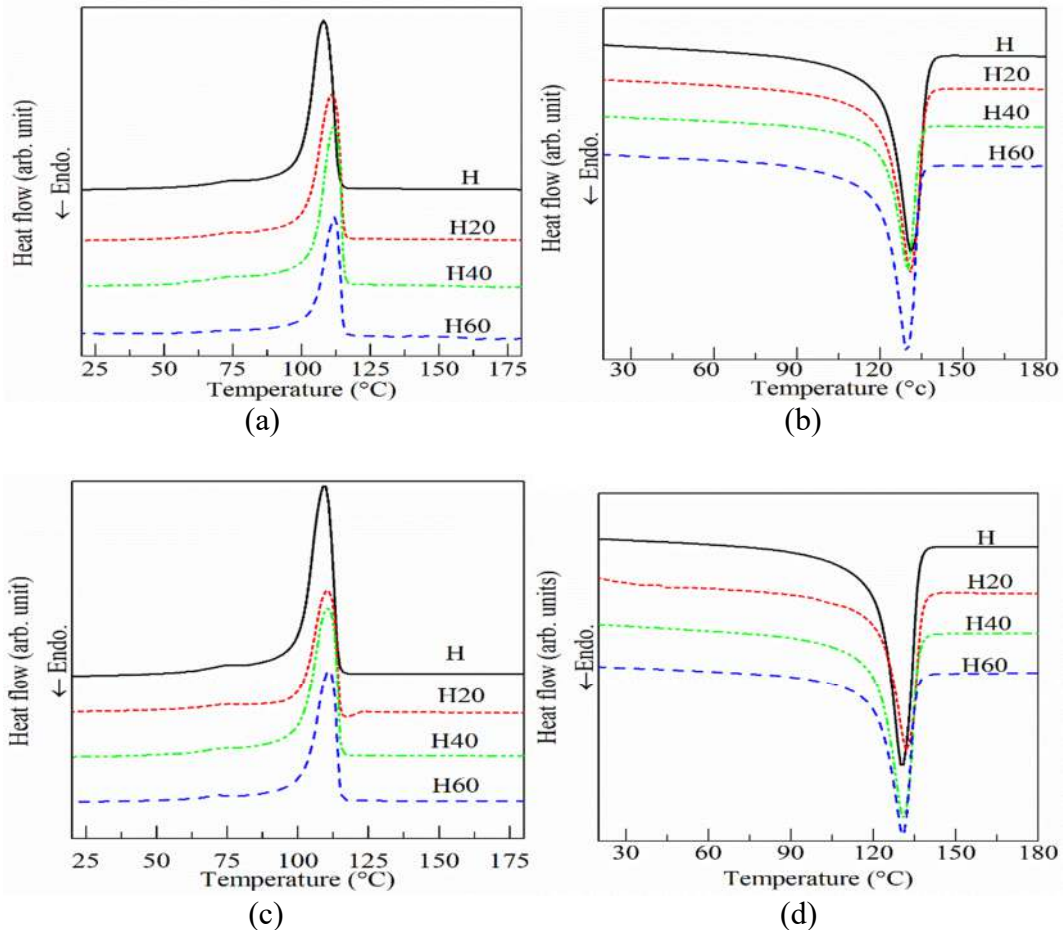


Figure 3.13 DSC thermograms for crystallization peak from cooling cycle in (a) filament (c) 3D prints and melting peak from second heating cycle in (b) filament (d) 3D prints.

Printed specimen follows a similar trend. α_{cryst} dropped from 57.1 (H) to 39.9% (H60) in prints. Degree of crystallinity is higher in prints compared to their respective filaments. Printed samples are allowed to cool through natural convection mode in the build chamber of the 3D printer while filaments are rapidly cooled in the water bath post extrusion leading to such an observation (Wasiak et al. 1999). Further, as filament gets quenched in a water bath there is not enough time and energy for the melt to crystallize (Yang et al. 2017). Drop in α_{cryst} of foams is due to the hindrance caused by filler particles to the polymer chain movement in addition to the reduction of crystal domain in HDPE (Deepthi M V et al. 2010, Panupakorn et al. 2013, Sewda and N. Maiti 2010).

3.5 XRD analysis of filament and 3D prints

Effect of cenospheres addition on the crystallinity of HDPE is investigated by conducting XRD analysis. The results of XRD analysis are summarized in Table 3.6. XRD pattern for feedstock filament and printed material is presented in Figure 3.14a and Figure 3.14b respectively. It is a well-known fact that based on processing condition and parameters HDPE is having monoclinic, orthorhombic and monoclinic crystal structure (Bassett 1976, Takahashi et al. 1988). Neat HDPE filament XRD spectra show two intense peak one at each 21.66° and 23.91° . These peaks represent the orthorhombic crystal structure of HDPE at (110) and (200) lattice plane (Lei et al. 2007, Lin et al. 2005).

Cenospheres/HDPE filament XRD pattern is similar to neat HDPE wherein peak positions are remained same while the reduction in peak intensity is observed as cenospheres percentage increases. Apart from two peaks one additional peak is also observed in foam material at around $\sim 25.2^\circ$ which corresponds to cenospheres (Shahapurkar et al. 2018). The drop in characteristic peak intensity and sharpness of peak indicates decreasing crystallinity. DSC results of filament also support this fact. There is no change in the diffraction pattern of printed foam samples compared to extruded foam filament, whereas printed neat HDPE peaks are more intense and narrower compared to extruded filament. This may be due to additional heating cycle

and more aligned pattern of material deposition which is reflected by crystallinity enhancement. The crystallinity percentage is in agreement with the DSC results.

Table 3.6 XRD data of neat HDPE and foam material.

| Material | Peak Position 2θ ($^{\circ}$) | | Peak Position 2θ ($^{\circ}$) | | α_{cryst} (%) | |
|----------|--|-------|--|-------|-----------------------------|-------|
| | Filament | 3DP | Filament | 3DP | Filament | 3DP |
| H | 21.66 | 23.91 | 21.22 | 23.67 | 49.33 | 54.03 |
| H20 | 22.26 | 23.73 | 21.08 | 23.40 | 42.52 | 45.25 |
| H40 | 22.36 | 23.76 | 21.06 | 23.42 | 38.45 | 40.23 |
| H60 | 22.30 | 23.80 | 21.10 | 23.48 | 35.56 | 37.98 |

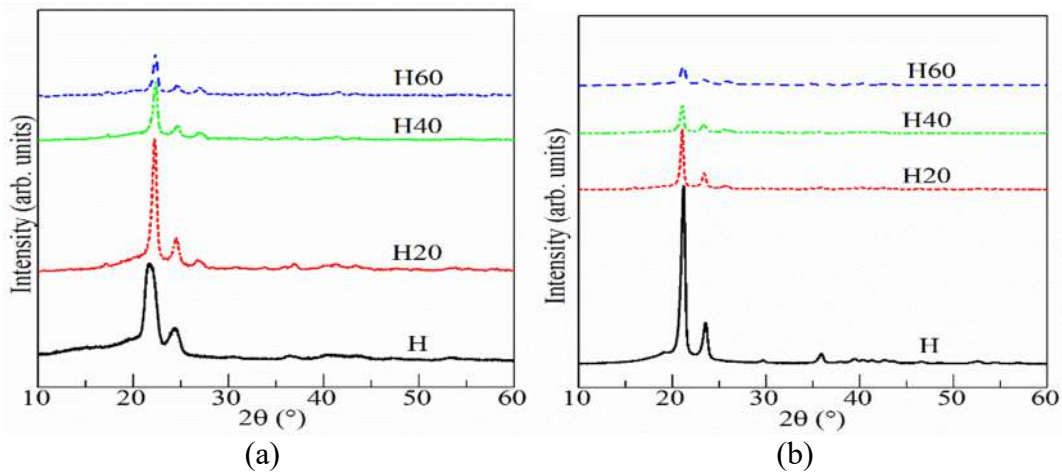


Figure 3.14 XRD pattern of (a) filament and (b) printed specimen.

3.6 Coefficient of thermal expansion of prints

Filler addition reduces CTE (Table 3.7) (Baglari et al. 2011, Shunmugasamy et al. 2012). Incorporation of cenospheres into neat HDPE provides dimensional stability at higher printing temperatures (Labella et al. 2014). CTE reduction signifies dimensional stability and lowers thermal stresses resulting in minimized warpage (Baglari et al. 2011). CTE of cenospheres ($3.3 \times 10^{-6}/^{\circ}\text{C}$) (Baglari et al. 2011) and HDPE ($127 \times 10^{-6}/^{\circ}\text{C}$) are quite apart and hence cenospheres loading decreases CTE substantially. CTE values give an insight into raster diffusion mechanism while printing. Part lifting and warpage are observed while printing pure HDPE due to higher CTE (Figure 3.15a). Warpage issues are not encountered while printing foam (Figure 3.15b). It resembles that, the gas of lower thermal conductivity inside hollow cenospheres is restricting the heat flow (Atagur et al. 2018, Labella et al. 2014). H60 composition registered lowest

CTE indicating minimum molten raster expansion in prints leading to under diffusion of adjacent rasters. As a consequence, the air gap in prints is seen (Figure 3.12d). CTE reduction leads to rise in air gaps making 3D printed components to be three-phase foam structures making them lighter than the closed cell foams.

Table 3.7 CTE values of 3D printed HDPE and their foams.

| Material | CTE $\times 10^{-6}$ ($^{\circ}\text{C}$) | % reduction w.r.t 'H' |
|----------|---|-----------------------|
| H | 127 \pm 4.29 | --- |
| H20 | 93.2 \pm 3.91 | 26.61 |
| H40 | 82.4 \pm 2.78 | 35.11 |
| H60 | 20.3 \pm 1.08 | 84.01 |

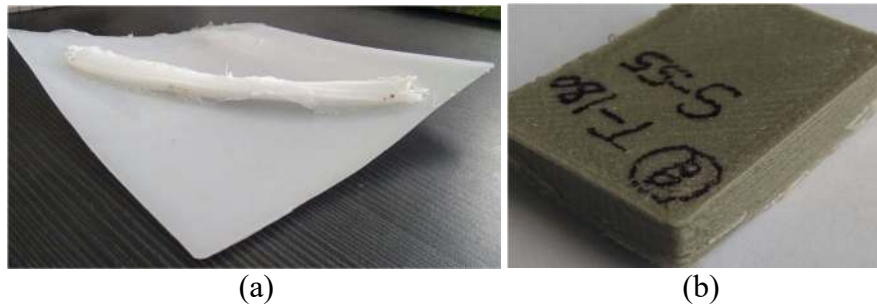


Figure 3.15 Representative images of (a) warped neat HDPE print and (b) intact non warped foam print.

4 TENSILE BEHAVIOR OF FILAMENT and 3D PRINTS

Recyclability potential of filaments at 10^{-2} , 10^{-3} and 10^{-4} and their prints at 10^{-3} are discussed in Section 4.1 and 4.2 respectively. Based on these pilot study results, Section 4.3 and 4.4 elaborates on finding of once extruded filament and their foam prints investigated under tensile loading condition as per ASTM D638-14.

4.1 Tensile behaviour of HDPE (1X, 2X and 3X) and H40 (2X, 3X) filament

Filament needs to meet a certain requirement to be utilized as feedstock material in the 3D printer without changing functional hardware and software. It must retain its shape without buckling while passing through drive rollers to absorb frictional forces (Lombardi et al. 1997). Buckling can be prevented making the filament stiff enough to resist drive roller push without getting deformed and fractured in the printer head. HDPE resin shows a ductile behavior with necking and plastic deformation. Similar deformation pattern for H-2X and 3X filaments is observed at all strain rates. In comparison, failure mode of the H40-2X and 3X filaments is observed to be brittle without any visible sign of necking, which is also observed in injection molded syntactic foams (Bharath Kumar et al. 2016). Inclusion of stiffer cenospheres in relatively soft and compliant HDPE matrix leads to such a behavior.

Figure 4.1a-e presents stress-strain plots for neat HDPE (1X, 2X and 3X) and H40 (2X and 3X) filaments at different strain rates. Most filaments fracture at a lower strain of 12-15% compared to the injection molded ones (over 100% strain) (Bharath Kumar et al. 2016). The modulus and yield strength (0.2% strain offset method) values for HDPE filaments are listed in Table 4.1. The modulus is 11, 2 and 6% higher for H-3X filament compared to H-1X at strain rates of 10^{-4} , 10^{-3} and 10^{-2} , respectively. Although this change is very small, the values are higher for all strain rates for filaments compared to the injection molded specimens. HDPE extrusion cycles leads to alignment of polymer chains (Picot 1984), resulting in increase in yield strength and modulus. At the same time, thermal processing of HDPE leads to crosslinking in the individual polymer chains, increasing stiffness as reported previously by other groups (Yin et al. 2015). Increase in strain rate increases filament modulus and strength. Ultimate tensile

strength (UTS) values of the 1X, 2X and 3X filaments at the same strain rates show an increasing trend, further backing the hardening process due to crosslinking.

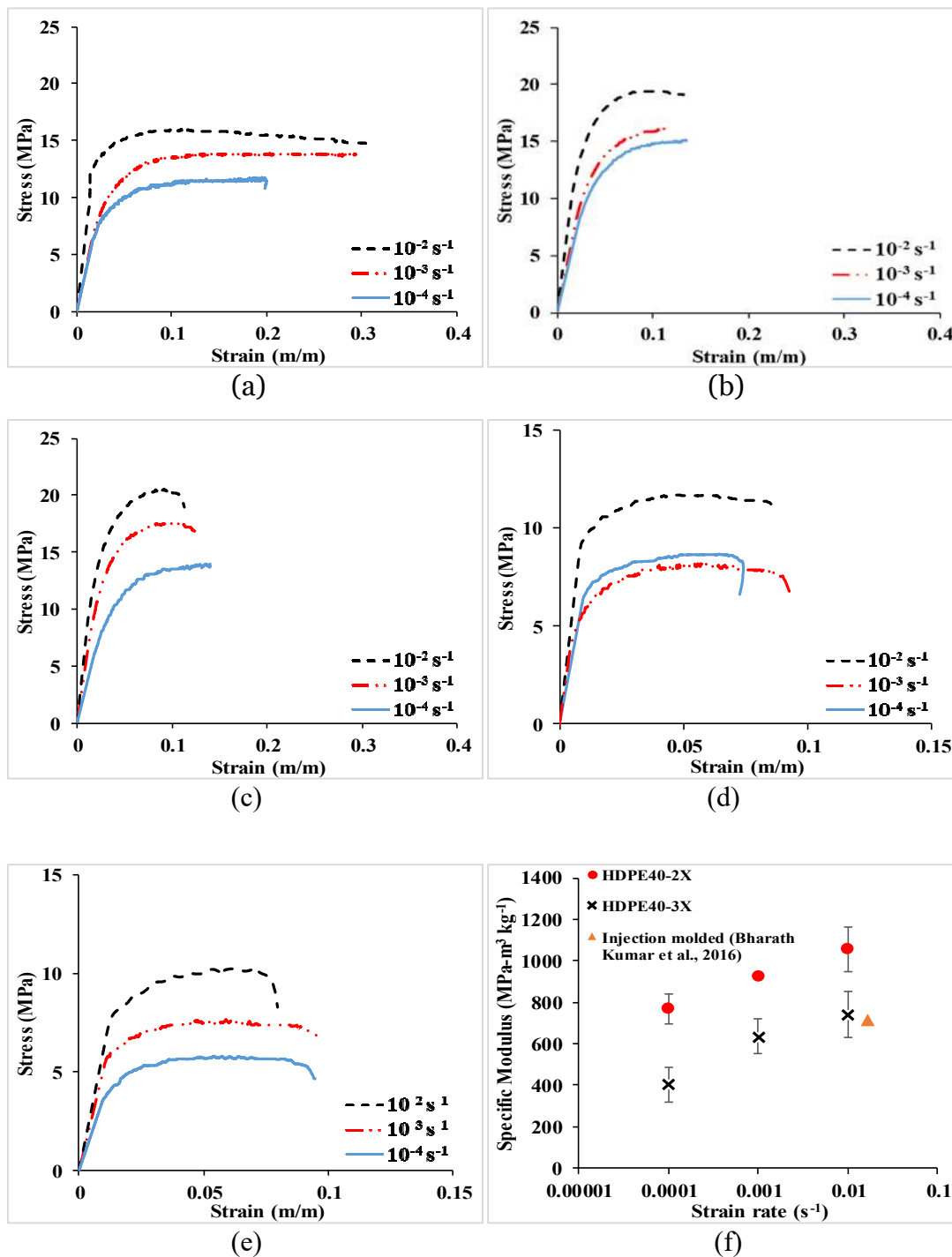


Figure 4.1 Representative stress vs. strain curves for tensile behavior of (a) H-1X (b) H-2X (c) H-3X (d) H40-2X (e) H40-3X filaments and (f) The specific modulus versus strain rate plot for H40 filaments versus injection molded H40.

A similar trend in modulus with strain rate is noted for H40-2X and 3X specimens (Figure 4.1d-e and Table 4.1). The only anomaly of this trend is observed in yield strength and ultimate tensile strength of H40-2X at 10^{-3} s^{-1} , which shows lower values than 10^{-4} s^{-1} strain rates as observed in Figure 4.1d. Nonetheless, given trends of all other materials in this study, this one test condition results are anomaly. Since densities of both these filaments are about the same, reduction in mechanical properties of H40-3X is likely because of orientation of broken fragments of cenospheres during extrusion process, leading to failure due to stress concentration effects. Thin walled ceramic fragments have two orders of magnitude higher stiffness than the matrix resin and sharp edges, which can cause severe stress concentration effects at the interface and initiate cracks. The strength of syntactic foams in all extruded conditions is in a narrow range, which can be useful in 3D printed components by making their properties more predictable and reliable.

Table 4.1 Tensile properties of extruded HDPE and H40 filaments.

| Filament | Strain rate (s^{-1}) | Modulus (MPa) | Yield strength (MPa) | Ultimate tensile strength (MPa) |
|----------|---------------------------------|---------------|----------------------|---------------------------------|
| H-1X | 10^{-4} | 353±28 | 6.7±1.5 | 11.5±0.6 |
| | 10^{-3} | 536±26 | 8.0±0.2 | 12.7±0.9 |
| | 10^{-2} | 687±33 | 13.3±0.7 | 16.1±0.3 |
| H-2X | 10^{-4} | 380±39 | 8.8±0.8 | 14.6±0.8 |
| | 10^{-3} | 521±10 | 10.0±0.4 | 17.3±0.6 |
| | 10^{-2} | 719±13 | 12.3±0.3 | 20.3±1.0 |
| H-3X | 10^{-4} | 397±55 | 6.1±1.7 | 13.9±1.3 |
| | 10^{-3} | 545±70 | 10.3±1.6 | 17.8±0.9 |
| | 10^{-2} | 732±59 | 13.1±1.2 | 21.0±1.0 |
| H40-2X | 10^{-4} | 744±71 | 7.2±0.2 | 8.6±0.3 |
| | 10^{-3} | 897±9 | 5.1±0.2 | 8.0±0.1 |
| | 10^{-2} | 1020±11 | 9.8±0.4 | 11.7±0.0 |
| H40-3X | 10^{-4} | 403±83 | 5.6±1.6 | 7.0±0.8 |
| | 10^{-3} | 620±84 | 6.4±0.6 | 8.8±0.7 |
| | 10^{-2} | 722±11 | 6.9±1.5 | 9.0±1.3 |

Figure 4.1f summarizes the results of tensile behavior for H40 processed by injection molding and filament extrusion methods. H40-2X and 3X filaments show an increasing trend in specific modulus with the strain rate. The specific modulus of H40-3X filament

is similar to that of injection molded specimen (Bharath Kumar et al. 2016). The specific modulus is strongly influenced by the number of intact particles in the matrix during processing. The results suggest that the particle survival rate is similar in both processes.

Figure 4.2a-b present tensile failure features in H40-2X filament at 10^{-4} s^{-1} strain rate. Plastic deformation of HDPE matrix can be observed in the form of long fibrils. In addition, some broken and intact cenospheres are also observed in these micrographs. Due to extremely high failure strain in thermoplastic resins and poor interfacial bonding between particle and matrix, the appearance of excessive plastic deformation of matrix and relatively unaffected particles is common for such materials, which is also observed in studies related to injection molded specimens (Bharath Kumar et al. 2016).

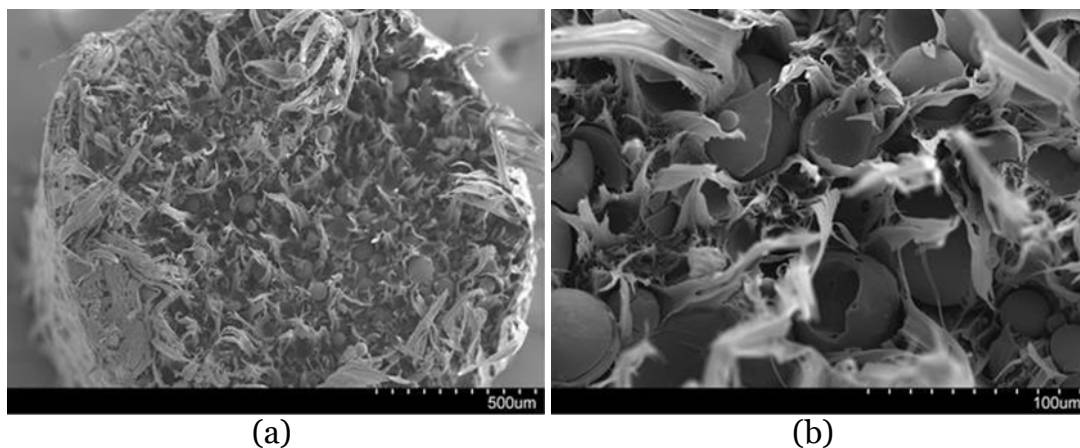
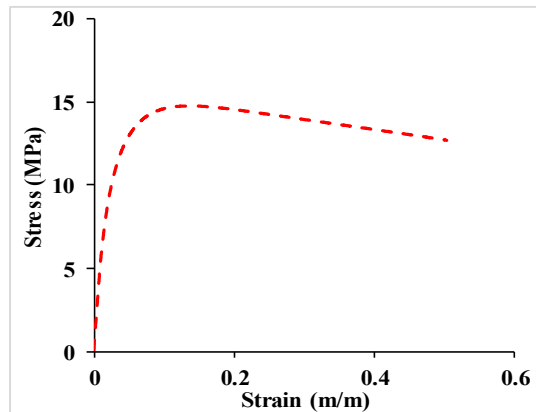


Figure 4.2 Tensile fracture surface of H40-2X filament tested at 10^{-4} s^{-1} at (a) low and (b) higher magnifications.

4.2 Tensile behaviour of HDPE and H40 (2X, 3X) prints

A representative stress-strain graph for 3D printed HDPE specimen is shown in Figure 4.3a. Tests are stopped at 50% strain. A linear section in the elastic region is used to calculate the modulus and yield strength is obtained by using the 0.2% offset method. The plot shows a peak at 13% strain followed by a slow drop in stress. The elastic modulus, yield strength and ultimate tensile strength are 632 ± 76 , 6.6 ± 0.6 and 14.3 ± 0.3 MPa, respectively. 3D printed HDPE shows 18% higher modulus and 17.5% lower yield strength compared with extruded filament at strain rate of 10^{-3} s^{-1} .



(a)



(b)

Figure 4.3 (a) Representative stress-strain curve for HDPE tensile samples at 10^{-3} s^{-1} strain rate, and (b) failure mode for HDPE tensile bar at 50% strain.

Compared to injection molded HDPE, the modulus of 3D printed HDPE is 16% higher (Bharath Kumar et al. 2016). Failure mode of a 3D printed HDPE specimen at 50% strain is shown in Figure 4.3b where a fibrous fracture is observed due to elongation of individual filaments extended in longitudinal directions, which causes separation of the printed layers. Although 3D printed specimens perform comparably to the molded specimens, further process improvements could be conducted to obtain monolithic specimens from 3D printing.

The tensile behavior of a representative set of 3D printed H40-2X and 3X specimens is compared in Figure 4.4a. Unlike HDPE samples, stress-strain curves do not show a peak and the stress rises with strain until failure due to increased brittleness of the material caused by the presence of ceramic particles. Failure strain is less than 6% for all the 3D printed H40 specimens, which is 30-40% lower than H40 filaments, indicating that the material becomes brittle by the 3D printing process. The failure of H40-2X is brittle in nature as shown in Figure 4.4c. Tensile modulus of 3D printed H40-

2X and 3X (Table 4.2) are 1.6 and 2.6 times higher than that of 2X and 3X filaments, respectively. This enhancement is likely due to additional crosslinking and realignment of polymer chains during the high temperature extrusion process during printing as suggested by some of the existing studies (Picot 1984, Yamaguchi and Suzuki 2002). Crystallization of HDPE due to thermal gradients can also contribute to such enhancement in mechanical properties (Bin et al. 2015). The fracture surface of a H40-3X specimen is shown in Figure 4.4b. The primary failure mode of the specimens is matrix fracture by plastic deformation. Cenospheres are intact on the fracture surface.

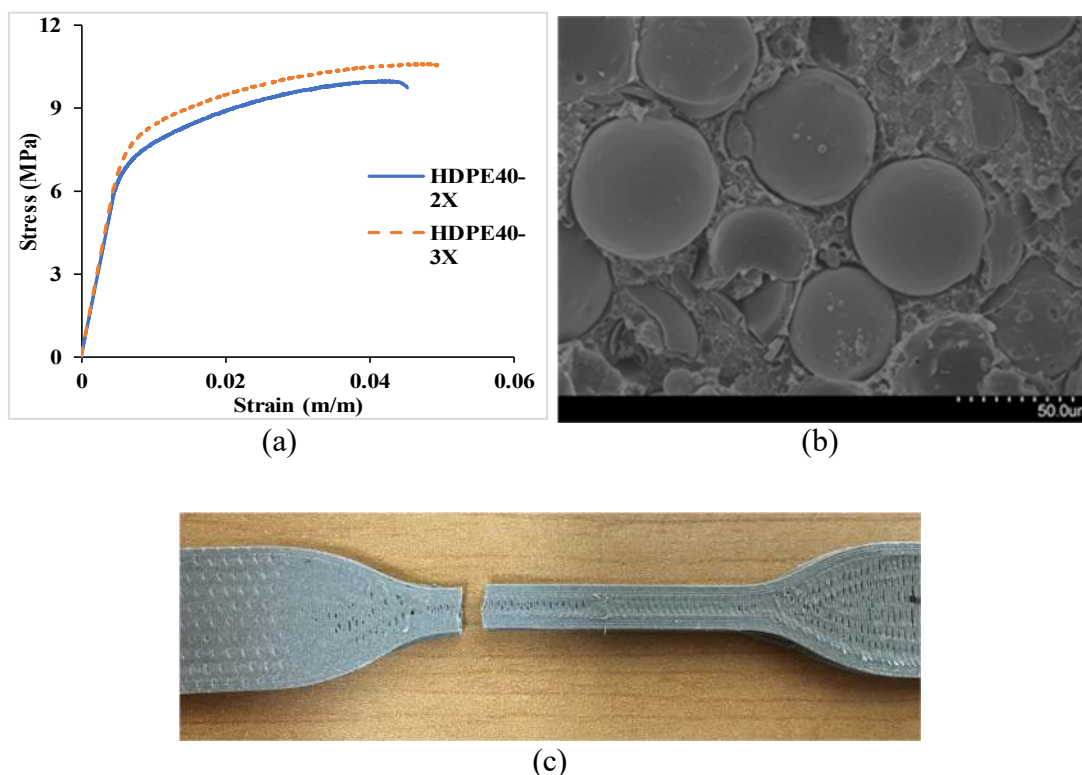


Figure 4.4 (a) Representative stress-strain plots for 3D printed H40-2X and H40-3X tensile specimens, (b) intact cenospheres on the fracture surface of a tensile tested H40-3X specimen and (c) failure mode in H40-2X specimen.

The specific modulus of molded H40 obtained in an earlier study at $1.6 \times 10^{-2} \text{ s}^{-1}$ strain rate was $717 \pm 27 \text{ MPa-cm}^3/\text{g}$, which is 51% and 44% that of 3D printed H-2X and 3X specimens tested at 10^{-3} s^{-1} (Bharath Kumar et al. 2016, Bharath Kumar et al. 2016). The mechanical properties of cenosphere/HDPE syntactic foams are highly strain rate sensitive and show an increasing trend with strain rate. Therefore, it is expected that

the mechanical properties of 3D printed H40-2X and 3X will be even higher at the comparable strain rates.

Table 4.2 Tensile properties of 3D printed H40-2X and 3X specimens.

| Material | Elastic modulus (MPa) | Density (g/cm ³) | Specific elastic modulus (MPa-cm ³ /g) | Yield strength (MPa) | UTS (MPa) | Fracture strain (%) |
|--|-----------------------|------------------------------|---|----------------------|-----------|---------------------|
| H40-2x | 1337±109 | 0.950 | 1407±115 | 7.0±0.4 | 10.1±0.1 | 5.2±0.5 |
| H40-3x | 1569±143 | 0.959 | 1636±149 | 7.4±0.5 | 10.7±0.2 | 5.1±0.1 |
| Injection Molded H40 (Bharath Kumar et al. 2016) | 723±27 | 1.008 | 717±27 | ----- | 12.1±0.44 | 9.42±0.72 |

As mentioned earlier, henceforth in the thesis, investigations are carried out for once extruded filaments and their prints at strain rates as mentioned in the respective ASTM standards (Tensile, Flexural and Compression).

4.3 Tensile behaviour of HDPE, H20, H40 and H60 filament

Higher filler loading increases filament modulus by 7.72-12.79% as compared to HDPE (Table 4.3). Filament stiffness increases due to stiffer intact cenospheres presence in compliant HDPE matrix. Figure 4.5 presents representative stress-strain plots (for clarity only up to 30% strain is included) of HDPE and their foam filaments. It is observed that pure HDPE filament undergoes elongation more than 200% strain and the test is discontinued due to time and machine span length constraint. Such higher elongation values without filament failure are due to the ductile nature of HDPE.

On the contrary, foam filaments failed within 30% stain. Among the foam filaments, H20 composition registered the highest ultimate strength (10.30 MPa) and strain at break (26.20%). Filament micrography (Figure 3.7) reveal voids across the cross-section of the filament which gets elongated leading to coalesce when pulled under tensile load to get fractured finally. The decreasing trend in strength and break strain is

likely due to the incorporation of stiffer cenospheres and the subsequent reduction in the ductile phase (HDPE).

Table 4.3 Tensile properties of filament and 3D printed material.

| Material | Modulus (MPa) | | UTS (MPa) | | Elongation at UTS (%) | | Fracture strength (MPa) | | Fracture strain (%) | |
|----------|---------------|----------------|----------------|----------------|-----------------------|----------------|-------------------------|----------------|---------------------|----------------|
| | Filament | 3DP | Filament | 3DP | Filament | 3DP | Filament | 3DP | Filament | 3DP |
| H | 813.26 ±22 | 946.20 ±35 | 14.90 ±0.22 | 18.84 ±0.28 | 13.9 ±0.23 | 12.99 ±0.26 | --- | 6.78 ±0.29 | --- | 142.9 ±5.89 |
| H20 | 876.05 ±31 | 1125.10 ±39 | 10.30 ±0.34 | 12.31 ±0.39 | 6.70 ±0.29 | 5.99 ±0.33 | 7.73 ±0.29 | 11.45 ±0.33 | 26.20 ±0.15 | 8.23 ±0.33 |
| H40 | 895.19 ±34 | 1351.60 ±44 | 7.56 ±0.32 | 11.25 ±0.41 | 3.90 ±0.31 | 1.46 ±0.35 | 5.34 ±0.19 | 10.89 ±0.25 | 15.00 ±0.22 | 1.51 ±0.06 |
| H60 | 971.25 ±38 | 1622.37 ±57 | 5.62 ±0.23 | 12.50 ±0.53 | 2.30 ±0.11 | 1.44 ±0.21 | 4.33 ±0.14 | 12.09 ±0.19 | 3.30 ±0.31 | 1.51 ±0.07 |

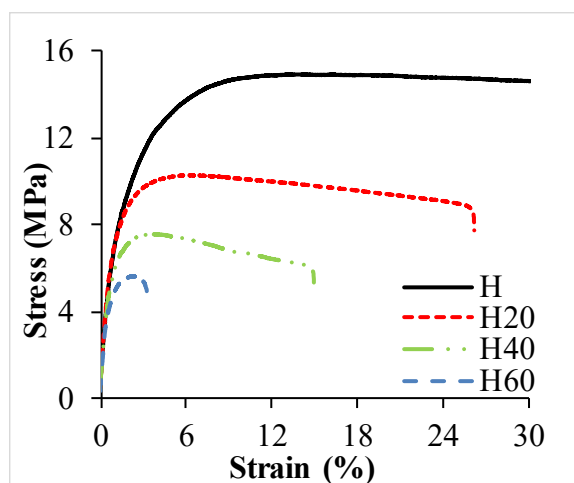


Figure 4.5 Representative stress-strain plot of neat HDPE and syntactic foam feedstock filament.

4.4 Tensile behaviour of HDPE, H20, H40 and H60 prints

Tensile tested printed samples response is plotted in Figure 4.6 and the results are summarized in Table 4.3. HDPE filament exhibits different response (Figure 4.5) as compared to a printed counterpart (Figure 4.6a). HDPE filament did not break even after 1000% strain while printed sample failed below 150% strain (Figure 4.6a) indicating brittle behavior post printing. A similar observation is noted in foams as well. Neat HDPE shows failure strain over 130% whereas syntactic foam specimens

exhibited failure at ~1.5-8%. Neat HDPE underwent plastic deformation from ~60-130% strain. Long necking region is clearly evident in HDPE (Figure 4.7a) due to fibrillation of individual raster resulting in broom-like fibrous ends. Printed foam exhibit brittle failure without remarkable plastic deformation (Figure 4.7b). Failure of syntactic foam specimens is initiated with plastic deformation of matrix phase at raster planes in the presence of stiff intact cenospheres (Figure 4.7c). Infusion of stiffer cenospheres into matrix leads to such behavior. Compared to injection molded HDPE, printed HDPE registered higher elastic modulus (78.86%) with comparable UTS, elongation at ultimate strength and fracture strain while fracture strength gets doubled (Bharath Kumar et al. 2016). Foam modulus increases as filler percentage increases (Table 4.3). H60 registered the highest modulus among other foam compositions and is 71.46% higher compared to its HDPE counterpart. 3D printed HDPE and foams modulus is 1.16, 1.28, 1.51 and 1.67 times better than the respective feedstock due to the realignment of the polymer chain and additional crosslinking during 3D printing.

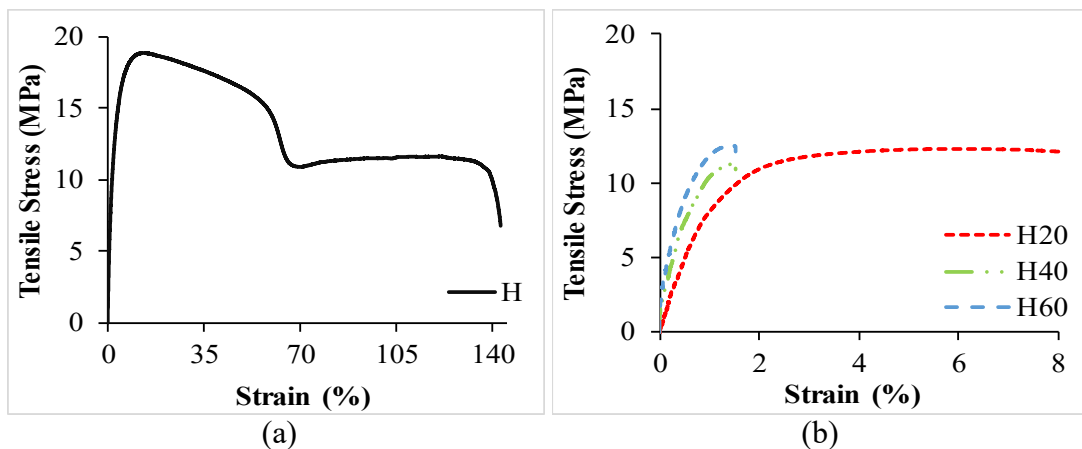


Figure 4.6 Representative stress-strain plot for 3D printed (a) HDPE and (b) their foams.

Modulus of printed cenosphere/HDPE foams is higher in the range of 96.01 to 144.45% as compared to injection molded ones (Bharath Kumar et al. 2016) indicating 3D printing potential in replacing injection molded components with zero lead time and tooling cost. UTS of foams is lower as compared to printed HDPE as constituents are blended without any surface treatment and thereby does not promote interfacial adhesion. UTS and fracture strength of printed material is almost equal to injection

molded material (Bharath Kumar et al. 2016). Printed foam registered lower elongation at UTS as compared to injection molded foams. Presence of stiffer cenospheres results in absence of necking and plastic deformation in printed foams (Figure 4.7b) and is also reflected in the stress-strain plot (Figure 4.6b). Fracture strength of printed foam is 1.78 times higher as compared to neat HDPE. Specific properties of the foams are vital in weight sensitive structures as printing renders the flexibility of integrated components with complex geometry. The specific strength of neat HDPE ($0.01985 \text{ MPa}/(\text{kg}/\text{m}^3)$) is higher as compared to foams (Table 4.4). H60 registered the highest specific strength among foams. Printed foams have the potential to be used in weight saving the application as depicted by E/ρ , E/ρ^2 and E/ρ^3 values in Table 4.4.

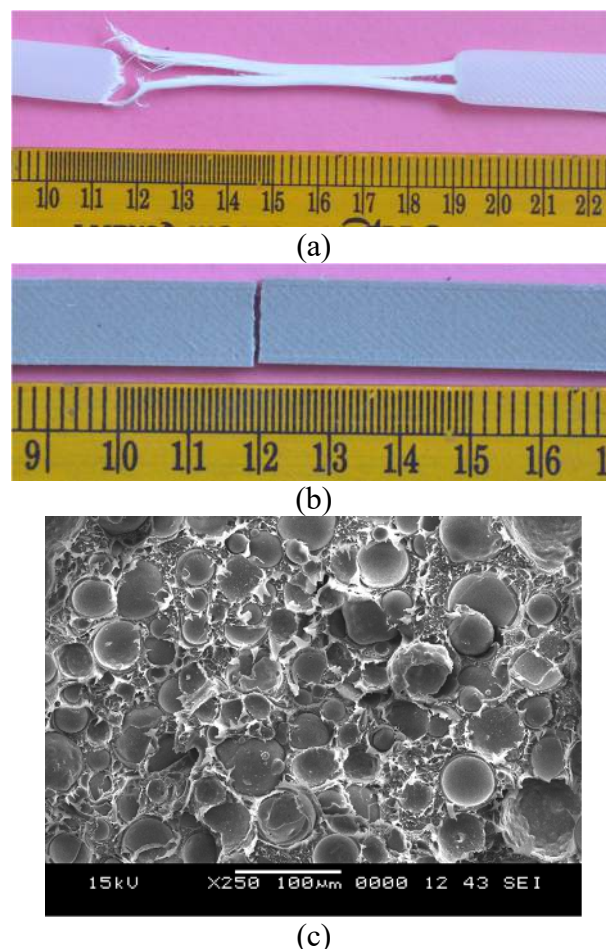


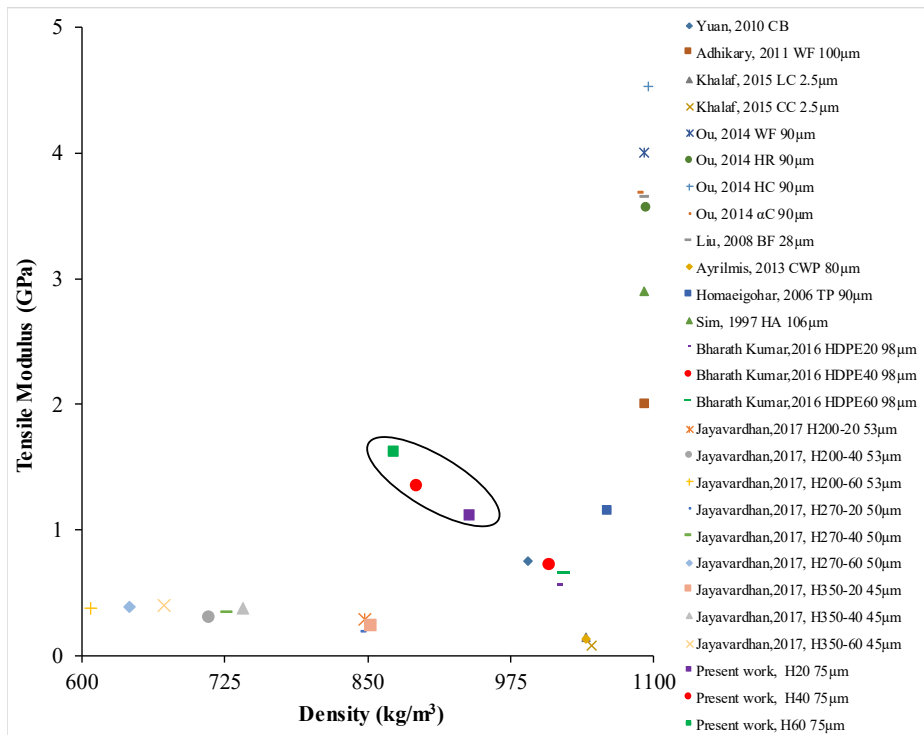
Figure 4.7 Representative failed 3D printed sample of (a) HDPE (b) H60 and (c) SEM of H60 post tensile test.

Table 4.4 Specific properties of syntactic foams fabricated using a 3D printer.

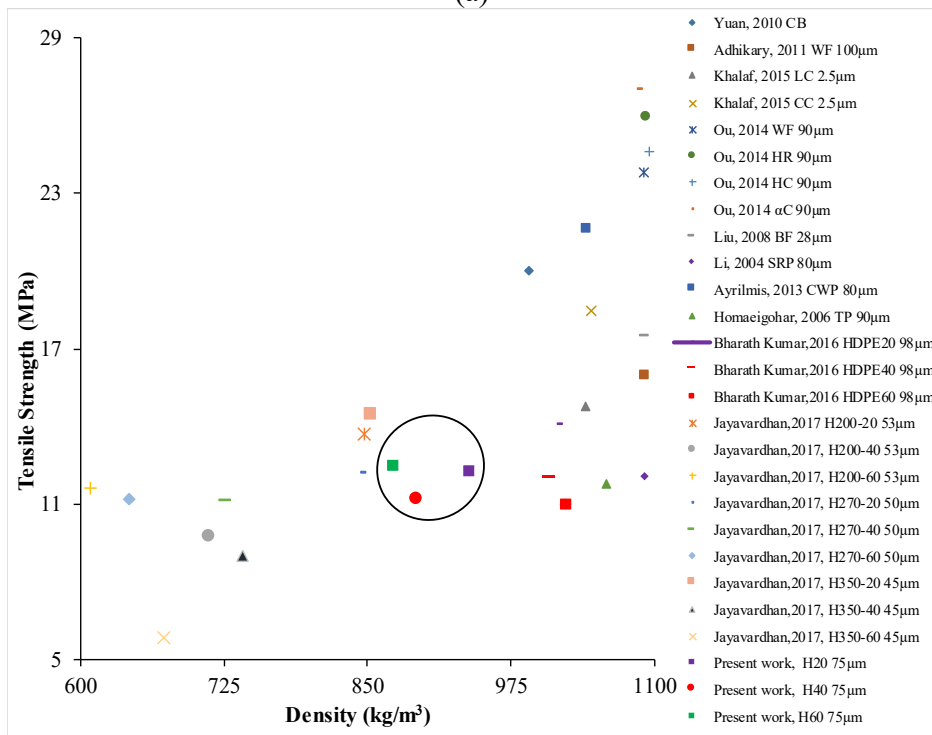
| Materials | Specific UTS (MPa/kg/m ³) × 10 ⁻³ | E/ρ (MPa/kg/m ³) | E/ρ ² (MPa/(kg/m ³) ²) × 10 ⁻³ | E/ρ ³ (MPa/(kg/m ³) ³) × 10 ⁻⁶ |
|-----------|--|---------------------------------|--|--|
| H | 19.85 | 1.00 | 1.05 | 1.11 |
| H20 | 13.12 | 1.20 | 1.28 | 1.36 |
| H40 | 12.61 | 1.52 | 1.70 | 1.90 |
| H60 | 14.33 | 1.86 | 2.13 | 2.45 |

4.5 Property map

Tensile data (extracted from literature) is graphed against the HDPE composites density in Figure 4.8a-b (Adhikary et al. 2011, Ayrimis 2013, Bharath Kumar et al. 2016, Homaeigohar et al. 2006, Khalaf 2015, Liu et al. 2008, Ou et al. 2014, Sim et al. 1997, Yuan et al. 2010). It is clear that composites with solid particle reinforcement have higher modulus with a higher density as a common trend. However, hollow particle filled composite provide lower density advantage over solid particles. Present study results show that the density of printed foam falls between compression molded engineered glass microballoon and injection molded cenosphere based closed cell foams. Modulus of printed syntactic foam is higher compared to carbon black, lignocellulose, calcium carbonate, wood, cenospheres, and glass microballoon based systems. Whereas strength is almost comparable with injection and compression molded composites.



(a)



(b)

Figure 4.8 Tensile modulus and (b) strength of HDPE composites plotted against density (Adhikary et al. 2011, Ayrilmis 2013, Bharath Kumar et al. 2016, Homaeigohar et al. 2006, Khalaf 2015, Liu et al. 2008, Ou et al. 2014, Sim et al. 1997, Yuan et al. 2010).

Conclusions

Eco-friendly lightweight cenosphere/HDPE closed cell foam filament is successfully used in FFF based 3D printer. It is highly desired to increase the available selection of filament materials for printing components that can be put into service directly after printing. Developed foam filament and prints are analyzed using mechanical tests to address their suitability and feasibility to be utilized for 3D printing applications. Filament recyclability potential is also addressed. HDPE and H40 filaments are used for 3D printing tensile test specimens. Printing parameters for H40 are optimized, and 3D printed parts are subjected to tensile testing at 10^{-3} s^{-1} strain rate. Tensile properties of 3D printed specimens are compared with those of injection molded specimens. Results are summarized as below:

Cenosphere/HDPE blends

- MFI of neat HDPE has decreased with increase in cenospheres content. Rheological results indicate a considerable increase in complex viscosity, loss and storage modulus with increasing cenospheres content.
- Complex viscosities values are maximum at a lower frequency but decrease with an increasing frequency indicating cenospheres/HDPE foams shear thinning behaviour. Both storage and loss modulus showed an increasing trend with filler loading and frequency.
- Neat HDPE and foam filaments exhibit lower crystallinity as compared to respective printed material. Filler addition in HDPE matrix reduces CTE remarkably.

Recyclability potential and tensile behavior of filaments at lower strain rates

- Developed feedstock material exhibit recyclability potential making them greener filaments.
- Density of H40 foams increased in up to two extrusion passes due to cenosphere breakage and porosity consolidation.
- Tensile modulus and yield strength of neat HDPE filaments increased with each extrusion pass.

- H40 filaments show increasing trend in modulus and strength with strain rate. H40 foams also show higher mechanical properties than the HDPE specimens under comparable processing conditions.
- Specific modulus values of extruded filaments are higher than that of injection molded samples at the same strain rates.

3D Prints

- Warping of the specimen is reduced and quality is improved by optimizing printer speed, layer thickness, print temperature and cooling conditions.
- 3D printed HDPE has 18% higher modulus and 17.5% lower yield strength than the HDPE filament.
- Microstructure of 3D printed H40 is similar to that of molded H40. Cenospheres are uniformly distributed and survived the 3D printing process.
- Specific modulus of 3D printed H40-2X and 3X are 1.6 and 2.6 times higher than the respective filaments, however, fracture strain decreases by up to 40%.
- Comparison of specific mechanical properties shows promise in 3D printed syntactic foam components in replacing some of the molded specimens for weight-reduction applications.
- Compared to injection molded HDPE, printed HDPE registered 78.86% higher tensile modulus and two-fold fracture strength. 3D printed HDPE and foams modulus is 1.16, 1.28, 1.51 and 1.67 times better than respective feedstock material. Tensile modulus of prints is higher in the range of 96.01 to 144.45% as compared to the same composition injection molded ones.
- Property map reveals 3D printing potential over other composites synthesized through different processing routes.
- Cenosphere/HDPE three-phase foam prints without warpage having weight saving potential can be used in marine applications.

These results show that the developed filaments have potential to be used in 3D printing as the properties are comparable to the injection molded specimens. Use of 60 vol. % less polymer and possibility of recycling make these filaments greener and more environmental friendly than the filaments of neat resin.

5 FLEXURAL RESPONSE

5.1 Flexural modulus and strength

Flexural test is conducted on 3D printed sample in two configurations (top face up - printed surface facing printing nozzle (Figure 5.1a), top face down - printed surface facing machine bed (Figure 5.1b)). Results obtained from both configurations reveals that second configuration has shown slightly better flexural modulus and strength compared to first configuration (Table 5.1). Flexural loading is a combination of compression and tension wherein compressive stresses act on top surface (loading arm contact surface) and tensile stresses act on outer most surface of the sample. The top face down configuration (Figure 5.1b) has performed better due to compressive load acts on the base layers that are well diffused. Wherein in case of top face up configuration (Figure 5.1), compressive load is acting on the top surface raster that may not be well diffused compared to bottom layer rasters. Nonetheless, modulus and strength values for both approaches are within the standard deviation overlap making them independent of chosen configurations.

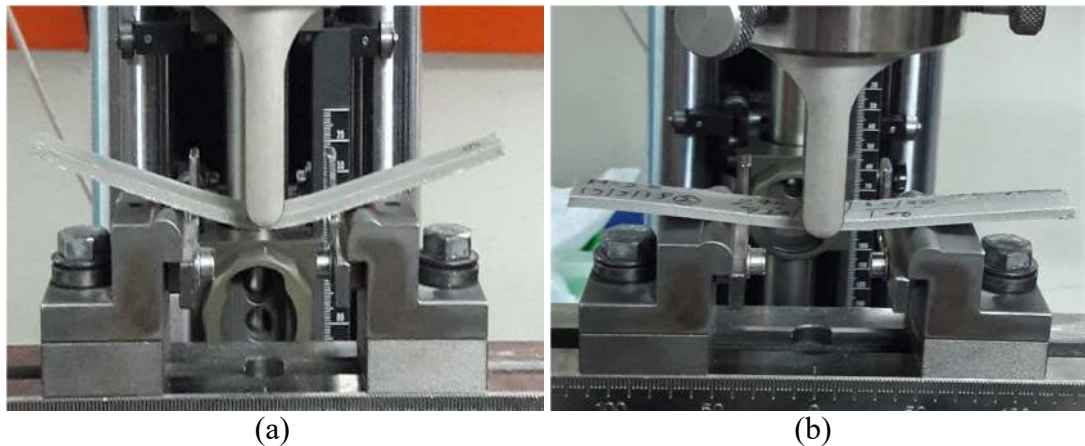


Figure 5.1 Flexural test configuration (a) sample with top face up (b) sample with top face down.

Neat HDPE specimen did not show any failure sign up to 10% strain (Figure 5.2a-b) while foams fractured in a brittle manner. From post-test images, (Figure 5.3) crack is clearly visible in H60 composition whereas no crack is seen for H20 composition, which is attributed to the ductile HDPE phase.

Flexural modulus increases with cenosphere content (Figure 5.4) due to intact filler in the HDPE matrix (Figure 5.5). Highest modulus is exhibited by H60 and is 1.56 times better than neat HDPE sample. Strength drop might be due to poor interfacial bonding between constituents and air gaps between the raster.

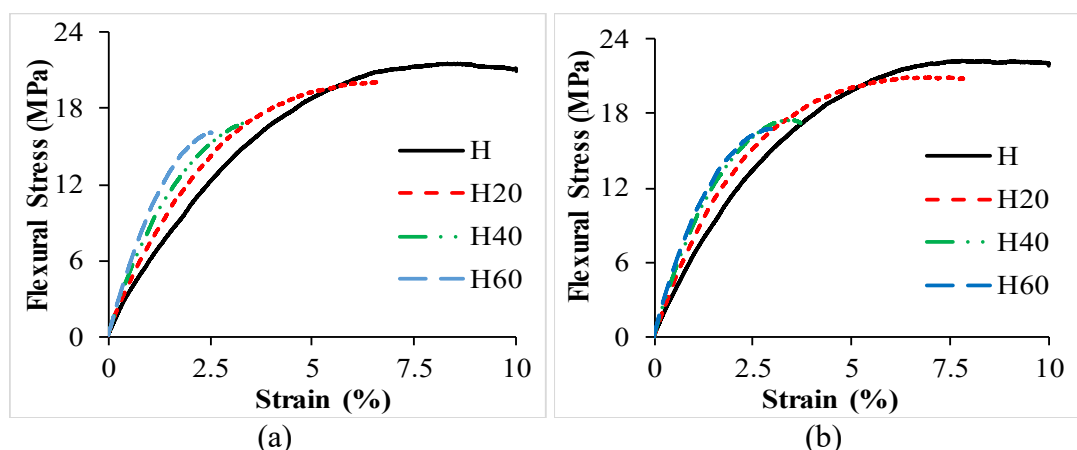


Figure 5.2 Representative flexural stress strain plot for (a) top face up and (b) top face down configuration.

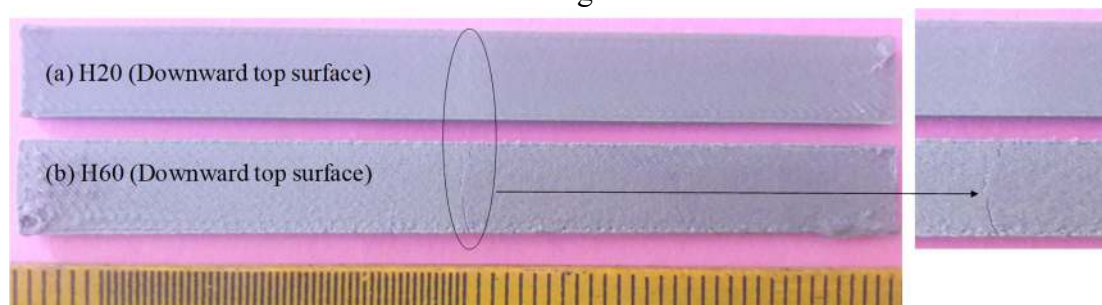


Figure 5.3 Flexural tested foam samples (a) H20 (b) H60.

Table 5.1 Flexural properties of printed HDPE and their syntactic foams.

| Material | Flexural modulus (MPa) | | Flexural strength (MPa) | | Fracture strength (MPa) | | Fracture strain (%) | |
|----------|------------------------|-------------------|-------------------------|----------------|-------------------------|----------------|---------------------|---------------|
| | Top face up | Top face down | Top face up | Top face down | Top face up | Top face down | Top face up | Top face down |
| H | 720.52 ±25.21 | 734.76 ±31.28 | 21.50 ±1.35 | 22.24 ±1.12 | --- | --- | --- | --- |
| H20 | 867.65 ±43.22 | 883.86 ±39.56 | 20.11 ±1.07 | 20.92 ±1.58 | 20.06 ±1.54 | 20.80 ±1.48 | 6.60 ±0.11 | 7.83 ±0.19 |
| H40 | 1040.71 ±50.21 | 1049.17 ±41.87 | 16.90 ±0.54 | 17.48 ±0.47 | 16.89 ±0.85 | 17.25 ±0.41 | 3.41 ±0.35 | 3.71 ±0.11 |
| H60 | 1120.35 ±53.65 | 1149.28 ±51.23 | 16.10 ±0.23 | 16.76 ±0.72 | 16.08 ±0.62 | 16.74 ±0.79 | 2.50 ±0.12 | 2.97 ±0.07 |

Table 5.2 Specific flexural modulus and strength for top face down configuration.

| Material | Sp. Flexural Strength (MPa/kg/m ³)× 10 ⁻³ | Sp. Flexural Modulus (MPa/kg/m ³) |
|----------|---|--|
| H | 23.44±1.19 | 0.77±0.03 |
| H20 | 22.30±1.16 | 0.94±0.01 |
| H40 | 19.59±0.59 | 1.18±0.08 |
| H60 | 19.22±0.45 | 1.32±0.02 |

Variation in Specific flexural modulus and strength with cenosphere is plotted in Figure 5.6. Specific flexural modulus follows the increasing trend with cenospheres percentage. Specific flexural modulus is 1.71 times higher as compared to neat HDPE (Table 5.2) 3D printed HDPE showed around 3% higher modulus compared to injection molded foams. H20, H40 and H60 foam registered 25.37, 13.67 and 9.08% lower modulus compared to respective injection molded foams while printed H, H20, H40, and H60 registered 1.62, 1.0, 11.78 and 14.38% lower strength as compared to injection molded ones (Bharath Kumar et al. 2016). This might be due to air gaps between adjacent raster in 3D printing as compared to fully dense molded sample.

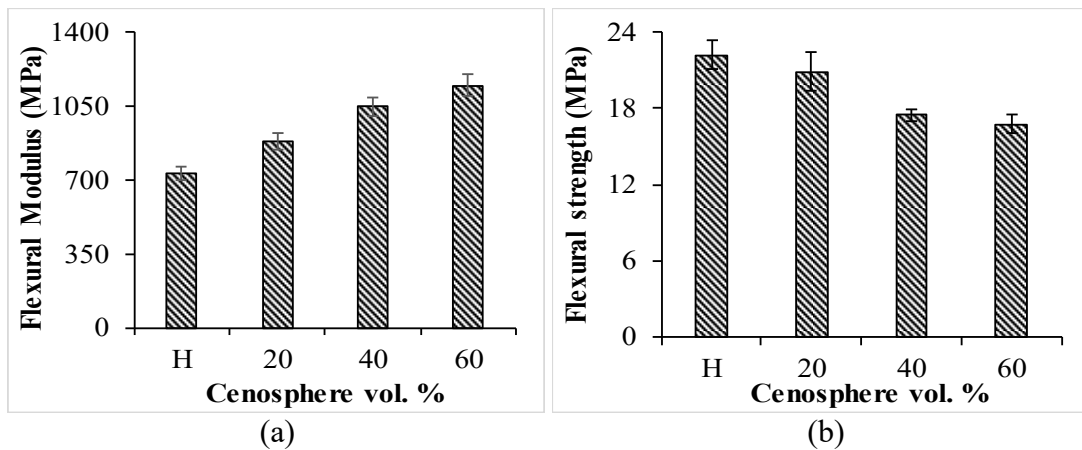


Figure 5.4 Experimentally measured flexural (a) modulus and (b) strength of HDPE and their syntactic foams.

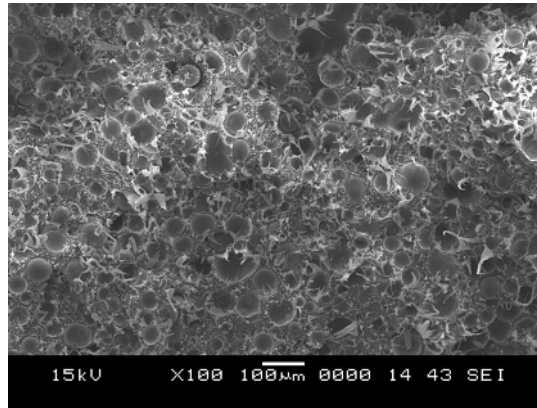


Figure 5.5 Micrograph of H60 post flexural test.

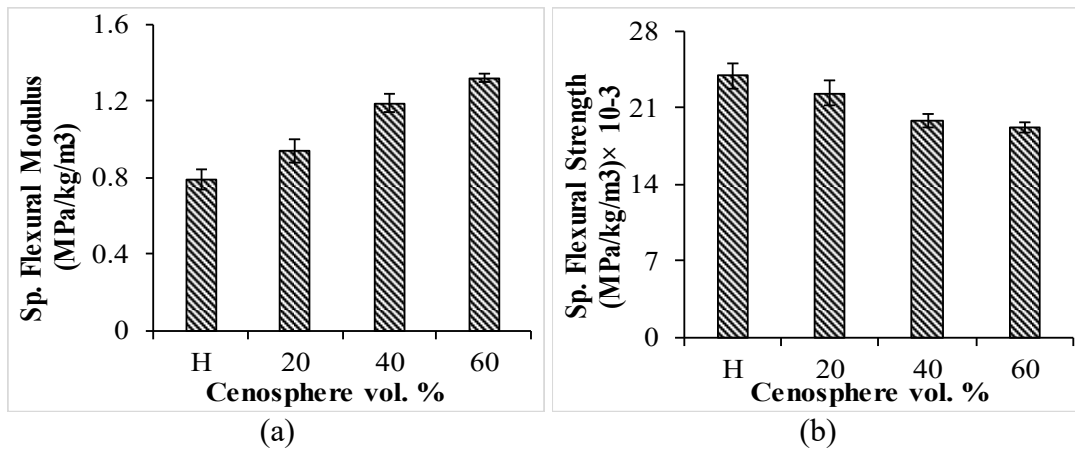
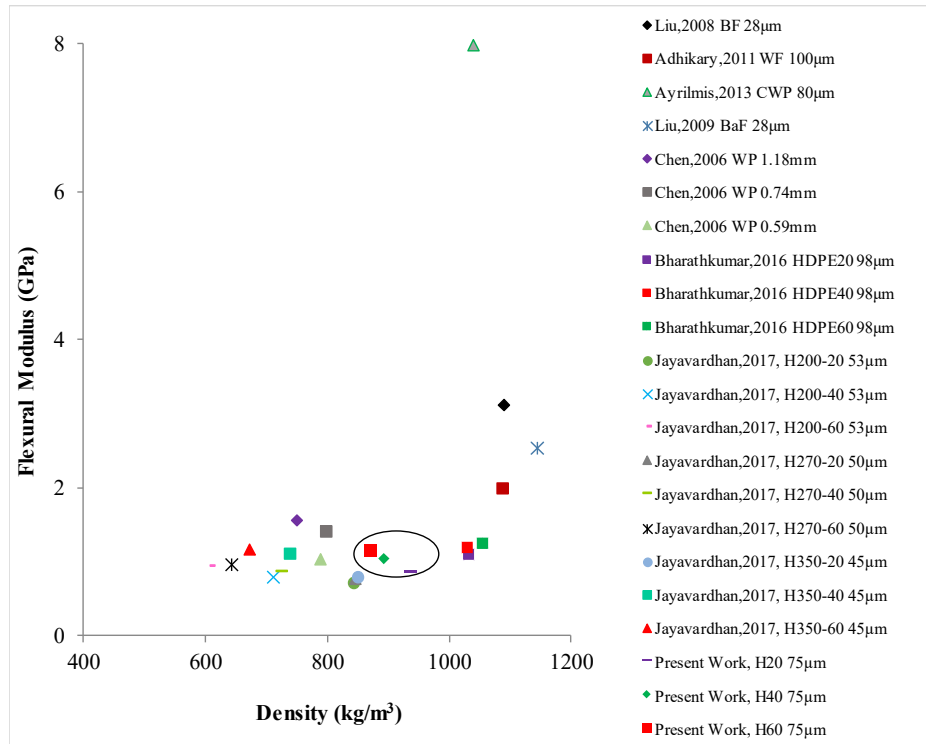


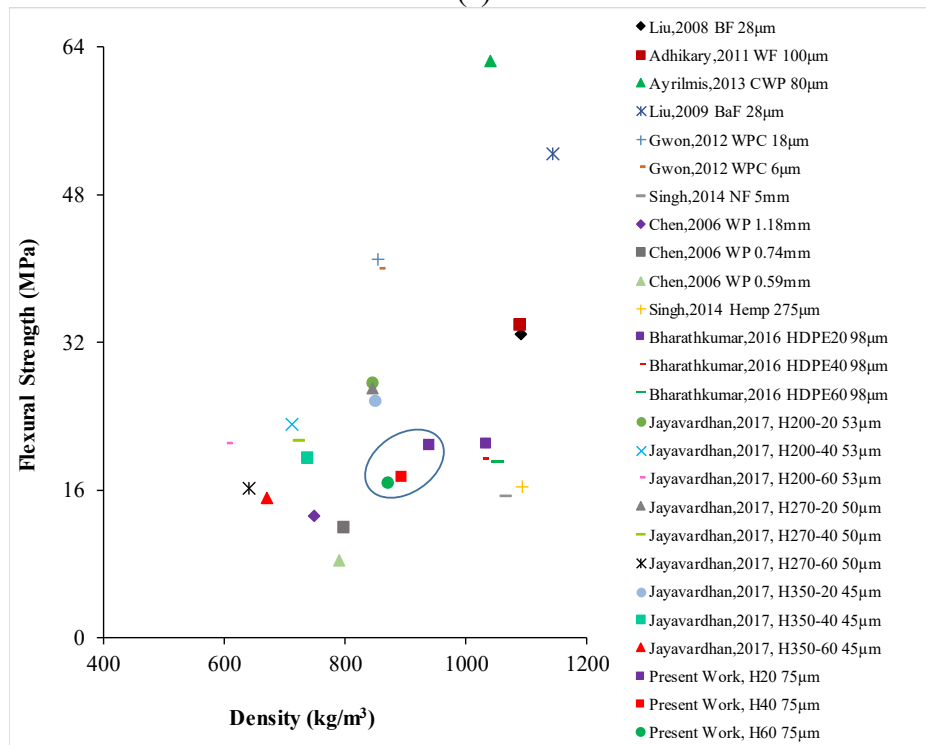
Figure 5.6 Experimentally measured specific flexural (a) modulus and (b) strength of HDPE and their syntactic foams.

5.2 Property map

Flexural properties data (extracted from literature) is graphed against the HDPE composites density in Figure 5.7 (Adhikary et al. 2011, Ayrilmis 2013, Bharath Kumar et al. 2016, Chen et al. 2006, Gwon et al. 2012, Liu et al. 2008, Liu et al. 2009, Singh et al. 2014, Sood 2014). Flexural modulus of printed foam is lower as compared to injection molded and comparable with compression molded foams. Flexural strength of printed foam is higher as compared to natural fiber and wood powder filled composite, lower compared to injection molded samples and is comparable with compression molded composites. Choice of appropriate extrusion and printing parameters with minimum filler breakage leads to density reduction. By controlling, filler percentage and printing parameters flexural properties can be exploited well over a wider range as seen from Figure 5.7.



(a)



(b)

Figure 5.7 Flexural modulus and (b) strength of HDPE composite plotted against density (Adhikary et al. 2011, Ayrilmis 2013, Bharath Kumar et al. 2016, Chen et al. 2006, Gwon et al. 2012, Liu et al. 2008, Liu et al. 2009, Singh et al. 2016, Sood 2014).

Conclusions

- Neat HDPE sample has not shown any fracture sign below 10% strain, due to ductile nature of material, cenosphere addition caused brittleness of foam.
- Top face down configuration registered slightly better performance for flexural modulus and strength as compared to top face down condition.
- Flexural modulus increases with cenosphere content. Highest modulus is exhibited by H60 which is 1.56 times better than neat HDPE sample.
- Presence of air gaps lowers flexural modulus and strength as compared to fully dense injection molded sample.

6 COMPRESSIVE BEHAVIOR OF 3D PRINTS

6.1 Quasi static compressive behavior of 3D prints

Measured densities (ASTM D792-13) of HDPE, H20, H40 and H60 filament are 949.32 ± 15 , 940.73 ± 21 , 897.41 ± 29 and 886.28 ± 38 kg/m^3 and are respectively lower by 0.071, 0.34, 4.32 and 4.90 % compared to the theoretical densities (rule of mixture) signifying entrapped porosity during extrusion.

Figure 6.1 presents circular cross section of H60 filament post freeze fracture. Matrix porosity clearly indicates three-phase structure in the extruded filament as seen from Figure 6.1a. Such a structure might help in additional cushioning effect during compression and might enhance damping. Cenospheres are seen to be intact post extrusion and are uniformly distributed in HDPE as observed from Figure 6.1a and is also confirmed earlier through micro CT scans as observed from Figure 3.5a (Singh et al. 2018).

3D printed HDPE, H20, H40 and H60 have densities of 948.93 ± 23 , 938.32 ± 30 , 892.14 ± 37 and 872.11 ± 42 kg/m^3 respectively. Measured values of printed specimens are 0.11, 0.60, 4.89 and 6.43% lower compared to theoretical values. Closer density values of 3D printed samples as compared to their respective filaments indicate the porosity survival post 3D printing (Figure 6.1b-c). Rheology of material flow gets affected by higher filler content resulting in elongated pores (Figure 6.1c) as compared to more circular pores in H20 (Figure 6.1b).

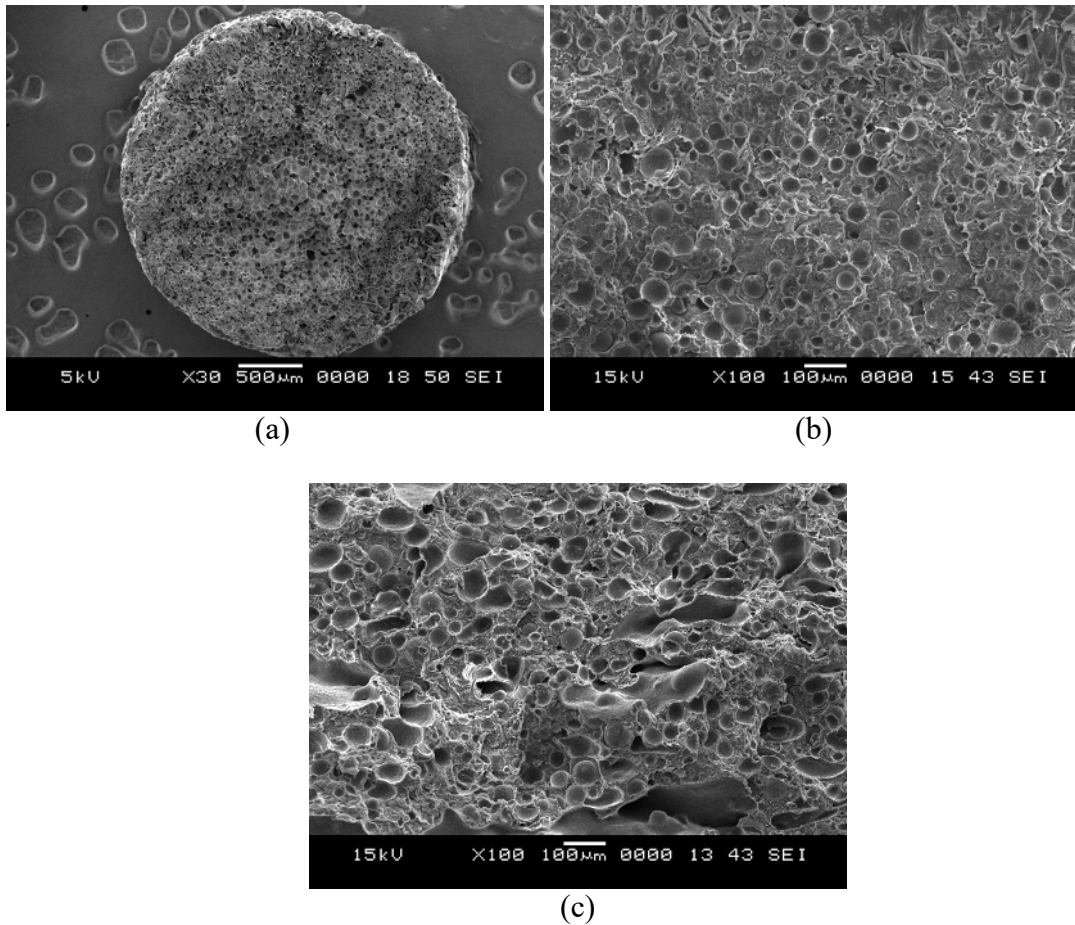


Figure 6.1 Micrograph of freeze fractured (a) extruded syntactic foam filament showing circular cross-section of representative H60 filament (b) 3D printed H20 and (c) H60 sample.

3D printed foams follow similar trend in quasi-static compressive mode (Figure 6.2) as reported in fully dense two-phase foams (Bharath Kumar et al. 2016, Jayavardhan and Doddamani 2018). Modulus of neat HDPE is higher for all strain rates as compared to foams (Table 6.1) which is due to HDPE's viscoelastic behavior (Bharath Kumar et al. 2016). H60 registered highest modulus at all strain rates among foams. With increasing filler content, stress plateau region becomes distinguishable signifying lower strain hardening resulting in higher energy absorbing capabilities. Yield strength of neat HDPE is comparable with all foam composition at all strain rates indicating potential of complex 3D printed parts to be replaced with compression and injection molded components in marine systems. Specific yield strength and yield strain values confirms that 3D printed foams may lower the overall structural weight by further increasing porosity at lower filler loadings.

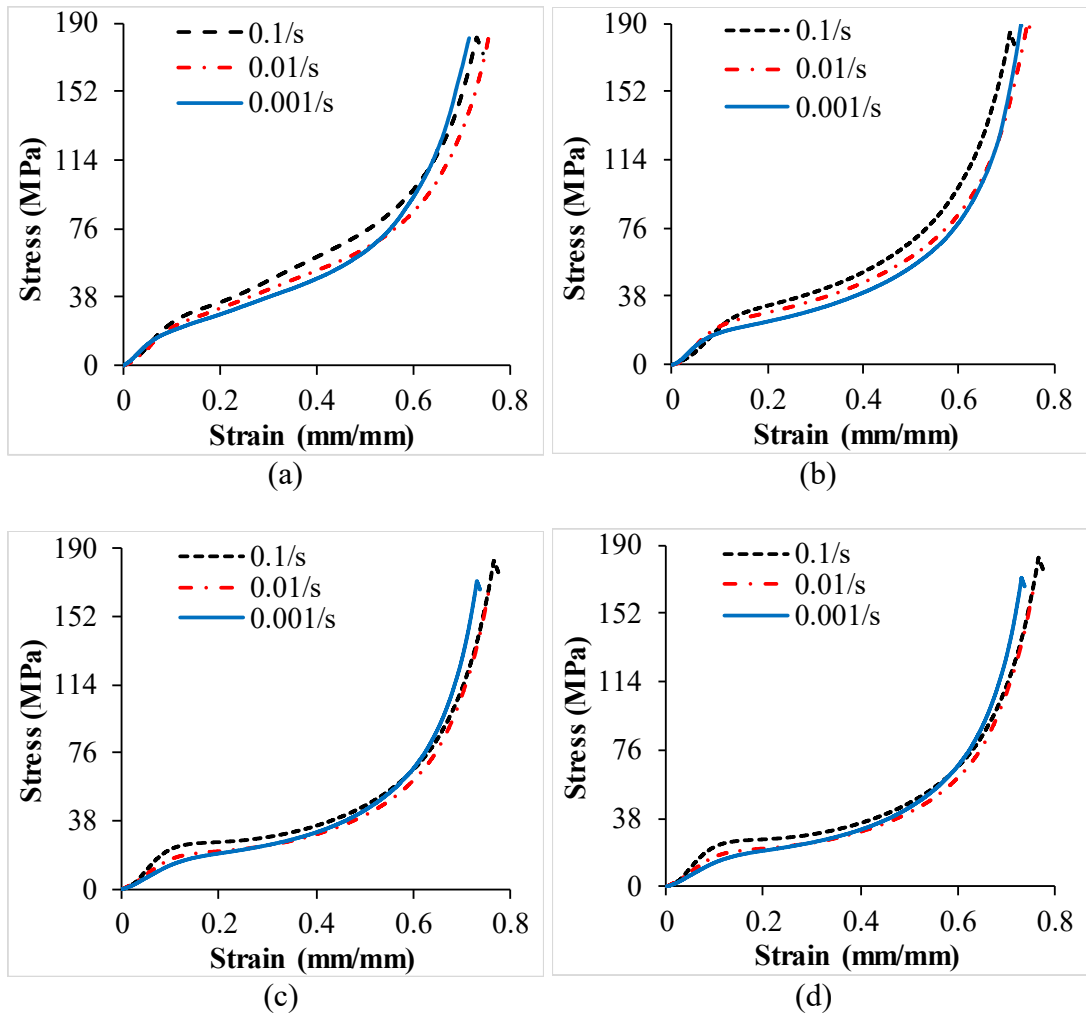


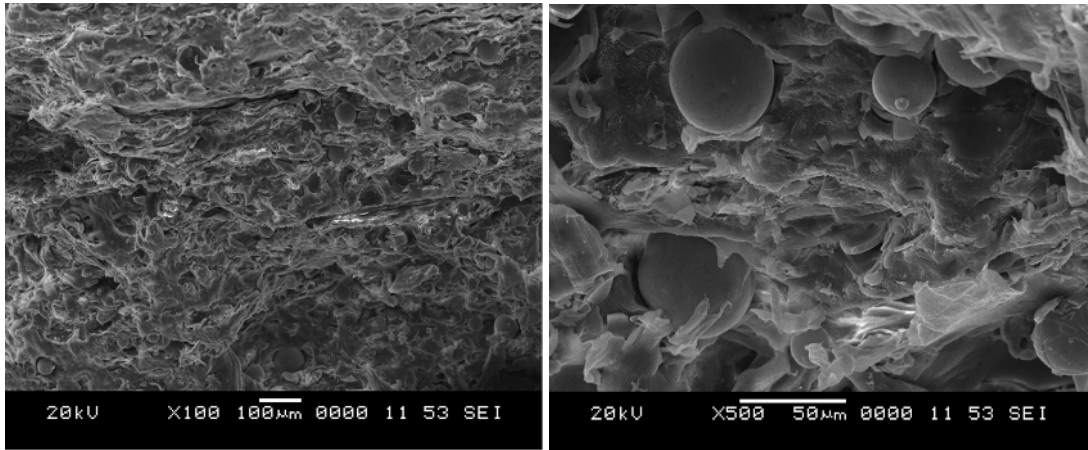
Figure 6.2 Representative stress-strain plots for Quasi-static (a) HDPE (b) H20 (c) H40 and (d) H60.

During compression, initial densification is initiated by matrix porosities collapse (Figure 6.3a, c and e). As stress level rises, cenospheres start to break resulting into further densification. At higher magnification (Figure 6.3b, d and f) deformed resin, intact cenospheres and debris are visible at 0.1 s^{-1} strain rate.

Post tested specimen micrographs have no much difference in appearance of fractured surfaces with respect to strain rate. Stress-strain curve shows similar level of strains in all the specimens at all strain rates when test is stopped making deformation and densification features appear similar.

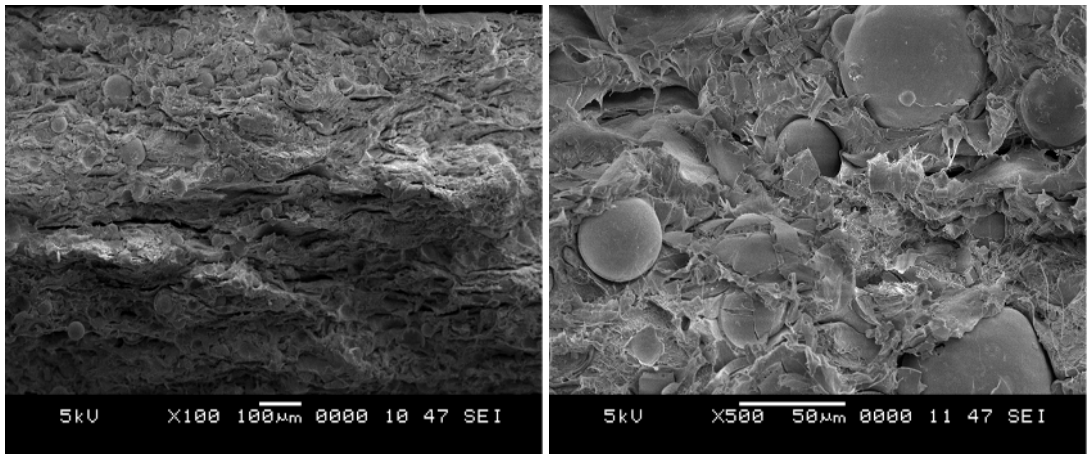
Table 6.1 Quasi-static compression data of 3D printed HDPE and their foams.

| Material | Strain rate (s ⁻¹) | Modulus (MPa) | Yield strength (MPa) | Yield strain (%) | Energy absorbed at 40% strain (MJ/m ³) | Densification on stress (MPa) | Densification on strain (%) | Specific modulus (MPa/kg/m ³) | Specific yield strength (MPa/kg/m ³) × 10 ⁻³ |
|----------|--------------------------------|---------------|----------------------|------------------|--|-------------------------------|-----------------------------|---|---|
| H | 0.001 | 239.84±10.32 | 16.79±0.87 | 8.53±0.11 | 13.09±0.76 | ----- | ----- | 0.253 | 17.69 |
| | 0.01 | 239.36±10.28 | 23.31±1.03 | 12.01±0.18 | 13.09±0.87 | ----- | ----- | 0.252 | 24.84 |
| | 0.1 | 271.32±11.47 | 27.45±1.14 | 12.16±0.25 | 13.28±0.94 | ----- | ----- | 0.286 | 28.93 |
| H20 | 0.001 | 151.86±6.13 | 15.34±0.79 | 7.95±0.12 | 11.96±0.65 | 68.45±2.14 | 54.45±1.44 | 0.161 | 16.34 |
| | 0.01 | 187.56±8.61 | 21.86±1.14 | 10.13±0.11 | 12.13±0.64 | 70.42±2.41 | 56.43±1.07 | 0.200 | 23.29 |
| | 0.1 | 208.81±10.02 | 24.54±1.65 | 11.69±0.14 | 12.21±0.45 | 76.87±2.73 | 58.27±1.95 | 0.222 | 26.15 |
| H40 | 0.001 | 214.15±10.41 | 11.09±0.88 | 5.76±0.07 | 12.22±0.45 | 58.42±2.08 | 55.43±1.57 | 0.240 | 13.34 |
| | 0.01 | 219.03±11.68 | 19.85±1.02 | 10.01±0.08 | 12.23±0.59 | 72.31±3.07 | 58.41±1.74 | 0.245 | 22.25 |
| | 0.1 | 241.08±11.17 | 22.98±1.44 | 10.47±0.16 | 12.28±0.56 | 72.39±3.18 | 58.42±1.45 | 0.270 | 25.76 |
| H60 | 0.001 | 222.94±11.26 | 14.58±0.98 | 10.12±0.06 | 13.05±0.38 | 52.58±1.09 | 52.04±1.87 | 0.255 | 16.71 |
| | 0.01 | 239.34±21.15 | 19.35±1.05 | 9.57±0.11 | 13.23±0.55 | 48.42±2.45 | 48.12±1.44 | 0.274 | 22.18 |
| | 0.1 | 242.54±25.56 | 22.6±1.12 | 10.12±0.12 | 13.35±0.22 | 52.58±2.11 | 52.40±2.25 | 0.278 | 25.91 |



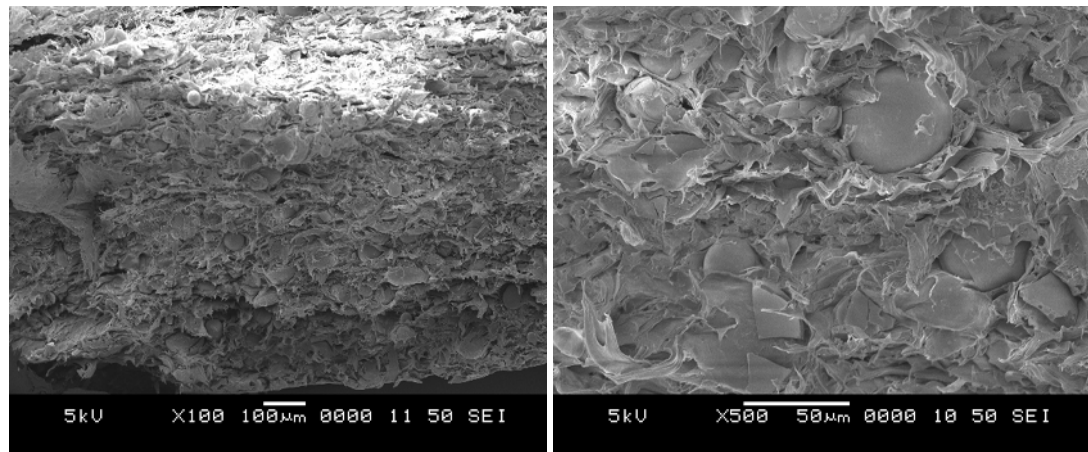
(a)

(b)



(c)

(d)



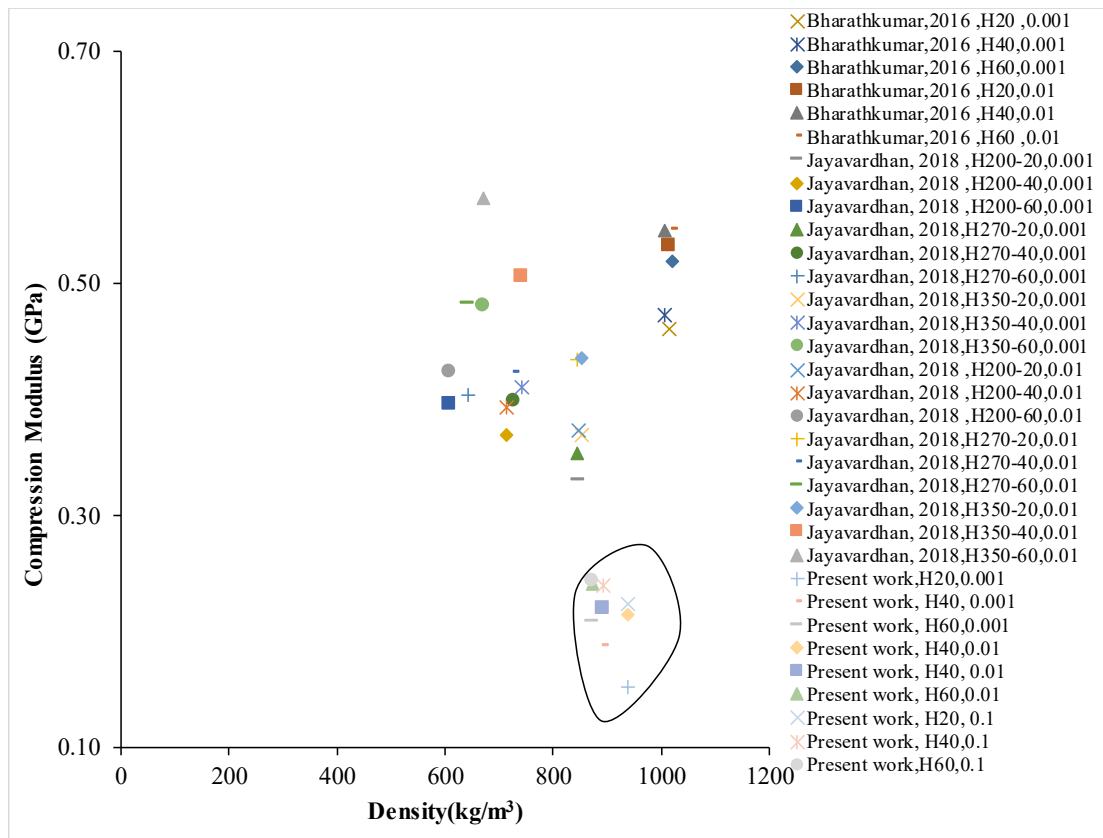
(e)

(f)

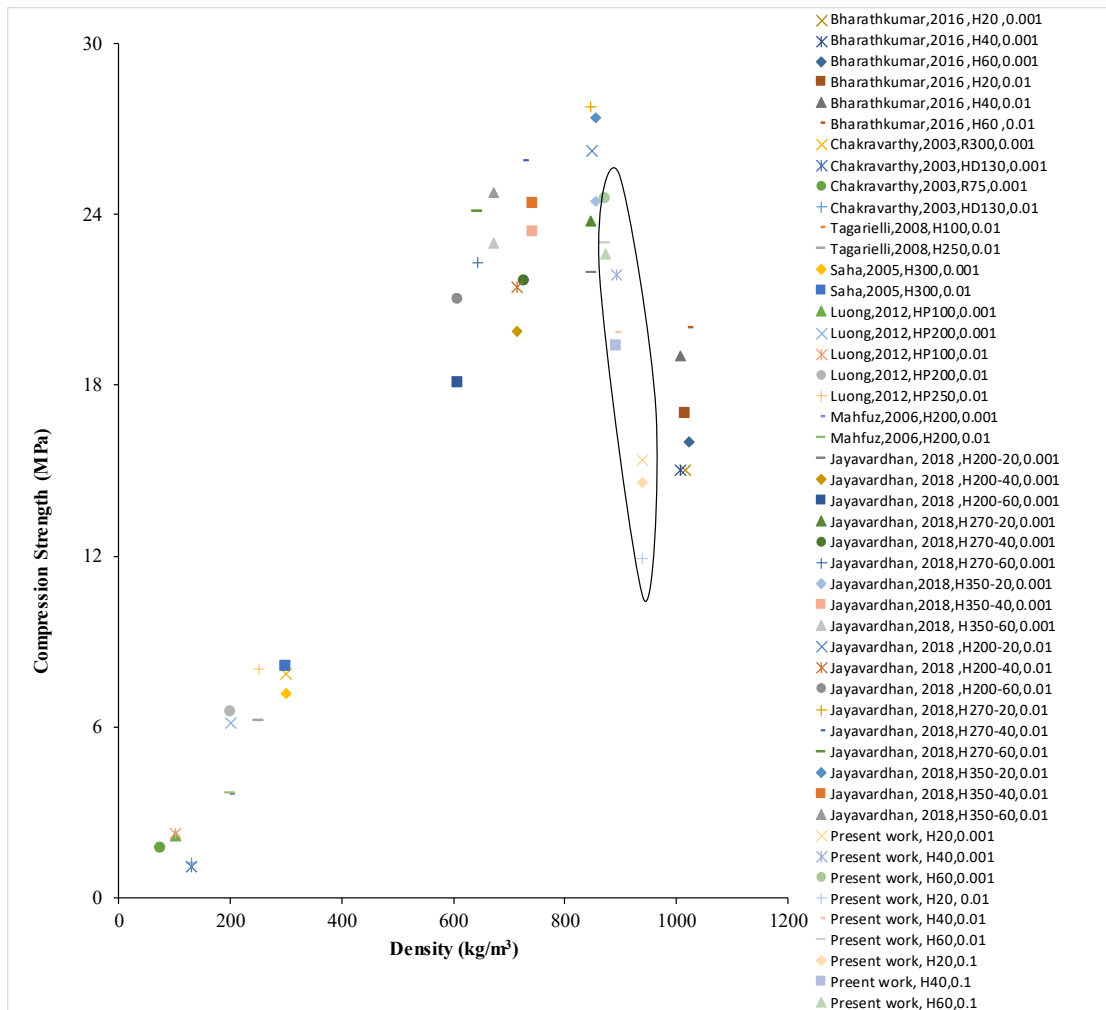
Figure 6.3 SEM of compression tested samples at 0.1 s^{-1} for H20 (a-b), H40 (c-d) and H60 (e-f) at lower and higher magnifications.

Property map

Quasi-static compressive strength and modulus values are plotted with respect to density for thermoplastic syntactic foams containing different fillers tested at strain rates of 0.001 s^{-1} , 0.01 s^{-1} and 0.1 s^{-1} are presented in Figure 6.4 (Bharath Kumar et al. 2016, Chakravarty et al. 2003, Jayavardhan and Doddamani 2018, Luong et al. 2013, Mahfuz et al. 2006, Saha et al. 2005, Tagarielli et al. 2008). The results extracted from the published literature are presented and is compared with the present study. Results from present study shows that, the 3D printed syntactic foams have lower modulus and density, possessing nearly equal strength compared to injection molded syntactic foam at the same strain rate. Choice of appropriate printing parameters and filler concentration tailored the compression properties of the 3D printed foams over wide range. Such property map come handy and useful for selection of particular foam for a given application.



(a)



(b)

Figure 6.4 Compressive modulus and strength of thermoplastic composites plotted against density from available studies (Bharath Kumar et al. 2016, Chakravarty et al. 2003, Jayavardhan and Doddamani 2018, Luong et al. 2013, Mahfuz et al. 2006, Saha et al. 2005, Tagarielli et al. 2008)

Conclusions

Entrapped porosity in the filaments is retained in 3D printed samples lowering the density. At 100% infill and H60 3D printed samples are 6.43% lighter than the theoretical density. Yield strength of neat HDPE is comparable to foams indicating 3D printing potential over expensive injection and compression molding for complex geometries. Highest specific compressive modulus and yield strength is observed for H60 and H20 respectively at 0.1 s^{-1} among foams. 3D printed syntactic foams show good strain rate sensitivity. Developing complex geometries with 3D printed three-

phase syntactic foams make them potential candidate materials for buoyant weight sensitive structures.

7 DYNAMIC MECHANICAL ANALYSIS

7.1 Temperature sweep

Storage modulus as a function of temperature for 3D printed HDPE, H20, H40 and H60 at 1 Hz is plotted in Figure 7.1a. As the glass transition temperature of the HDPE matrix is approximately -100°C (Khanna et al. 1985), the experiments are conducted in temperature range of $30\text{-}125^{\circ}\text{C}$. In the present study experiments are conducted entirely in rubbery region thus the variations of the dynamic properties with temperature does not show step changes or peaks which indicate phase transitions. From Figure 7.1a it is observed that all temperatures the syntactic foam have higher storage modulus than that of neat HDPE, except H20. Storage modulus increases with increasing hollow particle content, though the difference between H, H20 and H40 is not much. From Table 7.1 it can be observed that the standard deviations of these compositions overlap at the three selected reference temperatures. H60 has shown highest storage modulus throughout the temperature range indicating that significantly higher filler content may be responsible for the increased stiffening effect. It is also observed that the syntactic foams are able to withstand approximately 5°C higher temperature before the storage modulus drops below the 35 MPa threshold.

Loss modulus results are presented in Figure 7.1b and at selected temperatures in Table 7.2. As with storage modulus, the loss modulus is higher at all temperatures for syntactic foams and increases with increasing hollow particle content. Loss modulus is observed to be highest for H60 as compared to other cenosphere/HDPE foams and neat HDPE. The peak observed in loss modulus is at around 50°C corresponds to the α -relaxation in HDPE (Khanna et al. 1985). The peak appears to occur at higher temperatures with increasing particle loading. $\tan \delta$ results are presented in Figure 7.1c and at selected temperatures in Table 7.3. This property, also known as the damping parameter, loss factor or loss tangent, is the ratio of the loss and storage moduli and represents the relative magnitudes of the elastic and viscous behavior of the material. While all of the syntactic foams have lower damping parameter than the virgin HDPE at all temperatures, the damping parameter is less sensitive to the hollow particle content than the storage and loss moduli.

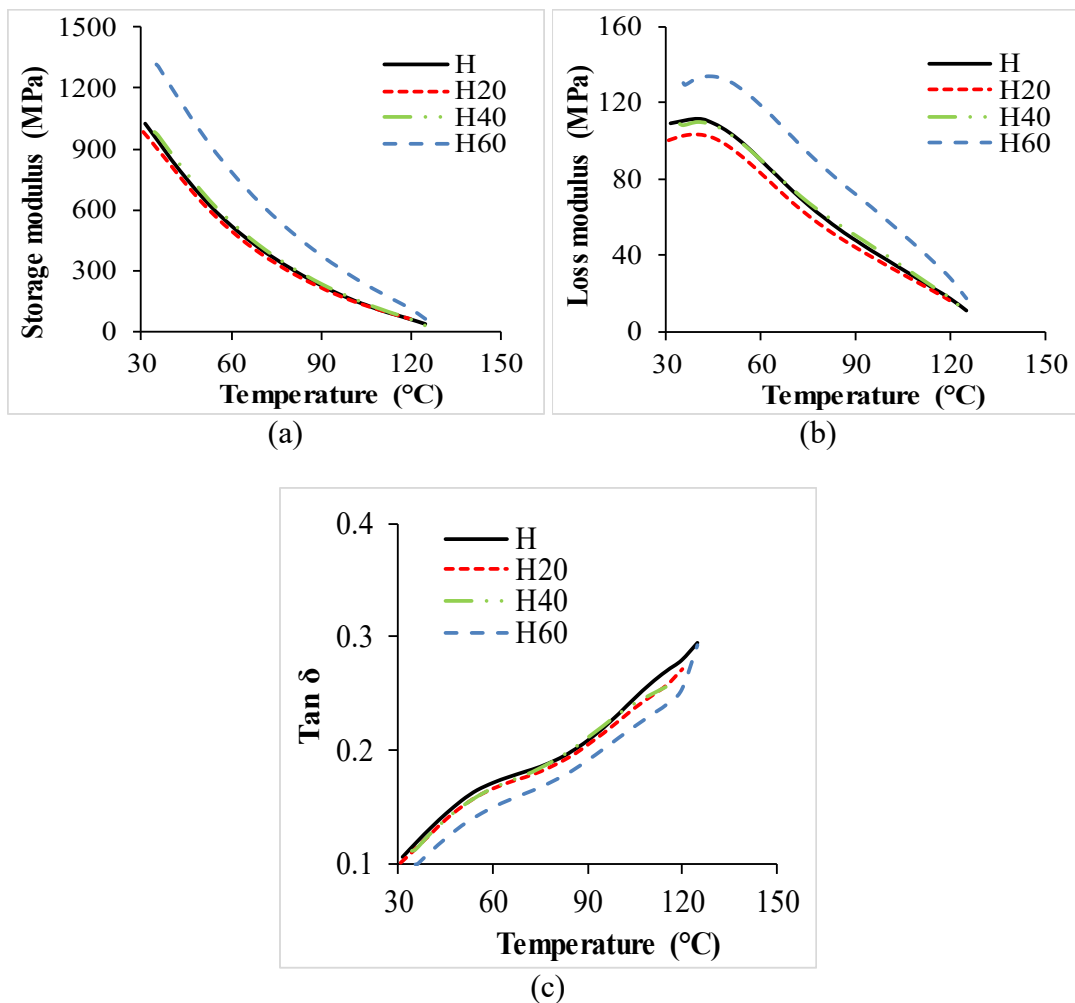


Figure 7.1 (a) Storage modulus (b) loss modulus and (c) Tan δ results at 1 Hz.

Table 7.1 Comparison of storage modulus at three representative temperatures.

| Material | E' at 50 °C (MPa) | E' at 80 °C (MPa) | E' at 120 °C (MPa) |
|----------|------------------------|------------------------|-------------------------|
| H | 668.27±3.2 | 309.87±4.5 | 60.95±1.3 |
| H20 | 640.89±3.7 | 290.50±5.2 | 59.71±1.7 |
| H40 | 689.13±7.2 | 318.39±3.6 | 62.10±2.3 |
| H60 | 984.90±12.8 | 492.53±4.3 | 109.35±3.1 |

Table 7.2 Comparison of loss modulus at three representative temperatures.

| Material | E'' at 50 °C (MPa) | E'' at 80 °C (MPa) | E'' at 120 °C (MPa) |
|----------|-------------------------|-------------------------|--------------------------|
| H | 104.33±0.2 | 59.45±2.3 | 17.06±1.2 |
| H20 | 96.70±1.3 | 54.65±4.7 | 16.21±2.4 |
| H40 | 103.34±2.1 | 61.14±5.2 | 17.00±2.3 |
| H60 | 131.19±5.1 | 85.70±4.2 | 27.76±5.1 |

Table 7.3 Comparison of damping parameter at three representative temperatures.

| Material | Tan δ at 50 °C ($\times 10^{-2}$) | Tan δ at 80 °C ($\times 10^{-2}$) | Tan δ at 120 °C ($\times 10^{-2}$) |
|----------|---|---|--|
| H | 15.61 \pm 0.006 | 19.20 \pm 0.005 | 28.00 \pm 0.002 |
| H20 | 15.09 \pm 0.002 | 18.82 \pm 0.003 | 27.15 \pm 0.003 |
| H40 | 15.00 \pm 0.003 | 19.19 \pm 0.001 | 27.00 \pm 0.001 |
| H60 | 13.32 \pm 0.004 | 17.40 \pm 0.005 | 25.40 \pm 0.001 |

Conclusions

Effect of temperature on the dynamic mechanical properties of 3D printed syntactic foam is presented. Effects of temperature and cenosphere volume fraction on the storage modulus, loss modulus and damping parameter are analyzed. The following conclusions are drawn from the analysis of experimental results:

- Neat HDPE 3D printed sample has registered slightly higher storage modulus compared to H20.
- Storage modulus of H60 is highest among all the samples.
- Storage modulus decreased with temperature for neat and foam samples. Deviations at low temperature between H, H20, H40 and H60 is high and reduces with increasing temperature.
- Loss modulus difference among H, H20 and H40 throughout the temperature range is in narrow range.
- H60 registered highest loss modulus followed by H40, H20 and H at higher temperature.
- Neat HDPE is having highest damping capacity indicating damping parameter is characterised elastic component. As cenosphere concentration increases viscous component increases which reduces the damping capacity of foam.

8 3D PRINTED INDUSTRIAL COMPONENTS

HDPE is widely used in manufacturing consumer products. Many of the existing components can be identified where cenosphere filled HDPE syntactic foams can be beneficial either to provide lightweight or to reduce HDPE consumption to make the part cheaper and more eco-friendly. Reduction in failure strain may be a limitation for some applications. In addition, concerns such as mismatch in coefficient of thermal expansion of particle and matrix leading to interfacial separation or material failure can be important considerations. Therefore, the potential applications of such new materials should be carefully selected. Several existing HDPE components are identified and the process parameters optimized in the present work are used to print these parts in syntactic foams using 3DP. A snapshot of the printed parts is presented in Figure 8.1 and close-up images of few components are shown in Figure 8.2

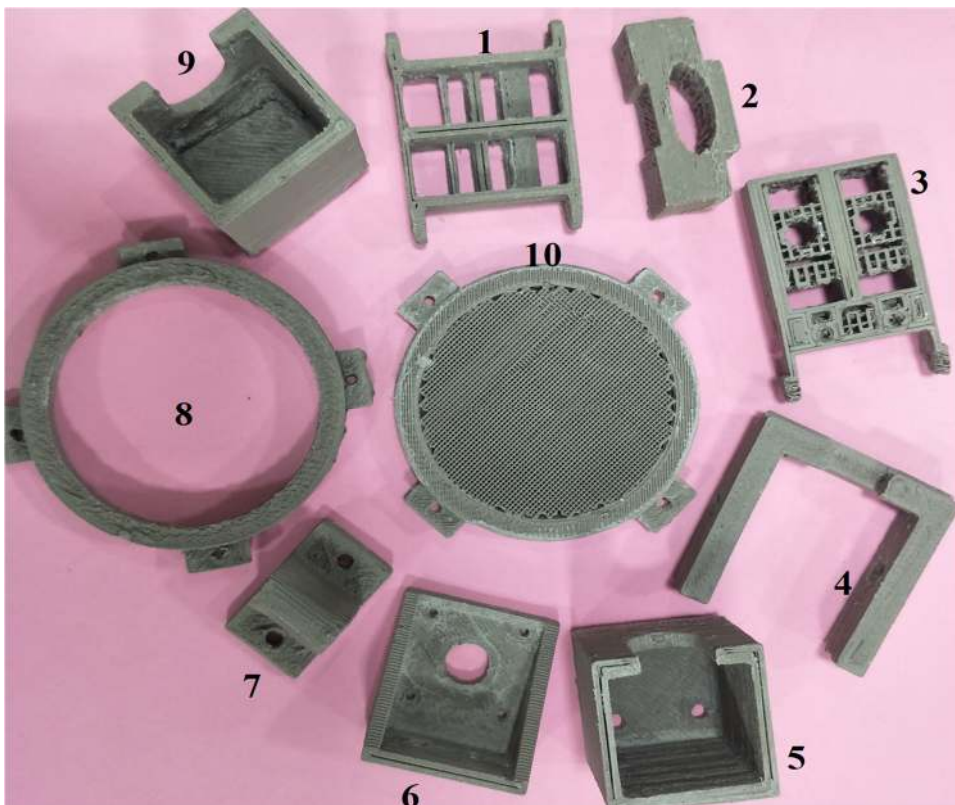


Figure 8.1 Eco-friendly components printed using 3DP technique 1. Arduino rack 2. Bearing holder 3. Arduino rack upper head 4. Support channel 5. Motor mount with fillet 6. Motor mount 7. Rod end holder 8. Filter ring 9. Motor cover 10. Filter end cap.

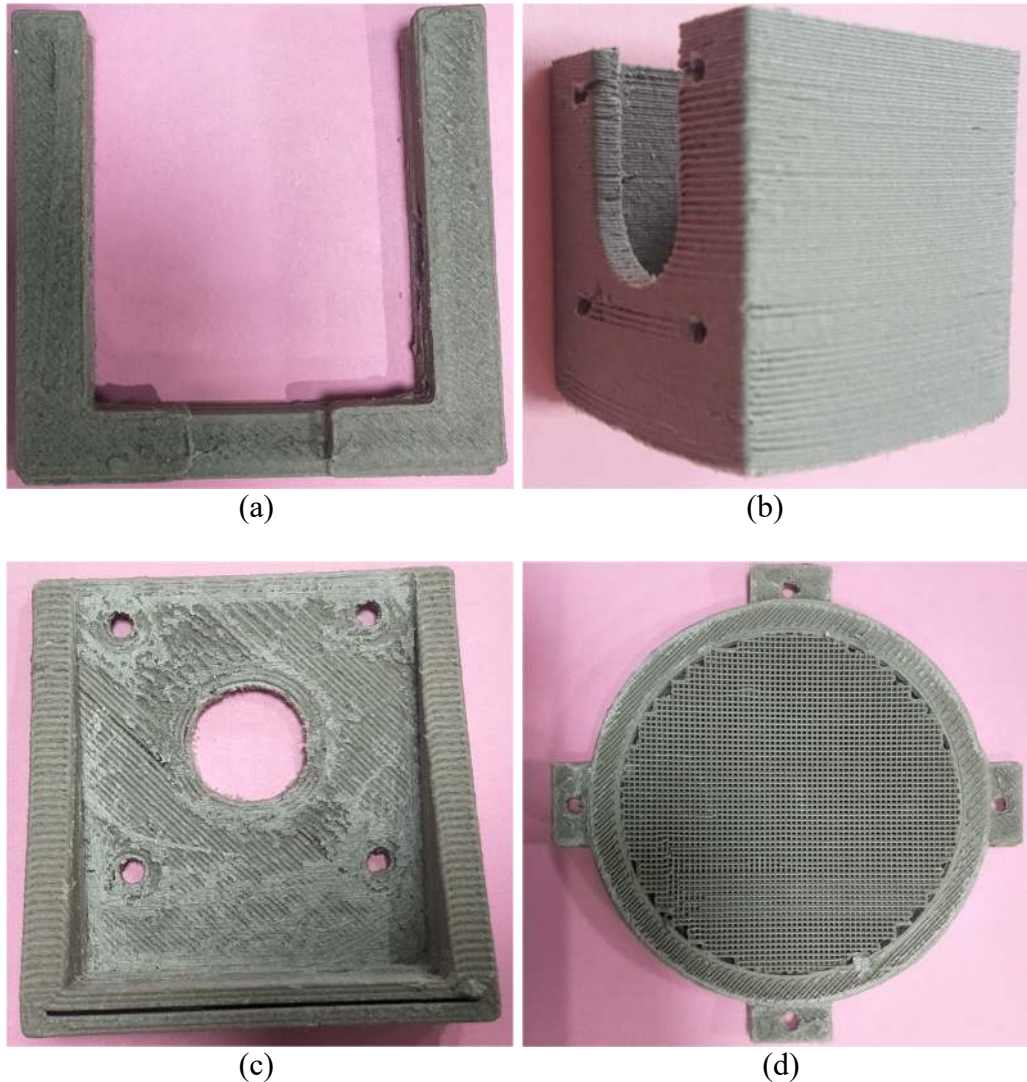


Figure 8.2 Prototype components printed in the study: (a) Support channel (b) Motor mount with fillet (c) Motor mount (d) Filter end cap.

Table 8.1 provides details on each of these components and the impact of using syntactic foams for their manufacture. The parts are 3DP with an aim of reducing the weight of the component by 8% using H60 filament. From Figure 8.2 it is very clear that, complex shaped, thin sectioned, intricate parts can be manufactured in large volume leading to lower costs. Further, the product is more eco-friendly due to use of fly ash. It is also noted that apart from mixing cenospheres in the initial feed, the overall 3D printer settings and parameters have been maintained constant so that the industrial adaptation of lighter components can be easily adopted. Based on the estimate of using

HDPE in the selected 10 components, cenosphere usage can save around 4.64 million tons of HDPE globally per year.

Table 8.1 Details of 3DP syntactic foam components.

| No. | Component Name | Wt. of HDPE component (g) | Wt. of Composite Component (g) | Wt. saving (%) | Features | Component functionality | *Annual total HDPE Saving |
|-----|-------------------------|---------------------------|--------------------------------|----------------|---|---|---------------------------|
| 01 | Arduino rack | 15.4 | 14.2 | 7.8 | Thin section, Multiple slots in different planes | Fixture for electrical connectors | |
| 02 | Bearing holder | 18.1 | 16.7 | 7.7 | Thick section, Oval shaped hole | Sustain better torque, support element | |
| 03 | Arduino rack upper head | 24 | 22.1 | 7.9 | Thick section, Multiple slots in different planes | Connector for robot linkages | |
| 04 | Support channel | 19.4 | 17.9 | 7.7 | Thick section with holes | Dimensional stability, bending and torsional strength | |
| 05 | Motor mount with fillet | 34.8 | 32.0 | 8.1 | Thin section, with intricate holes | Close dimensional tolerance, fixture for motor | |
| 06 | Motor mount | 16.72 | 15.4 | 7.9 | Thin section, with intricate holes | Dimensional and load sustainability | |
| 07 | Rod end holder | 15.3 | 14.1 | 7.8 | Thick section, with holes | Dimensional stability, good strength | |
| 08 | Filter ring | 23.5 | 21.6 | 8.0 | Thick section | Good compressive strength | |
| 09 | Motor cover | 37.1 | 34.2 | 7.8 | Thin section, U shaped slot | Dimensional stability, Support element | |
| 10 | Filter end cap | 31.2 | 28.7 | 8.0 | Thin section, complex mesh structure | Dimensional stability, Filtering liquid | |

*Report on Global HDPE demand to grow 4.2% annually through 2022, March 9, 2015 by Canadian plastics, Toronto, Canada. <http://www.canplastics.com/materials/global-hdpe-demand-to-grow-4-2-annually-through-2022-report/1003434693>

Summary and conclusive remarks of this study are presented hereafter.

SUMMARY AND CONCLUSIVE REMARKS

Summary

A comprehensive investigation is carried out to fabricate and characterize HDPE and fly ash cenosphere/HDPE syntactic foam filament, investigations for recyclability potential and their usage as eco-friendly lightweight feedstock filament to be used in 3D printing. Use of cenospheres in structural applications can reduce the landfill burden and help in effectively addressing the environmental concern of fly ash disposal. In the present study, thermoplastic based 3D printing technique named FFF/FDM is used to develop the cenosphere/HDPE syntactic foam prints and are characterized for mechanical properties. Syntactic foam filaments are fabricated using cenosphere/HDPE blends having 20, 40 and 60 vol. % of cenospheres in HDPE matrix. The effect of filler volume fraction on filament and 3D printed samples are investigated.

Cenosphere/HDPE blend is prepared and characterized to develop foam filament. Viability and recycling potential of foam filament to be used in 3D printer is carried out using thermal and tensile tests. Further printing parameters for foam filament are optimized for minimum filler breakage. Tensile, flexural, compressive and DMA on 3D prints is carried out finally. Extensive scanning electron microscopy and Micro CT scanning is performed to study the structure-property correlations and investigate the failure mechanisms.

Properties of 3D prints are compared with the data extracted from available literature in the form of property map which comes handy for industrial practitioners and acts as a guideline for choosing appropriate process/composition for the envisaged application. As a outcome of thesis, industrial scale components are printed.

Conclusions

The main conclusions are summarized as:

Blend characterization

- MFI of neat HDPE has decreased with increase in cenospheres content. Rheological results indicate a considerable increase in complex viscosity, loss and storage modulus with increasing cenospheres content.
- Complex viscosities values are maximum at a lower frequency but decrease with an increasing frequency.
- Both storage and loss modulus showed an increasing trend with filler loading and frequency.

Density

- Reduction in the experimental density of composites filament and 3D prints is observed as compared to the theoretical ones.
- At 100% infill, H60 3D printed samples are 6.43% lighter than the theoretical density.
- The void content and weight saving potential increases with increase in filler content and their values are higher for 3D prints than respective filament.

Filament development and recycling potential

- Density of H40 foams increased in up to two extrusion passes due to cenosphere breakage and porosity consolidation.
- Developed filaments exhibit three-phase foam structure.
- Tensile modulus and yield strength of neat HDPE filaments increased with each extrusion pass affirming recyclability potential of the developed filaments.
- Higher filler loading increases filament modulus by 7.72-12.79% as compared to HDPE.
- Specific modulus values of extruded filaments are higher than that of injection molded samples at the same strain rates.

Optimization of 3D printing parameters and tensile behavior

- Neat HDPE and foam filaments exhibit lower crystallinity as compared to respective printed material. Filler addition in HDPE matrix reduces CTE remarkably.
- Warping of the specimen is reduced and quality is improved by optimizing printer speed, layer thickness, print temperature and cooling conditions.
- Cenosphere/HDPE three-phase foam prints without warpage having weight saving potential can be used in marine applications.
- Voids present in the respective filament are carried over during printing indicating retention of three-phase foam structure in 3D printed samples.
- Microstructure of 3D printed HDPE40 is similar to that of molded H40.
- Compared to injection molded HDPE, printed HDPE registered 78.86% higher tensile modulus and two-fold fracture strength.
- 3D printed HDPE and foams modulus is 1.16, 1.28, 1.51 and 1.67 times better than respective feedstock material.
- Tensile modulus of prints is higher in the range of 96.01 to 144.45% as compared to the same composition injection molded ones.
- Comparison of specific mechanical properties shows promise in 3D printed syntactic foam components in replacing some of the molded specimens for weight-reduction applications.
- Property map reveals 3D printing potential over other composites synthesized through different processing routes.

Flexural behavior

- Neat HDPE sample is not shown any fracture sign below 10% strain, due to ductile nature of material, cenosphere addition caused brittleness of foam.
- Flexural modulus increases with cenosphere content.
- Highest modulus is exhibited by H60 which is 1.56 times better than neat HDPE sample.

- Presence of air gaps lowers flexural modulus and strength as compared to fully dense injection molded sample.

Quasi-static compression

- Highest specific compressive modulus and yield strength is observed for H60 and H20 respectively at 0.1 s^{-1} among foams.
- 3D printed syntactic foams show good strain rate sensitivity.
- Developing complex geometries with 3D printed three-phase syntactic foams make them potential candidate materials for buoyant weight.

Dynamic Mechanical Analysis

- Neat HDPE 3D printed sample has registered slightly higher storage modulus compared to H20.
- Storage modulus of H60 is highest among all foams.
- H60 registered highest loss modulus followed by H40, H20 and H at higher temperature.
- Neat HDPE is having highest damping capacity
- Cenosphere addition increases viscous component resulting in reduction in damping capacity of the foam.

Present work successfully demonstrates development and recyclability potential of eco-friendly syntactic foam filament for 3D printing process. Thermal, rheological and mechanical characterization of both filament and 3D prints are investigated. Composites are eco-friendly, lightweight and more importantly provides about 7% weight savings potential. Further, usage of fly ash cenospheres reduces landfill burden and environmental linked issues. Experimental results presented as part of this work can be used by 3D printing industry professionals for component development in specific applications. H60 is the best choice based on the work presented here.

SCOPE OF FUTURE WORK

Present work demonstrates 3D printing feasibility and recycling potential of syntactic foam filaments. Geometrical imperfections and irregular wall thickness of fly ash cenospheres needs to be addressed for structure-property correlations. Further, considering the filament extrusion, 3D printing parameters and interaction between the hollow particles and HDPE matrix theoretical models can be developed to print complex foam structures of desired mechanical properties. Further matrix and filler are used in as received condition to fabricate filament. It will be worth studying the influence of treated constituents over filament and 3D printed foam properties.

REFERENCES

- Abdullah, A. M., Rahim, T. N. A. T., Mohamad, D., Akil, H. M. and Rajion, Z. A. (2017). "Mechanical and physical properties of highly ZrO₂/β-TCP filled polyamide 12 prepared via fused deposition modelling (FDM) 3D printer for potential craniofacial reconstruction application." *Materials Letters*, 189, 307-309.
- Adhikary, K. B., Park, C. B., Islam, M. R. and Rizvi, G. M. (2011). "Effects of Lubricant Content on Extrusion Processing and Mechanical Properties of Wood Flour-High-density Polyethylene Composites." *Journal of Thermoplastic Composite Materials*, 24(2), 155-171.
- Agarwal, B. D. and Broutman, L. J. (1980). "Analysis and performance of fiber composites." *Journal of Polymer Science: Polymer Letters Edition*, 18(10), 689-690.
- Alaimo, G., Marconi, S., Costato, L. and Auricchio, F. (2017). "Influence of meso-structure and chemical composition on FDM 3D-printed parts." *Composites Part B: Engineering*, 113, 371-380.
- Alkan, C., Arslan, M., Cici, M., Kaya, M. and Aksoy, M. (1995). "A study on the production of a new material from fly ash and polyethylene." *Resources, conservation and recycling*, 13(3-4), 147-154.
- Arza, S. (2012). "Fillers." *Encyclopedia of Polymer Science and Technology*, 4th edition, John Wiley & Sons, New York.
- Arzamasov B. (1989). *Material Science*. Mir Publishers, Moscow.
- ASTM C618-15, *Standard Specification for Coal Fly Ash and Raw or Calcined Natural Pozzolan for Use in Concrete*, ASTM International, PA, USA.
- ASTM D638-14, *Standard Test Method for Tensile Properties of Plastics*, ASTM, International, PA, USA.
- ASTM D696-13, *Standard Test Method for Coefficient of Linear Thermal Expansion of Plastics Between -30⁰C and 30⁰C with a Vitreous Silica Dilatometer*, ASTM, International, PA, USA.

ASTM D790-17, *Standard Test Methods for Flexural Properties of Unreinforced and Reinforced Plastics and Electrical Insulating Materials*, ASTM International, PA, USA.

ASTM D792-13, *Standard Test Methods for Density and Specific Gravity (Relative Density) of Plastics by Displacement*, ASTM International, PA, USA.

ASTM F2792-10, *Standard Terminology for Additive Manufacturing Technologies*, ASTM International, PA, USA.

Atagur, M., Sarikanat, M., Uysalman, T., Polat, O., Elbeyli, I. Y., Seki, Y. and Sever, K. (2018). "Mechanical, thermal, and viscoelastic investigations on expanded perlite-filled high-density polyethylene composite." *Journal of Elastomers & Plastics*, 50(8), 747-761.

Ayrilmis, N. (2013). "Combined effects of boron and compatibilizer on dimensional stability and mechanical properties of wood/HDPE composites." *Composites Part B: Engineering*, 44(1), 745-749.

Baglari, S., Kole, M. and Dey, T. K. (2011). "Effective thermal conductivity and coefficient of linear thermal expansion of high-density polyethylene — fly ash composites." *Indian Journal of Physics*, 85(4), 559-573.

Banat, R. and Fares, M. M. (2015). "Thermo-gravimetric stability of high density polyethylene composite filled with olive shell flour." *American Journal of Polymer Science*, 5(3), 65-74.

Bassett, D. C. (1976). "Chain-extended polyethylene in context: a review." *Polymer*, 17(6), 460-470.

Benchechou, B., Coni, M., Howarth, H. and White, R. (1998). "Some aspects of vibration damping improvement in composite materials." *Composites Part B: Engineering*, 29(6), 809-817.

Bharath Kumar, B. R., Doddamani, M., Zeltmann, S., Gupta, N., Ramesh, M. R. and Ramakrishna, S. (2016). "Processing of cenosphere/HDPE syntactic foams using an

industrial scale polymer injection molding machine." *Materials and Design*, 92, 414-423.

Bharath Kumar, B. R., Doddamani, M., Zeltmann, S., Gupta, N., Uzma, Gurupadu, S. and Sailaja, R. R. N. (2016). "Effect of particle surface treatment and blending method on flexural properties of injection-molded cenosphere/HDPE syntactic foams." *Journal of Materials Science*, 51(8), 3793-3805.

Bharath Kumar, B. R., Doddamani, M., Zeltmann, S. E., Gupta, N., Ramesh, M. R. and Ramakrishna, S. (2016). "Data characterizing tensile behavior of cenosphere/HDPE syntactic foam." *Data in Brief*, 6, 933-941.

Bharath Kumar, B. R., Singh, A. K., Doddamani, M., Luong, D. D. and Gupta, N. (2016). "Quasi-Static and High Strain Rate Compressive Response of Injection-Molded Cenosphere/HDPE Syntactic Foam." *JOM*, 68(7), 1861-1871.

Bin, Y., Yan-Li, D., Gui-Jing, L., Ji-Bin, M., Ru, X., Jia-Sheng, Q., Peng, C. and Jing-Wang, L. (2015). "Solidification behavior of high-density polyethylene (HDPE) during injection molding: Correlation between crystallization kinetics and thermal gradient field." *IOP Conference Series: Materials Science and Engineering*, 87(1).

Bunn, P. and Mottram, J. (1993). "Manufacture and compression properties of syntactic foams." *Composites*, 24(7), 565-571.

Burgiel, J., Butcher, W., Halpern, R., Oliver, D., Tangora, P., Tangora, R. W. and Kirk, D. R. (1994). *Cost evaluation of automated and manual post-consumer plastic bottle sorting systems*. EPA report EPA/600/R-94/165, 1-10.

Burgueno, R., Quagliata, M. J., Mohanty, A. K., Mehta, G., Drzal, L. T. and Misra, M. (2004). "Load-bearing natural fiber composite cellular beams and panels." *Composites Part A: applied science and manufacturing*, 35(6), 645-656.

Byberg, K. I., Gebisa, A. W. and Lemu, H. G. (2018). "Mechanical properties of ULTEM 9085 material processed by fused deposition modeling." *Polymer Testing*, 72, 335-347.

- Chakravarty, U., Mahfuz, H., Saha, M. and Jeelani, S. (2003). "Strain rate effects on sandwich core materials: An experimental and analytical investigation." *Acta Materialia*, 51(5), 1469-1479.
- Chand, N., Sharma, P. and Fahim, M. (2010). "Correlation of mechanical and tribological properties of organosilane modified cenosphere filled high density polyethylene." *Materials Science and Engineering: A*, 527(21-22), 5873-5878.
- Chawla, K. K. (2001). *Composite Materials*. Springer, New York.
- Chen, F., Mac, G. and Gupta, N. (2017). "Security features embedded in computer aided design (CAD) solid models for additive manufacturing." *Materials & Design*, 128, 182-194.
- Chen, H. C., Chen, T. Y. and Hsu, C. H. (2006). "Effects of Wood Particle Size and Mixing Ratios of HDPE on the Properties of the Composites." *Holz als Roh- und Werkstoff*, 64(3), 172-177.
- Dakshinamurthy, D. and Gupta, S. (2018). "A Study on the Influence of Process Parameters on the Viscoelastic Properties of ABS Components Manufactured by FDM Process." *Journal of The Institution of Engineers (India): Series C*, 99(2), 133-138.
- Daver, F., Lee, K. P. M., Brandt, M. and Shanks, R. (2018). "Cork–PLA composite filaments for fused deposition modelling." *Composites Science and Technology*, 168, 230-237.
- Deepthi, M., Sailaja, R., Sampathkumaran, P., Seetharamu, S. and Vynatheya, S. (2014). "High density polyethylene and silane treated silicon nitride nanocomposites using high-density polyethylene functionalized with maleate ester: mechanical, tribological and thermal properties." *Materials & Design (1980-2015)*, 56, 685-695.
- Deepthi M V, Sharma, M., N, S. R. R., P, A., Sampathkumaran, P. and Seetharamu, S. (2010). "Mechanical and thermal characteristics of high density polyethylene–fly ash Cenospheres composites." *Materials & Design*, 31, 2051-2060.
- Divya, V., Khan, M. A., Rao, B. N. and Sailaja, R. R. N. (2015). "High density polyethylene/cenosphere composites reinforced with multi-walled carbon nanotubes:

mechanical, thermal and fire retardancy studies." *Materials & Design (1980-2015)*, 65, 377-386.

Divya, V. C., Pattanshetti, V. V., Suresh, R. and Sailaja, R. R. N. (2013). "Development and characterisation of HDPE/EPDM-g-TMEVS blends for mechanical and morphological properties for engineering applications." *Journal of Polymer Research*, 20(2), 51.

Domingo Espin, M., Puigoriol-Forcada, J. M., Garcia-Granada, A. A., Lluma, J., Borros, S. and Reyes, G. (2015). "Mechanical property characterization and simulation of fused deposition modeling Polycarbonate parts." *Materials & Design*, 83, 670-677.

Dul, S., Fambri, L. and Pegoretti, A. (2016). "Fused deposition modelling with ABS–graphene nanocomposites." *Composites Part A: applied science and manufacturing*, 85, 181-191.

El Achaby, M., Ennajih, H., Arrakhiz, F. Z., El Kadib, A., Bouhfid, R., Essassi, E. and Qaiss, A. (2013). "Modification of montmorillonite by novel geminal benzimidazolium surfactant and its use for the preparation of polymer organoclay nanocomposites." *Composites Part B: Engineering*, 51, 310-317.

Esha, S. and Rajaram. (1997). "Plastic Recycling in Bangalore - India." *Urban Waste Expertise Programme (UWEP)*, CS-Plast India, 8-10.

Faes, M., Ferraris, E. and Moens, D. (2016). "Influence of inter-layer cooling time on the quasi-static properties of ABS components produced via fused deposition modelling." *Procedia CIRP*, 42, 748-753.

Ferreira, R. T. L., Amatte, I. C., Dutra, T. A. and Burger, D. (2017). "Experimental characterization and micrography of 3D printed PLA and PLA reinforced with short carbon fibers." *Composites Part B: Engineering*, 124, 88-100.

Ferrigno, T. H. (1978). "Handbook of fillers and reinforcements for plastics." *H. S. Katz and J. V. Milewski eds*, Van Nostrand Reinhold, New York, 66-71.

Gardner, J. M., Sauti, G., Kim, J. W., Cano, R. J., Wincheski, R. A., Stelter, C. J., Grimsley, B. W., Working, D. C. and Siochi, E. J. (2016). "3-D printing of

- multifunctional carbon nanotube yarn reinforced components." *Additive Manufacturing*, 12, 38-44.
- Garg, H. and Singh, R. (2017). "Tribological Properties of Fe–Nylon6 Composite Parts Prepared Using Fused Deposition Modelling." *Transactions of the Indian Institute of Metals*, 70(5), 1241-1244.
- Garg, H. K. and Singh, R. (2015). "Comparison of wear behavior of ABS and Nylon6—Fe powder composite parts prepared with fused deposition modelling." *Journal of Central South University*, 22(10), 3705-3711.
- Gupta, N. (2007). "A functionally graded syntactic foam material for high energy absorption under compression." *Materials Letters*, 61(4), 979-982.
- Gupta, N., Maharsia, R. and Jerro, H. D. (2005). "Enhancement of energy absorption characteristics of hollow glass particle filled composites by rubber addition." *Materials Science and Engineering: A*, 395(1-2), 233-240.
- Gupta, N., Pinisetty, D. and Shunmugasamy, V. C. (2013). *Reinforced Polymer Matrix Syntactic Foams: Effect of Nano and Micro-Scale Reinforcement*. Springer, New York.
- Gupta, N. and Woldesenbet, E. (2004). "Microballoon wall thickness effects on properties of syntactic foams." *Journal of Cellular Plastics*, 40(6), 461-480.
- Gupta, N., Woldesenbet, E. and Mensah, P. (2004). "Compression properties of syntactic foams: effect of cenosphere radius ratio and specimen aspect ratio." *Composites Part A: applied science and manufacturing*, 35(1), 103-111.
- Gupta, N., Zeltmann, S. E., Shunmugasamy, V. C. and Pinisetty, D. (2014). "Applications of polymer matrix syntactic foams." *JOM*, 66(2), 245-254.
- Gwon, J. G., Lee, S. Y., Kang, H. and Kim, J. H. (2012). "Effects of sizes and contents of exothermic foaming agent on physical properties of injection foamed wood fiber/HDPE composites." *International Journal of Precision Engineering and Manufacturing*, 13(6), 1003-1007.
- Harris, B. (1999). *Engineering composite materials*. IOM communications, The university press, Cambridge.

- Homaeigohar, S. S., Sadi, A. Y., Javadpour, J. and Khavandi, A. (2006). "The effect of reinforcement volume fraction and particle size on the mechanical properties of β -tricalcium phosphate–high density polyethylene composites." *Journal of the European Ceramic Society*, 26(3), 273-278.
- Hwang, S., Reyes, E. I., Moon, K. S., Rumpf, R. C. and Kim, N. S. (2015). "Thermo-mechanical Characterization of Metal/Polymer Composite Filaments and Printing Parameter Study for Fused Deposition Modeling in the 3D Printing Process." *Journal of Electronic Materials*, 44(3), 771-777.
- Jayavardhan, M. L., Bharath Kumar, B. R., Doddamani, M., Singh, A. K., Zeltmann, S. E. and Gupta, N. (2017). "Development of glass microballoon/HDPE syntactic foams by compression molding." *Composites Part B: Engineering*, 130(Supplement C), 119-131.
- Jayavardhan, M. L. and Doddamani, M. (2018). "Quasi-static compressive response of compression molded glass microballoon/HDPE syntactic foam." *Composites Part B: Engineering*, 149, 165-177.
- Kazmer, D. (2017). "Three-Dimensional Printing of Plastics." *Applied Plastics Engineering Handbook*, (pp. 617-634) William Andrew Publishing, New York.
- Khalaf, M. N. (2015). "Mechanical properties of filled high density polyethylene." *Journal of Saudi Chemical Society*, 19(1), 88-91.
- Khanna, Y. P., Turi, E. A., Taylor, T. J., Vickroy, V. V. and Abbott, R. F. (1985). "Dynamic mechanical relaxations in polyethylene." *Macromolecules*, 18(6), 1302-1309.
- Kruger, R. A. (1997). "Fly ash beneficiation in South Africa: creating new opportunities in the market-place." *Fuel*, 76(8), 777-779.
- KSSPMA, (Karnataka Small Scale Plastic Manufacturers Association). (1992). *A Guide to Plastics*. Bangalore.

- Labella, M., Zeltmann, S. E., Shunmugasamy, V. C., Gupta, N. and Rohatgi, P. K. (2014). "Mechanical and thermal properties of fly ash/vinyl ester syntactic foams." *Fuel*, 121, 240-249.
- Lee, J. and Huang, A. (2013). "Fatigue analysis of FDM materials." *Rapid Prototyping Journal*, 19(4), 291-299.
- Lei, Y., Wu, Q., Clemons, C. M., Yao, F. and Xu, Y. (2007). "Influence of nanoclay on properties of HDPE/wood composites." *Journal of Applied Polymer Science*, 106(6), 3958-3966.
- Lin, Y., Du, W., Tu, D., Zhong, W. and Du, Q. (2005). "Space charge distribution and crystalline structure in low density polyethylene (LDPE) blended with high density polyethylene (HDPE)." *Polymer International*, 54(2), 465-470.
- Liu, H., Wu, Q., Han, G., Yao, F., Kojima, Y. and Suzuki, S. (2008). "Compatibilizing and toughening bamboo flour-filled HDPE composites: Mechanical properties and morphologies." *Composites Part A: applied science and manufacturing*, 39(12), 1891-1900.
- Liu, H., Wu, Q. and Zhang, Q. (2009). "Preparation and properties of banana fiber-reinforced composites based on high density polyethylene (HDPE)/Nylon-6 blends." *Bioresource Technology*, 100(23), 6088-6097.
- Lombardi, J. L., Hoffinan, R. A., Waters, J. A. and Popovich, D. (1997). "Issues associated with EFF & FDM ceramic filled feedstock formulation." *International Solid Freeform Fabrication Symposium, Austin*.
- Luong, D. D., Pinisetty, D. and Gupta, N. (2013). "Compressive properties of closed-cell polyvinyl chloride foams at low and high strain rates: Experimental investigation and critical review of state of the art." *Composites Part B: Engineering*, 44(1), 403-416.
- Mahfuz, H., Thomas, T., Rangari, V. and Jeelani, S. (2006). "On the dynamic response of sandwich composites and their core materials." *Composites Science and Technology*, 66(14), 2465-2472.

Manas, C. and Salil, R. (2006). "Plastic Technology " *Handbook*, CRC press, New York, 2-6.

Manz, O. E. (1999). "Coal fly ash: a retrospective and future look." *Fuel*, 78(2), 133-136.

Mohamed, O. A., Masood, S. H., Bhowmik, J. L., Nikzad, M. and Azadmanjiri, J. (2016). "Effect of process parameters on dynamic mechanical performance of fdm PC/ABS printed parts through design of experiment." *Journal of Materials Engineering and Performance*, 25(7), 2922-2935.

Mohanty, S. and Nayak, S. K. (2010). "Short Bamboo Fiber-reinforced HDPE Composites: Influence of Fiber Content and Modification on Strength of the Composite." *Journal of reinforced plastics and composites*, 29(14), 2199-2210.

Mohapatra, R. and Rao, J. R. (2001). "Some aspects of characterisation, utilisation and environmental effects of fly ash." *Journal of Chemical Technology & Biotechnology: International Research in Process, Environmental & Clean Technology*, 76(1), 9-26.

Nanavaty, K. (1997). "Recycling of Plastics: Indian Experience." *3rd International Plastics Exhibition and Conference on Environment/Recycling of Plastics*, New Delhi.

Nikzad, M., Masood, S. and Sbarski, I. (2011). "Thermo-mechanical properties of a highly filled polymeric composites for fused deposition modeling." *Materials & Design*, 32(6), 3448-3456.

Ning, F., Cong, W., Hu, Y. and Wang, H. (2017). "Additive manufacturing of carbon fiber-reinforced plastic composites using fused deposition modeling: Effects of process parameters on tensile properties." *Journal of Composite Materials*, 51(4), 451-462.

Ou, R., Xie, Y., Wolcott, M. P., Sui, S. and Wang, Q. (2014). "Morphology, mechanical properties, and dimensional stability of wood particle/high density polyethylene composites: Effect of removal of wood cell wall composition." *Materials & Design*, 58, 339-345.

- Panupakorn, P., Chaichana, E., Praserttham, P. and Jongsomjit, B. (2013). "Polyethylene/Clay Nanocomposites Produced by In Situ Polymerization with Zirconocene/MAO Catalyst." *Journal of Nanomaterials*, 2013, 9.
- Pardo, S. G., Bernal, C., Ares, A., Abad, M. J. and Cano, J. (2010). "Rheological, thermal, and mechanical characterization of fly ash-thermoplastic composites with different coupling agents." *Polymer Composites*, 31(10), 1722-1730.
- Pedlow, J. (1978). *Cenosphers, in Coal ash utilization Fly ash, Bottom ash, and Slag*. S. Torrey, eds., Noyes, New Jersey, 353-362.
- Perez, B. (2013). "Printing Pioneer Scott Crump's Kitchen Experiment." *South China Morning Post*.
- Picot, J. J. C. (1984). "Molecular orientation in film extrusion of high-density polyethylene." *Polymer Engineering & Science*, 24(6), 415-420.
- Porter, D. A., Hoang, T. V. T. and Berfield, T. A. (2017). "Effects of in-situ poling and process parameters on fused filament fabrication printed PVDF sheet mechanical and electrical properties." *Additive Manufacturing*, 13, 81-92.
- Rayegani, F. and Onwubolu, G. C. (2014). "Fused deposition modelling (FDM) process parameter prediction and optimization using group method for data handling (GMDH) and differential evolution (DE)." *The International Journal of Advanced Manufacturing Technology*, 73(1-4), 509-519.
- Reinhart, T. J. (1998). "Overview of composite materials " *Handbook of composites*, Springer, Boston.
- Riddick, J. C., Haile, M. A., Von Wahlde, R., Cole, D. P., Bamiduro, O. and Johnson, T. E. (2016). "Fractographic analysis of tensile failure of acrylonitrile-butadiene-styrene fabricated by fused deposition modeling." *Additive Manufacturing*, 11, 49-59.
- Saha, M. C., Mahfuz, H., Chakravarty, U. K., Uddin, M., Kabir, M. E. and Jeelani, S. (2005). "Effect of density, microstructure, and strain rate on compression behavior of polymeric foams." *Materials Science and Engineering: A*, 406(1), 328-336.

Scheetz, B. E. and Earle, R. (1998). "Utilization of fly ash." *Current Opinion in Solid State and Materials Science*, 3(5), 510-520.

Scott, G. G. (2000). "Polymers." *Polymer Degradation and Stability*, 68, 1-7.

Sewda, K. and N. Maiti, S. (2010). "Crystallization and melting behavior of HDPE in HDPE/teak wood flour composites and their correlation with mechanical properties." *Journal of Applied Polymer Science*, 118(4), 2264-2275.

Shahapurkar, K., Garcia, C. D., Doddamani, M., Mohan Kumar, G. C. and Prabhakar, P. (2018). "Compressive behavior of cenosphere/epoxy syntactic foams in arctic conditions." *Composites Part B: Engineering*, 135, 253-262.

Shaikh, A. and Channiwalla, S. (2006). "Experimental and analytical investigation of jute polyester composite for long continuous fiber reinforcement." *Journal of reinforced plastics and composites*, 25(8), 863-873.

Shaikh, H., Anis, A., Poulouse, A. M., Alam, M., A-Otaibi, M. N., Alam, M. A. and Al-Zahrani, S. M. (2016). "Studies on High Density Polyethylene Reinforced with Phosphate Ore Particles: Thermal, Rheological, Mechanical and Morphological Properties ". *Polymer-Plastics Technology and Engineering*, 55(17), 1831-1841.

Shaikh, H., Anis, A., Poulouse, A. M., Alam, M., A-Otaibi, M. N., Alam, M. A. and Al-Zahrani, S. M. (2016). "Studies on High Density Polyethylene Reinforced with Phosphate Ore Particles: Thermal, Rheological, Mechanical and Morphological Properties." *Polymer-Plastics Technology and Engineering*, 55(17), 1831-1841.

Shekhar, B. (2012). "Roadmap to 13 Million Tons." *Plastindia in-house journal*, 37, 6-11.

Shunmugasamy, V. C., Pinisetty, D. and Gupta, N. (2012). "Thermal expansion behavior of hollow glass particle/vinyl ester composites." *Journal of Materials Science*, 47(14), 5596-5604.

Sim, C. P., Cheang, P., Liang, M. H. and Khor, K. A. (1997). "Injection moulding of hydroxyapatite composites." *Journal of Materials Processing Technology*, 69(1), 75-78.

- Singh, A. K., Patil, B., Hoffmann, N., Saltonstall, B., Doddamani, M. and Gupta, N. (2018). "Additive Manufacturing of Syntactic Foams: Part 1: Development, Properties, and Recycling Potential of Filaments." *JOM*, 70(3), 303-309.
- Singh, R., Bedi, P., Fraternali, F. and Ahuja, I. P. S. (2016). "Effect of single particle size, double particle size and triple particle size Al₂O₃ in Nylon-6 matrix on mechanical properties of feed stock filament for FDM." *Composites Part B: Engineering*, 106, 20-27.
- Singh, R., Kumar, R. and Kumar, S. (2017). " Polymer Waste as Fused Deposition Modeling Feed Stock Filament for Industrial Applications." *Ref. module in "Materials Science and Materials Engineering"*, (pp. 1-12) Elsevier, U.K.
- Singh, R., Singh, N., Bedi, P. and Ahuja, I. P. S. (2016). "Polymer Single-Screw Extrusion With Metal Powder Reinforcement." *Ref. Module in "Materials Science and Materials Engineering"*, (pp. 1-18) Elsevier, U.K.
- Singh, R., Singh, S. and Fraternali, F. (2016). "Development of in-house composite wire based feed stock filaments of fused deposition modelling for wear-resistant materials and structures." *Composites Part B: Engineering*, 98, 244-249.
- Singh, R., Singh, S. and Mankotia, K. (2016). "Development of ABS based wire as feedstock filament of FDM for industrial applications." *Rapid Prototyping Journal*, 22(2), 300-310.
- Singh, S., Deepak, D., Aggarwal, L. and Gupta, V. K. (2014). "Tensile and Flexural Behavior of Hemp Fiber Reinforced Virgin-recycled HDPE Matrix Composites." *Procedia Materials Science*, 6, 1696-1702.
- Sood, M. (2014). "Investigation of Flexural behavior of hybrid natural fiber composite with recycled polymer matrix." *American International Journal of Research in Science, Technology, Engineering & Mathematics*, 6(3), 237-240.
- Srinivasan, N. K. and Ramakrishnan, S. S. (1983). *The science of engineering materials*. Oxford & IBH, New Delhi.

- Tagarielli, V. L., Deshpande, V. S. and Fleck, N. A. (2008). "The high strain rate response of PVC foams and end-grain balsa wood." *Composites Part B: Engineering*, 39(1), 83-91.
- Tagliavia, G., Porfiri, M. and Gupta, N. (2010). "Analysis of flexural properties of hollow-particle filled composites." *Composites Part B: Engineering*, 41(1), 86-93.
- Takahashi, Y., Ishida, T. and Furusaka, M. (1988). "Monoclinic-to-orthorhombic transformation in polyethylene." *Journal of Polymer Science Part B: Polymer Physics*, 26(11), 2267-2277.
- Tekinalp, H. L., Kunc, V., Velez-Garcia, G. M., Duty, C. E., Love, L. J., Naskar, A. K., Blue, C. A. and Ozcan, S. (2014). "Highly oriented carbon fiber-polymer composites via additive manufacturing." *Composites Science and Technology*, 105, 144-150.
- Tian, X., Liu, T., Wang, Q., Dilmurat, A., Li, D. and Ziegmann, G. (2017). "Recycling and remanufacturing of 3D printed continuous carbon fiber reinforced PLA composites." *Journal of Cleaner Production*, 142, 1609-1618.
- Tuan Rahim, T. N. A., Abdullah, A. M., Md Akil, H., Mohamad, D. and Rajion, Z. A. (2015). "Preparation and characterization of a newly developed polyamide composite utilising an affordable 3D printer." *Journal of reinforced plastics and composites*, 34(19), 1628-1638.
- Viviane Alves Escocio, Elen Beatriz Acordi Vasques Pacheco, Ana Lucia Nazareth da Silva, André de Paula Cavalcante and Visconte, L. L. Y. (2015). "Rheological Behavior of Renewable Polyethylene (HDPE) Composites and Sponge Gourd (*Luffa cylindrica*) Residue." *International Journal of Polymer Science*, 2015, 7.
- Wang, J., Xie, H., Weng, Z., Senthil, T. and Wu, L. (2016). "A novel approach to improve mechanical properties of parts fabricated by fused deposition modeling." *Materials & Design*, 105, 152-159.
- Wang, L. and Gardner, D. J. (2017). "Effect of fused layer modeling (FLM) processing parameters on impact strength of cellular polypropylene." *Polymer*, 113, 74-80.

- Wasiak, A., Sajkiewicz, P. and Woźniak, A. (1999). "Effects of cooling rate on crystallinity of i-polypropylene and polyethylene terephthalate crystallized in nonisothermal conditions." *Journal of Polymer Science Part B: Polymer Physics*, 37(20), 2821-2827.
- Weng, Z., Wang, J., Senthil, T. and Wu, L. (2016). "Mechanical and thermal properties of ABS/montmorillonite nanocomposites for fused deposition modeling 3D printing." *Materials & Design*, 102, 276-283.
- Yamaguchi, M. and Suzuki, K.-I. (2002). "Enhanced strain hardening in elongational viscosity for HDPE/crosslinked HDPE blend. II. Processability of thermoforming." *Journal of Applied Polymer Science*, 86(1), 79-83.
- Yang, C., Tian, X., Li, D., Cao, Y., Zhao, F. and Shi, C. (2017). "Influence of thermal processing conditions in 3D printing on the crystallinity and mechanical properties of PEEK material." *Journal of Materials Processing Technology*, 248, 1-7.
- Yao, T., Deng, Z., Zhang, K. and Li, S. (2019). "A method to predict the ultimate tensile strength of 3D printing polylactic acid (PLA) materials with different printing orientations." *Composites Part B: Engineering*, 163, 393-402.
- Yao, X., Luan, C., Zhang, D., Lan, L. and Fu, J. (2017). "Evaluation of carbon fiber-embedded 3D printed structures for strengthening and structural-health monitoring." *Materials & Design*, 114, 424-432.
- Yin, S., Tuladhar, R., Shi, F., Shanks, R., Combe, M. and Collister, T. (2015). "Mechanical reprocessing of polyolefin waste: A review." *Polymer Engineering & Science*, 55, 2899–2909.
- Yuan, Q., Bateman, S. A. and Wu, D. (2010). "Mechanical and conductive properties of carbon black-filled high-density polyethylene, low-density polyethylene, and linear low-density polyethylene." *Journal of Thermoplastic Composite Materials*, 23(4), 459-471.
- Zaldivar, R. J., Witkin, D. B., McLouth, T., Patel, D. N., Schmitt, K. and Nokes, J. P. (2017). "Influence of processing and orientation print effects on the mechanical and

thermal behavior of 3D-Printed ULTEM® 9085 Material." *Additive Manufacturing*, 13, 71-80.

Zou, R., Xia, Y., Liu, S., Hu, P., Hou, W., Hu, Q. and Shan, C. (2016). "Isotropic and anisotropic elasticity and yielding of 3D printed material." *Composites Part B: Engineering*, 99, 506-513.

RESEARCH OUTCOME IN PRINT MEDIA

Research outcome on Syntactic foam filament development and 3D printing is reported by TWO leading National News Papers, DECCAN HERALD (14.03.2018) and TIMES OF INDIA (16.03.2018) in India.

Districts

Dakshina Kannada & Udupi

Three students get Postal Dept scholarship

MANGALURU, DHNS: Three students of St Aloysius High School, Kodialbail, received a scholarship from the Department of Posts (DoP), India.

The Office of the Senior Superintendent of Post office, Balmatta, conducted a quiz (1 round) for philately students of 8th and 9th standard in several disciplines such as philately, science, history and current affairs.

Four students qualified for the second round and were asked to present a project in order to qualify for the Philately scholarship under the scheme "Deen Dayal Sparsh Yojana" (scholarship for the promotion of aptitude and research in stamps as a hobby). Of the four, three students of St Aloysius High School, Kodialbail got selected for the scholarship. Desmond D'Cunha (class 8), Lester Lobo and Suman Pinto (class 9) are those who received the scholarship. They will be receiving an amount of Rs 6,000 during the academic year.

No ticket for Shiroor Mutt seer, says BJP

UDUPI: District BJP president Mattar Rathnakar Hegde said that there is no question of Shiroor Mutt seer Sri Lakshmvira Theertha Swami getting the BJP ticket to contest the forthcoming Assembly elections from Udupi.

Speaking to reporters, the BJP district president said that the seer's decision to contest the elections has nothing to do with the BJP or its ideologies. The seer is associated with Hindutva and is a close associate of the BJP.

"The BJP ticket is only for those who are working for the party and are associated with the party since years," he added.

The president said he spoke to the seer and had discussed the issue with him. He is ignorant of the seer's intentions and his opinion about district BJP. "The district BJP is perfect in all angles and there is no need for an outsider to come in and set right the unit. The party's high command will take care of the district unit," said Hegde.

He said the seer is under confusion and is of double standard, which he himself should clarify.

DH News Service

Symposium on human dignity in M'loru today

MANGALURU, DHNS: St Aloysius College will organise a symposium on "Champion Human Dignity: Translate Fear Into Hope" at LF Rasquinha Hall, LCRI Block, at 9 am on March 14.

Actor Prakash Rai will speak on "Just Asking: A Movement for Personal

Ensure proper water supply in peak summer: Madhwaraj

Officers directed to arrange for direct supply through tankers

UDUPI: District In-charge Minister Pramod Madhwaraj directed the officials to ensure that the district does not face shortage of water during peak summer. Priority should be given for supply of water till the onset of monsoon, he stated.



District In-charge Minister Pramod Madhwaraj chairs a meeting in Udupi on Tuesday.

Chairing a meeting convened to discuss on water supply with the City Municipal Council (CMC) engineers and PDOs on Tuesday, Madhwaraj directed the officials to make arrangement for a supply of water through tankers. Tenders should be invited for the supply, he added.

'Attend to public calls'

The minister directed the officials not to switch off their mobile phones but attend to the calls of the public with regard to shortage of water.

CMC environment officer Raghavendra said, "Tenders have been invited to supply

water to eight wards in Udupi. Measures have been taken to supply water in other wards. The water level in Baje reservoir that supplied drinking water to Udupi stood at 5.66 metre. If water is supplied round the clock, then it is sufficient for 65 to 70 days."

The sand bags placed in Shiroor dam have been removed. The inflow of water to the dam has also stopped.

CMC commissioner D Manjunathaiah said that officials have been deployed to monitor the supply of water in all the 35 wards.

He said that the CMC had conducted a trial run on rationing of water. Fifty-eight houses had encountered minor problems while receiving water.

Tanker to well

The minister expressed dis-

'My word to be followed'

The Handadi GP PDO said that the gram panchayat has resolved not to supply water through tankers..

The enraged minister said, "I am the president of the Task Force looking into the supply of water. Do what I ask you to do. Invite quotation for water supply."

pleasure for pouring water from tanker to a well and later supplying it to the residents through pipelines at Ambalpaday Gram Panchayat.

"The pouring of water into the well will result in wastage of water. Instead, water should be supplied through tankers directly," the minister said.

Electrification of houses

Elaborating the achievements of various development programmes, the minister said that 497 houses in the rural areas are given electricity connection and are undergo-

ing various stages of electrification. Out of 497, 167 are completely electrified.

The minister said that 3,540 BPL cards are distributed in the Adalat, while 3,373 are given under Tatkal and another 8,000 sent via post. As many as 1,490 title deeds are given under 94C and 94CC of Land Revenue Act.

He said that the applicants for BPL cards can immediately approach the Food section in respective Taluk offices with income certificates and get their cards done.

DH News Service

Lightweight filament for 3D printing developed

MANGALURU, DHNS: A novel lightweight filament for 3D printing developed by National Institute of Technology Karnataka (NITK), Surathkal, in collaboration with New York University, USA.

Dr Mrityunjay Doddamani from Mechanical Department, NITK said syntactic foams are hollow particle filled lightweight polymer composites. These foams are extensively used for Naval applications like in marine underwater vehicles and submarines, an area of urgent need for India. Syntactic foams have enabled the deep dive capabilities of underwater vehicles such as Bluefin-21 used in the search of Malaysia Airline flight 370 and construction of James Cameron's Deepsea Challenger submarine for the Mariana Trench dive.

One of the major challenges in developing vehicles for deep sea exploration is the failure of



Dr Mrityunjay Doddamani from Mechanical Department, NITK and his student who along with Prof Nikhil Gupta of Tandon School of Engineering, New York University, have developed a filament for 3D printing.

materials at joints. 3D printing can completely eliminate the need for joining panels to construct these vehicles. However, developing a syntactic foam filament for 3D printing has been a major challenge for researchers.

Syntactic foam filament

As part of collaborative efforts between the teams, Dr Mrity-

unjay Doddamani of Mechanical Engineering department, NITK, and Prof Nikhil Gupta of Tandon School of Engineering, New York University, recently reported development of a syntactic foam filament that can be used in commercial 3D printers for printing lightweight components.

This filament is made from high density polyethylene

plastic (HDPE) filled with ceramic hollow particles. HDPE is an industrial plastic and can be used in making industrial grade components. The filament was used in off-the-shelf commercial printers successfully to print specimens.

About the challenges faced by the researchers in this project, Dr Doddamani said "Optimisation of parameters related to mixing of particles in polymer and extrusion of filament are crucial to ensure that particles do not break in the process."

"Success of the mixing process without breaking particles was an important aspect in obtaining low density in the filament," added Dr Gupta. The low density filaments can provide buoyant low density structures needed for the underwater vehicles.

Balu Patil, a PhD student in Advanced Manufacturing Lab, Mechanical Department, working with Dr Doddamani

said, "Achieving close control over the filament diameter ensured that these filaments can be used in 3D printers without jamming the printer nozzles."

NITK Director Prof K Uma Maheshwar Rao applauded the success of the team and said, "This work is crucial to develop the next generation of underwater vehicles for the nation."

Prof S Narendranath, who is the head of the Mechanical Engineering department, NITK said, "Such projects can motivate the next generation to aim higher and develop cutting-edge technologies, that have industrial relevance. Future work of will focus on optimising the material properties for various applications such as designing syntactic foam with properties that are tailored for various depths of ocean for use in underwater vehicles."



Srajana Kaikini, a PhD student at the Manipal Centre for Philosophy and Humanities (MCPH), MAHE, Manipal; Dr Sandhya R Nambiar, principal and head of Department of English, MGM College; and K P Rao, retired professor, Manipal Institute of Technology, MAHE, Manipal, release the book at MGM College in Udupi.

MUP releases 'Dhvani and Epiphany: Essays in Criticism'

MANIPAL, DHNS: Manipal Universal Press released its 123rd publication, 'Dhvani and

the author himself. Srajana Kaikini, a PhD student at Manipal Centre for

Applications invited for artificial limb camp

MANGALURU, DHNS: Mangalore Refinery & Petrochemicals Limited (MRPL) will be organising the 17th artificial limb camp as part of its corporate social responsibility initiatives for the benefit of people with disabilities for three days, on March 30, 31 and April 1, at MRPL Employees Club, MRPL Township, Bala.

According to a press release, the camp is being arranged in two phases. In the first phase, only the measurement will be taken, and in the second phase, fittings of limbs will be carried out (approx

the measurement). People who are interested in availing this facility are requested to send their details such as name, address, age, phone number, particulars of the handicap etc, addressed to the CGM (CSR),

Mangalore Refinery and Petrochemicals Ltd., Post Kuthethur, via Katipalla, Mangalore-575030, Dakshina Kannada, on or before March 15. Polio affected people who are unable to walk can also participate in the camp.



JOCKEY FACTORY SECONDS UPTO 50% OFF
INNERWEAR • ACTIVEWEAR • LEISUREWEAR • KIDSWEAR

Venue in Mangaluru :



Demand to serve boiled rice in Indira Canteens

MANGALURU, DHNS: Minister for Food and Civil Supplies U T Khader said that there is a demand for a supply of boiled rice instead of white rice at the Indira Canteen.

"The measures will be taken to provide boiled rice shortly," he added.

Speaking to reporters here, he said that a demand for boiled rice was made by people when he visited an Indira Canteen recently.

"People have also demanded pickle with rice, rasam and curd rice for lunch. People from Dakshina Kannada district prefer boiled rice, while people from other districts prefer white rice. Changes in the menu will be discussed at a meeting of the committee headed by the deputy commissioner," explained the minister.

V Prasanna, project director, District Urban Development Cell, said the contractor

providing food at the Indira Canteens has agreed to make both boiled and white rice available. Indira Canteens have been built at Urwa Stores, near the service bus stand at State Bank, near Surathkal market and in Kavoor.

LPG cylinders under Anila Bhagya will be distributed in Dakshina Kannada shortly. The district has already received Rs 50 lakh grant for the distribution of LPG to beneficiaries.

To a query on Congress office-bearers and leaders participating in the distribution of title deeds in Mangaluru constituency, Khader said, "Government funds are not used to organise the programme. Hence, the local people organise the programme."

Those who had worked hard to get the title deeds for the poor were felicitated on the occasion.

New concrete road with Adani CSR opens in Yellur

UDUPI, DHNS: The Adani UPCL plant, which is operating at Yellur village, inaugurated the new concrete road constructed under its CSR activities, at the limits of Yellur gram panchayat, on Sunday.

The concrete road, measuring 250 metres in length from Veerabhadra Temple to Maniyuru village, was built at a cost of Rs 22.50 lakh.

Inaugurating the road, Adani UPCL joint president Kishore Alva said that Adani UPCL has declared a special CSR grant of Rs. 22.73 crores for rural infrastructure development works in seven gram

panchayats, where Yellur gram panchayat has been committed with infrastructure development works worth Rs. 3.75 crores for over a period of 3 years. From the annual commitment of CSR works of Rs. 1.25 crores in Yellur gram panchayat, UPCL has already executed development works worth Rs. 55.50 lakh.

UPCL has also provided a safe drinking water unit worth Rs 20 lakh to the villagers of Yellur and many other infrastructure development works, of which the erection of street lights on the roads are in progress.

AMITY | BANGALORE

CAMPUS PLACEMENTS AT AMITY GLOBAL BUSINESS SCHOOLS IN 2017

WORLD-CLASS LEARNING MEETS TOP PLACEMENTS

2018 SESSION ADMISSIONS OPEN

MBA + PGPM BBA + GDBA

FROM AMITY UNIVERSITY FROM AMITY GLOBAL BUSINESS SCHOOL

For full details on certification, etc. visit website

THE AMITY EDUCATION GROUP ADVANTAGE

- 150,000 students and 25 years experience in Mgmt. Education
- Over 2,000 management case studies developed by faculty bought across 99 countries by Harvard, McKinsey etc.
- B. School Network across 11 Indian metros & 10 International Campuses
- Industry interaction with top professionals from Deloitte, JP Morgan, Accenture, NDTV, Citibank etc.

Printed from

THE TIMES OF INDIA

Lightweight filament for 3D printing developed in NIT-K

TNN | Mar 16, 2018, 05.40 PM IST



MANGALURU: In a breakthrough research in the field of 3D printing technology, researchers at NIT-K, Surathkal in collaboration New York University, USA, have reported development of a syntactic foam filament that can be used in commercial 3D printers for printing lightweight components.

According to researcher, this is first time that such invention has gone behind filament while lots of work has done to improvise the 3D printers in the past.

The research is done as collaborative efforts between team, Mrityunjay Doddamani from mechanical engineering department of National Institute of Technology Karnataka Surathkal and Nikhil Gupta of New York University, Tandon School of Engineering (NYU), USA. They recently reported development of a syntactic foam filament that can be used in commercial 3D printers for printing lightweight components.

Explaining about new development, Doddamani said this filament is made from high density polyethylene (HDPE) plastic filled with ceramic hollow particles. HDPE is an industrial plastic and can be used in making industrial grade components. The filament was used in off the shelf commercial printers successfully to print specimens.

About the challenges faced by the researchers in this project, Doddamani said that optimization of parameters related to mixing of particles in polymer and extrusion of filament are crucial to ensure that particles do not break in the process.

Nikhil Gupta added that success of the mixing process without breaking particles was an important aspect in obtaining low density in the filament. "The low density filaments can provide buoyant low density structures needed for the underwater vehicles," he said.

Balu Patil, Ph.D scholar in advanced manufacturing lab, mechanical department said that achieving close control over the filament diameter ensured that these filaments can be used in 3D printers without jamming the printer nozzles.

K Uma Maheshwar Rao, director of NIT-K, applauded the success of the team and said that such work is crucial for the current needs of the nation for developing the next generation underwater vehicles.

While S Narendranath, head of the mechanical engineering department, NITK pointed out that such projects can motivate the next generation of students to aim higher and develop cutting-edge technologies that have industrial relevance. The future work of this team will focus on optimizing the material properties for various applications such as designing syntactic foam with properties that are tailored for various depths of ocean for use in underwater vehicles.

What is syntactic foam?

Syntactic foams are hollow particle filled lightweight polymer composites. These foams are extensively used for naval applications like in marine underwater vehicles and submarines, an area of urgent need for India. Syntactic foams have enabled the deep dive capabilities of underwater vehicles such as Bluefin-21 used in the search of Malaysia Airline flight 370 and construction of James Cameron's Deepsea Challenger submarine for the Mariana Trench dive.

Click here for more [Education News](#)

LIST OF PUBLICATIONS

INTERNATIONAL JOURNALS

1. “Compressive behavior of fly ash based 3D printed syntactic foam composite” *Materials Letters*, vol. 254, 246-249. (**Elsevier, 3.019**)
2. “Eco-friendly lightweight filament synthesis and mechanical characterization of additively manufactured closed cell foams” *Composite Science and Technology*, (Revision Submitted) (**Elsevier, 6.309**)
3. “Additive manufacturing of syntactic foams: Part 1: Development, properties, and recycling potential of filaments” *JOM*, 70(3), 303-309. (**Springer, 2.305**)
4. “Additive manufacturing of syntactic foams: Part 2: Specimen printing and mechanical property characterization” *JOM*, 70(3), 310-314. (**Springer, 2.305**)

INTERNATIONAL CONFERENCES

1. Praveen Jeyachandran, Balu Patil, Mrityunjay Doddamani, Srikanth Bontha and Vamsi Krishna Balla (2017). “Development of Thermoplastic Feedstock Filament for 3D Printing.” International Conference on Precision, Meso, Micro and Nano Engineering, December 6-9, 2017 Indian Institute of Technology - Madras, Chennai, Tamil Nadu, India.
2. Balu Patil, Kiran Shahapurkar and Mrityunjay Doddamani (2019). “Compressive behavior of 3D printed lightweight composite.” 27th Annual International Conference on Composites/Nano Engineering, July 15 - 21, 2019 Paris, France.

BIO-DATA

1. Name : Balu Patil
2. Father's Name : Parasharam Patil
3. Date of Birth : 04th July 1988
4. Nationality : Indian
5. Marital Status : Single
6. Address : Department of Mechanical Engineering
National Institute of Technology Karnataka
Surathkal, PO Srinivasnagar 575 025
Karnataka, India.
7. Mobile Number : +91 8971206446
8. E-mail id. : *bppatil353@gmail.com*
9. Educational Qualification :

| Qualification | University/Board | Year of Passing |
|----------------------------------|---|-----------------|
| Ph.D. (Mechanical Engineering) | National Institute of Technology Karnataka | 2019 |
| M.Tech. (Mechanical Engineering) | Visvesvaraya Technological University, Belgaum | 2013 |
| B.E. (Mechanical Engineering) | Visvesvaraya Technological University, Belgaum | 2010 |
